General Disclaimer

One or more of the Following Statements may affect this Document

- This document has been reproduced from the best copy furnished by the organizational source. It is being released in the interest of making available as much information as possible.

- This document may contain data, which exceeds the sheet parameters. It was furnished in this condition by the organizational source and is the best copy available.

- This document may contain tone-on-tone or color graphs, charts and/or pictures, which have been reproduced in black and white.

- This document is paginated as submitted by the original source.

- Portions of this document are not fully legible due to the historical nature of some of the material. However, it is the best reproduction available from the original submission.

CR 73184 4

Available to The Public

RESEARCH STUDY OF AN AIRCRAFT-CONTAINED RADAR ZERO-ZERO LANDING SYSTEM

FINAL REPORT

JANUARY TO DECEMBER 1967

VOLUME I

Prepared For
NATIONAL AERONAUTICS AND
SPACE ADMINISTRATION
AMES RESEARCH CENTER

LOCKHEED ELECTRONICS COMPANY
A DIVISION OF LOCKHEED AIRCRAFT CORPORATION
MILITARY SYSTEMS . . . PLAINFIELD, NEW JERSEY

RESEARCH STUDY OF AN AIRCRAFT - CONTAINED RADAR ZERO-ZERO LANDING SYSTEM

Final Report
January to December, 1967
Contract No. NAS2-4091

For

NATIONAL AERONAUTICS & SPACE ADMINISTRATION
Ames Research Center, Moffett Field,
California

David W. Young, Program Manager
James W. Suzansky, Project Engineer

VOLUME I

Report No. 4

LEC Project
22-4351-1000

December, 1967

LOCKHEED ELECTRONICS COMPANY
A DIVISION OF LOCKHEED AIRCRAFT CORPORATION
MILITARY SYSTEMS · PLAINFIELD, NEW JERSEY

ABSTRACT

Two rapid scan radar/display techniques (P^3I CBRS) were developed and demonstrated, utilizing the benefits of each technique to provide a pictorial, vertical, linear perspective display of a landing area and the terrain preceding and surrounding it. The resulting display is intended to be used in the performance of aircraft landings under conditions of zero visibility and zero ceiling and without the need for cooperative ground equipment.

An introduction to motion cue guidance is developed as a technique for designing radar, comparing radar/display results with normal vision, gaining insight into the experience of landing an aircraft, and drawing attention to the difficult task of visual landing as well as possible solutions which could lead to an instrument landing capability "better than visual".

This final report, together with addendums and references, can be used as a concept design guide for low level flight, specifically, approach to landing and touch down.

ACKNOWLEDGMENTS

This study program was monitored by, and coordinated with, Gilbert Robinson and Robert Griffin, Guidance and Control Systems Branch, Full Scale and Systems Research Division, NASA-Ames Research Center. Lockheed Electronics Company personnel who have contributed to this program include: Homer B. Tilton, Frank S. Gutleber, Robert W. Neher, George H. Boehm, Ansel H. Leffel and John F. Dey.

CONTENTS

VOLUME I

CONTENTS (Continued)

VOLUME I

VOLUME II

TABLES

ILLUSTRATIONS

ILLUSTRATIONS (Continued)

ILLUSTRATIONS (Continued)

1. SUMMARY

This Final Report (Volume I), together with the Addendums (Volume II), is the first attempt by the Airborne Radar Program personnel of Lockheed Electronics Company to assemble in one published report the concept of using longwave (radar) vision to produce a pictorial, linear perspective display/radar through techniques such as the P^3I (Processed PPI) and CBRS (Cross Beam Raster Scan). This report, as outlined by the summary, is intended as a concept design guide for low level flight, specifically, approach to landing and touchdown.

The intent of this study program, as defined by Contract NAS2-4091[1], is "to conduct a study of the feasibility of a radar display/system for landing of aircraft under conditions of zero visibility and zero ceiling without the aid or need of ground instrumentation." The display desired was pictorial - a radar display which would present the pilot the available landing cues in a form with which he is already familiar. These objectives have been met, as demonstrated by Figures 7, 58, and 59. Figures 58 and 59 are examples of the radar/display achieved by use of a rapid scanning antenna (the Variable Ridge Scanning Antenna) and circuitry for processing the radar data into a pictorial perspective display, described in Sections 6 and 7. Figure 7 is from the first flight-demonstration film of the Lockheed Electronics Company P^3I radar, accomplished by optical processing (rather than the electronic processing of Figures 58 and 59) of movies of the Lockheed Rotor Blade Antenna Radar. Although the radar data for Figure 7 was real-time flight data, data processing took place in the laboratory. It is recommended that a follow-on phase be pursued to implement a real-time flight demonstration of this radar-derived perspective display.

---

1. Note, References are listed in Section 7.8

Sections 2 through 4 develop the problem to be dealt with in the main body of the report. The radar/display objectives, concepts, and definitions are presented. The P^3I and CBRS radar/display techniques and a method for registration are developed.

Section 5 is an introduction to motion cue guidance as a technique for designing radar, comparing radar/display results with normal vision, gaining insight into the experience of landing an aircraft, and drawing attention to the difficult task of visual landing as well as possible solutions which could lead to an instrument landing capability which is "better than visual."

Included with this report are two Addendums which excerpt two unpublished reports prepared in 1962 and 1965. These addendums, as well as several of the references, are intrinsic to a full understanding of the concepts presented and of current and future design planning.

2. PROBLEM DEFINITION

The general problem is to make a zero-zero landing with self-contained (aircraft-contained) sensors and without electronic ground-based aids when using any type of aircraft. Specifically, the problem is to review the visual landing problem, develop new visual landing cue analytical techniques as required, analyze the motion cues, and, as a result of the motion cue study and the review of the visual landing (manual control) problem, define the parameters of a self-contained sensor/display system for use in zero-zero landings. This system is to be economically feasible to design and fabricate, and used as a flight-test research tool at NASA, Ames Research Center, for zero-zero landing flight research in the Convair 340 Flying Laboratory.[38] The results of tests with the Flying Laboratory could eventually lead to specification of a family of systems, each designed for a specific aircraft with specific missions.

The initial assumption is that by using other navigational methods (VOR, TACAN, etc.) the Convair 340 is guided to within 10,000 feet of the runway threshold. It is also assumed that the aircraft position is sufficiently accurate to allow the runway outline or terrain landmarks on each side of the proper course to be detected (by radar) approximately 2 miles from the runway to serve as checkpoints for proper alignment adjustment. Aircraft heading is expected to differ from runway heading by less than 15 degrees. These assumptions affect the desired radar range and azimuth angle to be scanned and displayed. Should these assumptions prove too restrictive in actual use, provision may be made for slewing the entire radar scanning field to search for landmarks and/or the runway.

The aircraft's altitude (above ground level, AGL) at the initiation of the problem will be dependent on the desired glide slope. The glide slope for this type of aircraft is normally in the range of 2.5 to 6.0 degrees, with 3.0 degrees (ILS approach) being the most common.[5, 11, 13, 19] This range of glide slopes, and the 3.0 degree and 6.0 degree glide slopes in

particular, will be used to limit the range of investigation. It is assumed that the glide slope is aimed at a point (aiming point or impact point) 1000 feet beyond the runway threshold on the runway centerline. The runways of interest, i.e., Moffett Field and Crows Landing, are 200 ft by 10, 000 ft.

This problem will include maintaining the aircraft on the glide slope, flaring the aircraft, touchdown, and rollout. It is assumed that this specific problem will end when the aircraft can first come to a full, controlled stop, and that additional taxiing will probably be guided primarily by an aircraft-contained horizontal (PPI) radar display or by use of radar reflector centerline markings. Existing aircraft altitude and attitude sensors will be used as required.

3. DISPLAY OBJECTIVE, CONCEPT, AND DEFINITION

The end result of the radar system's scanning of the earth is the presentation of information on terrain and runway status in a form the pilot can readily interpret and utilize. The primary method of achieving this will be a Vertical Situation Display (VSD), which presents an azimuth angle versus elevation/depression angle plot of the information gathered from the earth's surface by the radar. It thus contains a linear perspective* view of the earth geometrically identical to the view that would be seen by the pilot when looking out his windshield on a clear day. One of the goals is to present this perspective view on a "heads-up", see-through screen, with display content having a one-to-one aspect with the visual real world situation. This goal necessitates on "inside-out" display approach; specifically, the display presents the earth as seen from the aircraft (as opposed to "outside-in", with the aircraft as seen from the earth). The display center and the center of the pilot's visual cone, together with the center of the radar antenna and the aircraft's longitudinal axis, are assumed to be coincident. In Figure 1, the display center is represented by a cross. This cross remains fixed, while the displayed terrain and runway move with respect to the cross in the same manner as the earth moves with respect to the aircraft's nose. In fact, the cross is a substitute for the aircraft's nose, which has been found to be a useful cue element for landing.[8]

The display must also contain an earth-referenced horizon line in order to provide the pilot attitude information. This will also have an "inside-out" movement direction, e.g., a pitch down would be shown by the horizon (and display content) moving up. Roll would be shown by rotation of the

---

* The apparent convergence at the horizon of parallel lines due to the observer's viewpoint (an orthographic projection).

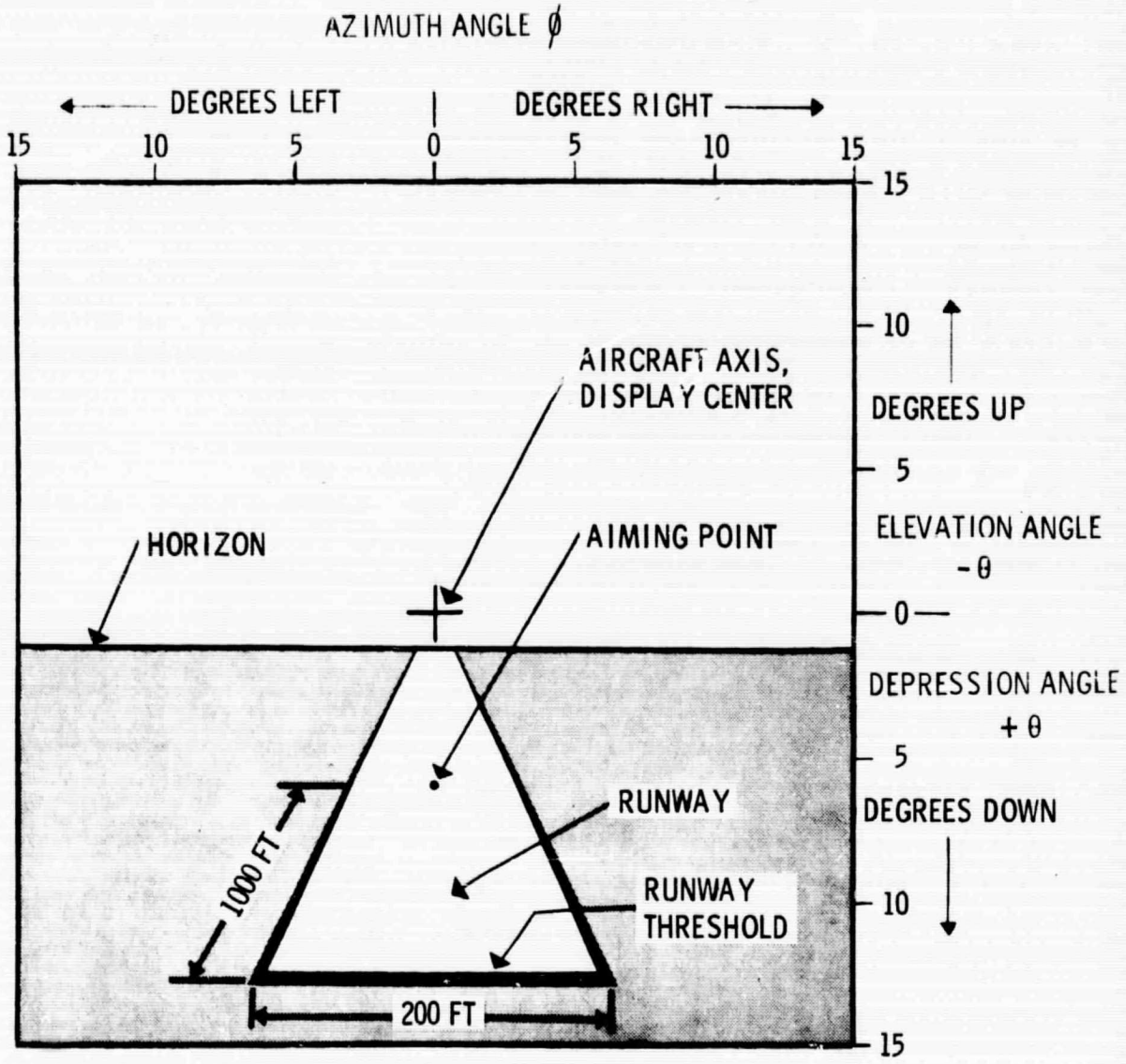

RUNWAY = 10,000 FT X 200 FT, 1000 FT
THRESHOLD TO AIMING POINT
RADAR RANGE ≈ 10,000 FT

AIRCRAFT AT 200 FT ALTITUDE,
6° GLIDE SLOPE,
ZERO ROLL AND PITCH
HEADING ALONG RUNWAY CENTERLINE

Figure 1. Display Definition

horizon about its center and corresponding perspective changes in the display content; a right roll would be shown by a counterclockwise rotation of the horizon, with the right side high and the left side low.

It is felt that such a display concept will present the pilot the same major visual cues available during a visual contact landing.[5, 6, 8, 11, 13, 17] (An excellent summary of these cues is given by Lane and Cumming.[8]) The runway is shown in perspective, providing the pilot the change-of-runway-perspective cues normally available. During a contact landing in which the horizon is visible, an important cue for maintaining a constant glide slope is the distance (in visual angle) between the horizon and the aiming (impact) point. For example, if the runway threshold is used as the aiming point, it should be a constant distance (nominally 3°) below the horizon from descent initiation to flareout. The aircraft is overshooting the threshold if the distance from the threshold to the horizon gets larger, and undershooting if this distance gets smaller. The intended VSD will provide the pilot this same capability, and will be more reliable than visual by always presenting a consistent horizon reference independent of haze, smog and fog. Some of the most important cues used during a contact landing are those resulting from relative terrain movement. The instantaneous aiming (impact) point is motionless, with other terrain points moving radially away at a rate that increases with distance from the aiming point. By sensing the direction of movement of several points, the pilot can triangulate to estimate his instantaneous aiming point. The intended terrain display will also provide these cues to the pilot. Because of their importance, the motion cues are analyzed in detail in Section 5.

It is a long term objective to achieve "better than visual" landings[37] by combining an enhanced radar perspective display with velocity vector intercept, etc., with additional cockpit information (flight director, etc.), and integrated flight controls.

Two radar design parameters are the inclusive scan angles (field of view) and the maximum range of the radar. The scan angle, both in elevation/depression and azimuth, must be defined in order to place practical limitations on the radar system and still provide a display of a portion of the earth that is large enough to facilitate a safe landing. Review of the literature

pertaining to landings made with a restricted field of view and with television or periscope displays[8, 15, 20, 21] suggests that a 25-degree by 25-degree field of view is adequate. However, a nominal 30-degree-square field of view will be used for convenient display analysis. This 30-degree field of view is depicted in Figure 1, showing a 15-degree scan both left and right of center and a 15-degree scan both up and down from center.

The required maximum range of the radar can best be determined by flight test. However, radar flight information has not previously been presented in this perspective form. Therefore, analytical studies and hypotheses will be used to specify the radar range. This has been accomplished through motion cue analysis and the assumption that the motion cues available during a landing are the most important cues. This analysis, presented in detail in Section 5, has resulted in the conclusion that the maximum desired range should be initially set at 10,000 feet in order to maximize the motion cues displayed.

These radar range and scan angle limitations are intended as values for initial system operation which must be evaluated in flight. If either proves to be too restrictive to ensure a safe landing, modifications must be made.

4. RADAR TECHNIQUES

4.1 P^3I SYSTEM CONCEPT

The P^3I (Processed Plan Position Indicator) is a radar system/display technique which results in the presentation of PPI-derived radar information in true linear perspective on a vertical (azimuth angle, $\emptyset$, vs. depression angle, θ) display without the use of cooperative ground equipment. (Figures 7, 58 and 59 demonstrate the P^3I appearance.) This section presents the basic logic which was followed in constructing the first P^3I radar system/display. Several of the constants presented were derived using the characteristics of the Fairchild 765 MH display (in particular, deflection voltage and display size) used with the first system. These values are included here to provide continuity in the logic. However, it must be clear that they may be changed to be compatible with a different display, once established.

The P^3I system/display is an extension of the same basic radar technology that produces a conventional PPI (Plan Position Indicator). The PPI is a polar plot of range and azimuth angle with the aircraft at the origin. The signal amplitude of the radar back-scattering terrain is plotted (as intensity modulation of the CRT) linearly with time from transmission, which is coincident with range. The basic PPI has no ability to present elevation/depression angle information.

The P^3I, a type of C-scope, is a linear plot of azimuth angle ($\emptyset$) versus depression angle (θ). Azimuth angle corresponds to the position of the radar fan beam. Processing the PPI-derived data from range to depression angle requires that the signal amplitude from the radar back-scattering terrain be plotted nonlinearly with time. The radar returns are made coincident with depression angle by taking into account attitude and altitude and assuming that the earth is relatively flat and horizontal in the vicinity of the airport. (If this is a poor assumption, it can be modified through an adjustment process called registration and discussed in Section 4.4.) Thus, in contrast

to the PPI, which presents the time delay of returns as slant range, the P^3I system converts the time delay to depression angle (θ), consistent with aircraft attitude and altitude.

Assuming a "flat earth," we have the relationship

$$\theta = \text{arc sin} \left(\frac{A}{R} \right)$$

where:

A = aircraft altitude above ground level (AGL), in feet

θ = depression angle from the earth-referenced horizontal to some point on the ground, in degrees

R = slant range from the aircraft to the above point, in feet.

Using the relationship $R = 500\ t$ as above, we have:

$$\theta = \text{arc sin} \left(\frac{A}{500\ t} \right)$$

where:

t = delay time of ground return at slant range R, in microseconds.

The geometry for this equation and the resultant θ vs. t curves for several aircraft altitudes are shown in Figure 2. Using the simplifying assumption that for small angles the sine of an angle is approximately equal to the angle expressed in radians results in:

$$\theta = 57.3 \left(\frac{A}{500\ t} \right) = \frac{0.115}{t} (A)$$

If we assume a display 18° (θ) by 30° (ϕ) that is 6 cm by 10 cm (usable) and requires a nominal deflection voltage of 0.1 volt/cm (compatible with the Fairchild 765 MH CRT display which was used for the first P^3I system), we obtain: 1 degree = 0.033^7 volt and $V_\theta = -0.033\ \theta$ (depression angle is positive), where V_θ is the deflection voltage required to move a distance corresponding to θ degrees and which defines the vertical sweep waveform. Therefore,

$$V_\theta = \frac{-(.033)(.115)}{t} A = \frac{-.00378}{t} A$$

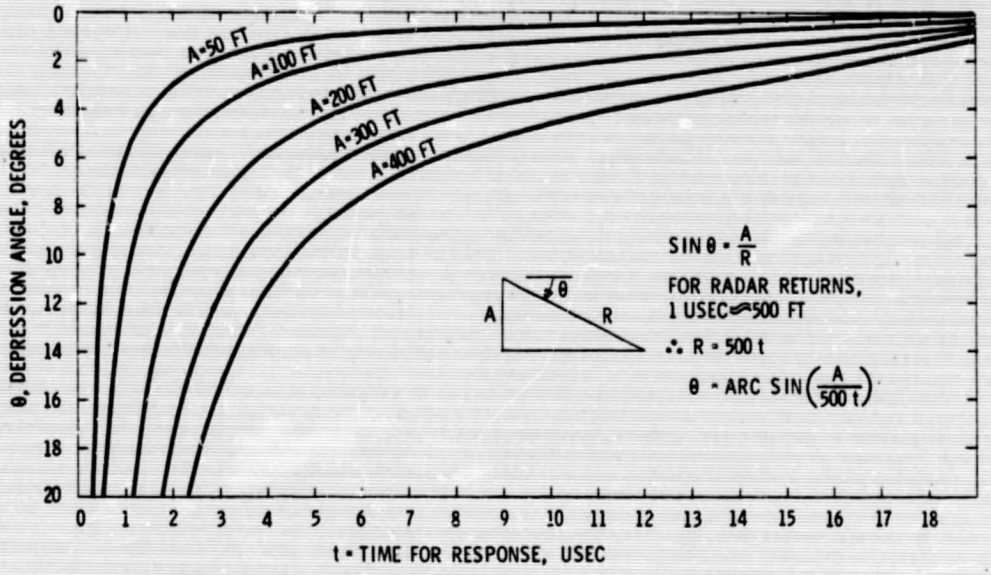

t USEC	θ (DEGREES)	.5	1	2	3	4	5	6	7	8	9	10	11	12	13	14	15	16	17	18
	FOR A = 50 FT	11.5	5.7	2.9	1.9	1.4	1.2	.96	.82	.72	.64	.58	.53	.48	.45	.41	.39	.36	.34	.33
	FOR A=100 FT	22.9	11.5	5.7	3.8	2.8	2.3	1.9	1.6	1.4	1.3	1.2	1.1	.96	.89	.83	.77	.73	.68	.65
	FOR A=200 FT		22.9	11.5	7.6	5.7	4.6	3.8	3.3	2.9	2.6	2.3	2.1	1.9	1.8	1.7	1.5	1.5	1.4	1.3
	FOR A=300 FT			17.2	11.5	8.6	6.9	5.8	4.9	4.3	3.8	3.5	3.2	2.9	2.7	2.5	2.3	2.2	2.1	2.0
	FOR A=400 FT			22.9	15.3	11.5	9.2	7.7	6.6	5.8	5.1	4.6	4.2	3.8	3.6	3.3	3.1	2.9	2.7	2.6

Figure 2. θ vs t Curves for Various Altitudes

Electronic implementation of this equation is then seen to be an inverse-time (hyperbolic) function generator amplified linearly by altitude. The altitude range of interest is from a maximum of 1000 ft to a minimum (wheels on ground) of 15 ft, resulting in an amplification range of 66.67. Applying this nonlinear vertical sweep to the vertical amplifier of the display will, neglecting roll and pitch, place the radar returns expressed as Z-axis (intensity) modulations in their proper depression angle (θ) location for each azimuth angle (ϕ) searched. The general system diagram is shown in Figure 3.

An additional input to the vertical amplifier is the attitude signal, which adjusts the amount and location of the ground picture shown on the vertical display to correspond to that which would be seen when looking out the windscreen under the existing pitch and roll conditions. This is accomplished by changing, from that visible in straight and level flight, the amount of display vertical sweep visible on the CRT. A change of pitch results in the corresponding addition (or subtraction) of a bias which is constant for all azimuth angles. A pitch-down attitude results in the addition of a positive bias, causing the ground to move up on the display; a pitch-up attitude results in the addition of a negative bias, causing the ground to move down on the display, consistent with what would be viewed out the windscreen. For the display considered above, this is represented by:

$$V_P = 0.033^{7}\,\theta_P$$

where

V_P = bias voltage due to pitch of aircraft, volts

θ_P = pitch angle of aircraft in degrees; down is positive, up is negative.

Both pitch and altitude affect the location of the display content. An error in pitch causes an error which is continuous on the display because it is simply a bias level, V_P. However, an error in altitude results in a vertically nonlinear error in the display presentation because altitude is represented as a gain level.

A roll attitude of the aircraft results in the corresponding addition (or subtraction) of bias which is linearly dependent on the azimuth position in question, expressed by:

$$V_R = .033\,\phi \tan \mathcal{B}$$

where:

V_R = bias voltage at some azimuth position ϕ due to roll of aircraft, volts

ϕ = azimuth position in degrees; to right of center is positive and to left of center is negative

$\mathcal{B}$ = roll angle of aircraft in degrees; to right is positive and to left is negative

The addition of V_R to the sweep function results in the ground moving up on the side of the roll and down on the opposite side, with the change of vertical sweep length increasing linearly for increasing angular distance from center. The vertical display thus shows the horizon moving in the direction opposite to the roll, and at an angle (from its "normal" position) equal to the roll angle, which is what would be seen when looking out the windscreen.

By summing V_R and V_P, a voltage is obtained which represents the sweep changes necessary to present a vertical display compatible with the roll and pitch conditions of the aircraft. It is necessary, due to its dependence on ϕ, that this attitude voltage ($V_R + V_P$) be synchronized to the horizontal sweep, which corresponds exactly to the position of the antenna, as shown in Figure 3. Thus, with proper synchronization between the horizontal and vertical sweeps and the antenna, the Z-axis modulations due to the reception of radar returns are placed in their proper vertical display position, i.e., in their proper (θ, ϕ) location.

4.2 P^3I OPTICAL DERIVATION

The appearance of a radar-derived vertical display is difficult to visualize; for this reason, it was decided to prepare P^3I demonstration material. An optical processing technique was developed to obtain both still and movie film of the P^3I display appearance. Although primarily intended for demonstration, the P^3I optical derivation method also provides an alternative to electronic derivation.

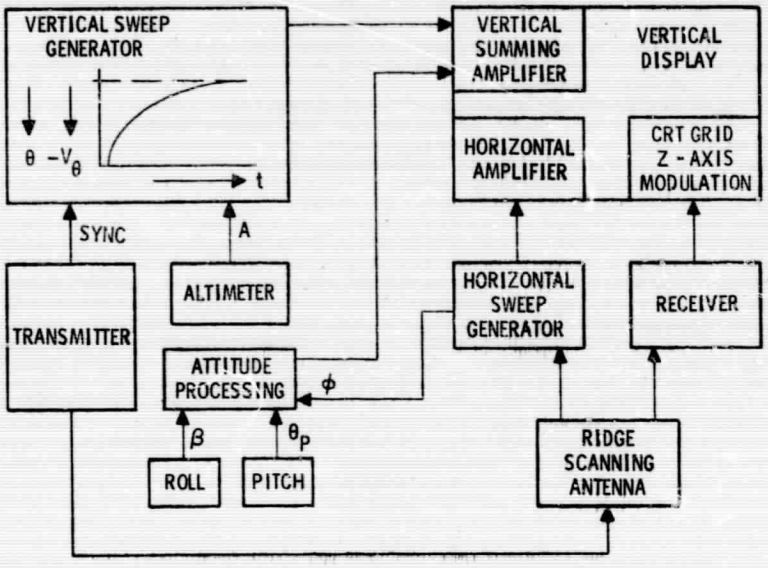

Figure 3. P^{3}I General System Diagram

The basic principle used in the P^3I optical derivation is that of the "pinhole projection" phenomena depicted in Figure 4. The perspective view which a human observer obtains of the world is due to the passage of light through the pupil of his eye and its projection on the retina.[25] The pupil is a small opening in the iris, so that light passing through it is in rays, with each point on the field of view (ideally) representing one ray passing through the pupil at an angle which is unique with respect to all other rays. The projection of these rays onto the retina produces a true perspective view of the world. This process is demonstrable by placing a pinhole in a plane vertical to a horizontal "ground" plane. The passage of light rays from the ground plane through the pinhole is similar to the passage of light rays through the pupil. If these light rays are then projected on a screen parallel to the plane of the pinhole, a true perspective view of the ground plane is attained which is very similar to what a human observer would see if located at the pinhole; i.e., a vertical perspective display is achieved. (The "pinhole projection" is inverted and the eye is difficult to focus, but these effects can be corrected.)

By moving the pinhole up and down in a plane at a right angle to the ground plane, the altitude changes of perspective are observed on the projection plane. Rotation of the projection plane about an axis perpendicular to it at its center results in perspective changes on the projection plane identical to those of a roll change of an aircraft. A change in the angle between the ground plane and the projection plane results in perspective changes identical to those of a pitch change of an aircraft. Thus, the combination of these movements can lead to perspective changes identical to those which an observer in an aircraft views during flight.

The appearance of the P^3I display can be demonstrated by optical processing of PPI-derived film in accordance with the pinhole projection concept. This processing was accomplished in the following manner. Using Lockheed Electronics Company's F-28 Enstrom Helicopter equipped with the Internal Research and Development Crossed-Beam Radar System[26] and the Helicopter Rotor Blade Antenna,[26, 27, 28] film records of an actual PPI radar display were obtained, along with synchronized cockpit views of the terrain from which the PPI data were derived. This PPI film was projected, one frame at

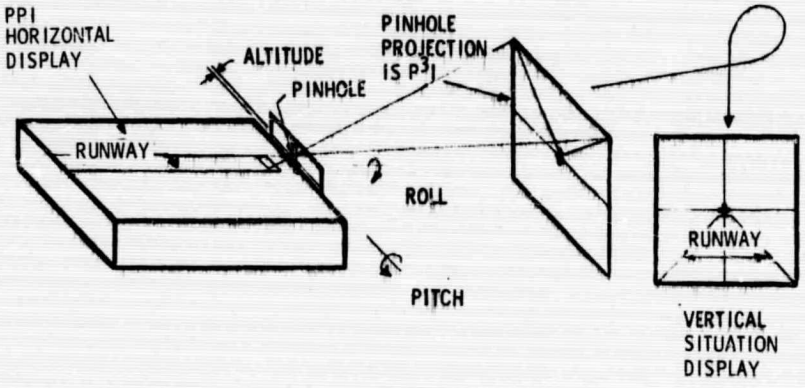

Figure 4. Pinhole Projection Technique

a time, on a white screen. The CRT grid was visible on the projection, with one grid space representing 450 or 900 ft, enabling the proper scaling of the photographic technique. A camera with the aperture stopped all the way down to approximate a "pinhole" was placed against the screen and looking up parallel to the screen. The camera aperture was centered at the altitude circle, which represents aircraft position, and placed a distance from the screen equal to aircraft altitude when using the projection scaling. The physical arrangement for this technique is shown in Figure 5.

Two cameras were used with this technique. A Polaroid was used initially to verify the theory and establish the procedures to be used. It was learned that exposure times of from 30 to 90 seconds were required to satisfactorily expose the film because of the small aperture used. (Larger apertures cause poor depth of focus.) It was also shown that the P^3I perspective changes due to pitch, roll or altitude changes, accomplished by movement of the camera with respect to the projection screen, were distinguishable. The second camera used was a Giannini Multidata Camera, Model III-B, which has the ability to expose one frame of 16mm movie film at a time, required by the long exposure times used. The camera was set at f/16 and a 1.7 ft focus, using 60 or 75 seconds exposure. Film was Ansco ASA 200 and Kodak Ektachrome.

A rather lengthy procedure was followed, with each frame of the PPI-derived film being processed to one frame of P^3I movie. Two series of P^3I films were made. The first film was prepared on May 15, 1967, using PPI films of the Raritan River area, near Middlesex, New Jersey. This film was intended to demonstrate the perspective and motion cues available on the P^3I display, but did not show the perspective changes that would result from altitude or attitude changes. A copy of this film was delivered to NASA-Ames Research Center in May, 1967.

To demonstrate the P^3I appearance during a landing approach, PPI films were obtained of approaches to Mercer Country Airport, Trenton, New Jersey, which was chosen for filming because it is fairly large and has relatively easy access. All approaches were on Runway 29, which is 150 x 3000 ft. The terrain preceding and surrounding the runways is primarily grassy fields, and all runways are either blacktop or concrete.

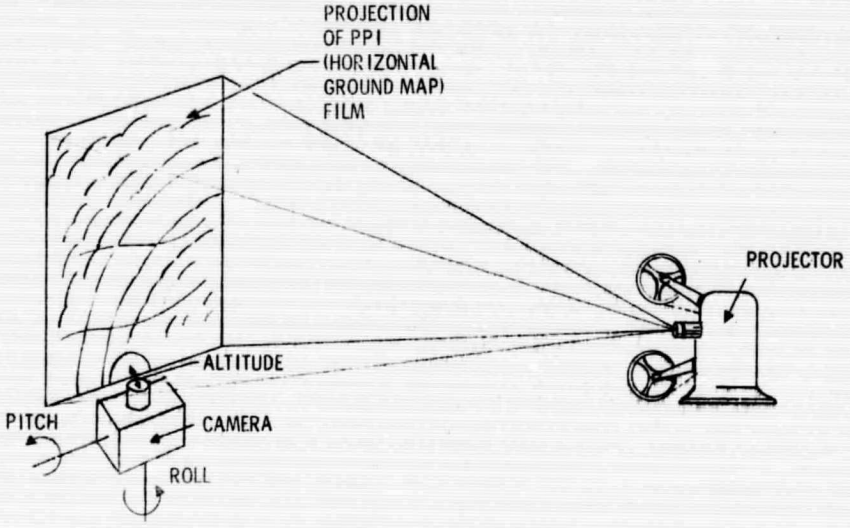

Figure 5. P^3I Optical Derivation Method

The films obtained show the PPI appearance during various types of landing approaches, both correct and incorrect: 3° and 6° approaches, crabbed approaches, and improperly aligned approaches. In addition, film was obtained of an autorotation approach with an approach angle of approximately 18°. The intent of this film is to demonstrate that the basic PPI changes very little with large and rapid altitude or attitude changes, and, therefore, has limited usage as a landing instrument. (However, the PPI with cross-beam can be used to perhaps CAT II with a fixed-wing, and has been demonstrated in an LEC helicopter to CAT II.[36])

One of the straight 6° approaches was selected to provide the PPI film, and this was processed into two P^3I film strips. The first film strip shows the P^3I appearance during a 6° approach from an altitude of 480 feet down to 150 feet, followed by a 4° pitch-up, a climb to 200 feet, and a leveling off. The second film is a fly-by at an altitude of 285 feet. This demonstrates the P^3I appearance during level flight, a left roll to 10° and return to level, a right roll to 10° and return to level, a pitch up to 4° and return to level, and a pitch down to 4° and return to level. Copies of these films were obtained by NASA-Ames during a trip by LEC personnel on September 7 and 8, 1967.

The nature of the films obtained is demonstrated by Figures 6 and 7. Figure 6 shows the PPI ground map of the entire runway/taxiway complex, with the approach runway as the dark vertical bar near the center of the figure. Other runways and taxiways appear as dark bars. The bright area in the right central portion of the picture is the hangar area. Figure 7 presents a comparison between visual perspective and P^3I perspective. The upper photograph shows the view from the helicopter cockpit during a landing approach. The runway on which the approach was made is seen in the upper portion of the photo to the left of the windscreen divider. Another runway crosses from the upper left to the lower right of the windscreen, in addition to a taxiway from center to upper right. Runways are 150 ft wide and taxiways are 75 ft wide. The helicopter is on a 6° glideslope at approximately a 150 ft altitude. The P^3I photograph corresponding to the cockpit view is shown in the lower half. Because the cockpit camera has a wide field of view (when compared to the P^3I field of view), the P^3I photograph is an enlargement of the central area of the cockpit view. The dark areas of the

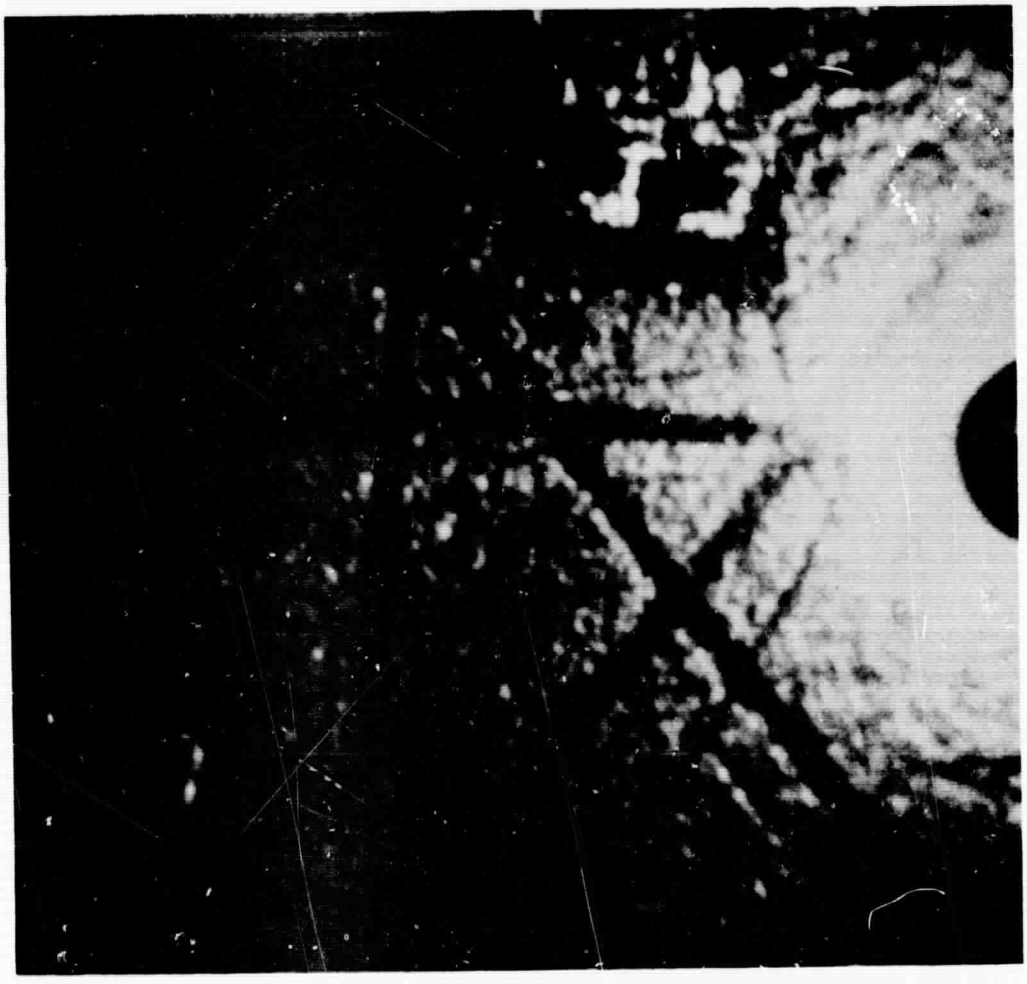

Figure 6. PPI of Mercer County Airport

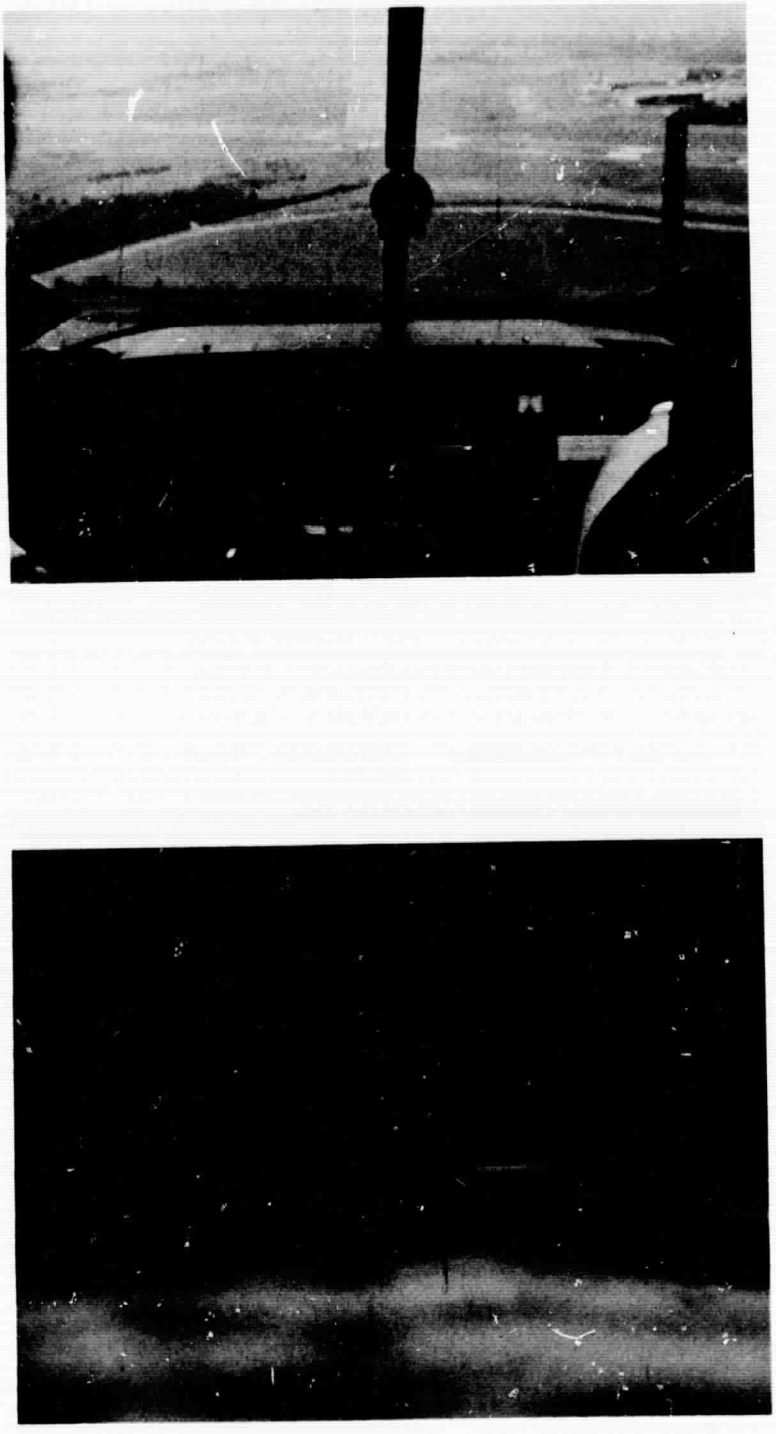

Figure 7. Comparison of Visual and Optically Derived P^3I Perspective

P^3I photograph represent the runways and taxiways. The vertical trapezoid in the center is the runway being approached, the dark band running from center left to lower right is the crossing runway, and the thin dark band running upward and across from the left is the crossing taxiway. The light areas represent the grass and soil surrounding the runways. Agreement between P^3I and visual perspective is noticeably good. The motion cues provided by the movie films demonstrate even more clearly the ability to "see" the runway in dynamic perspective. Providing the pilot with such a display gives him a capability not previously available - the ability to "see" the runway and the terrain surrounding it in a real-time perspective presentation while under IFR conditions and without the need for cooperative ground equipment.

4.3 P^3I WITH CBRS

The P^3I (Processed Plan Position Indicator) and CBRS (Cross Beam Raster Scan) radar techniques are two different but complementary ways of deriving and displaying radar data. The P^3I uses a PPI derivation which, assuming a flat-earth, is converted to a perspective display. The CBRS sequentially views the field of interest in nominally 1-degree by 1-degree squares, which results in a perspective display of the area scanned without relying on attitude or altitude sensors.[29, 30] Thus, the P^3I presents a derived perspective while the CBRS presents actual perspective. The two types of perspective will agree, provided the P^3I assumptions are met, namely that the earth is relatively flat and horizontal and that the altitude, roll, and pitch inputs are correct. If these assumptions are not correct, comparing the P^3I against the CBRS can provide an adjustment or "registration" of the P^3I display. This is an important benefit of the combined P^3I and CBRS sytem.

The two techniques, the P^3I and the CBRS, will be combined in a single system/display concept which obtains the resolution benefits of each. For the radar currently considered, the pulsewidth is such that a point target is displayed as having a resolution of 50 ft (0.1 μsec pulsewidth). The CBRS would present such a target as a 1 degree square (no matter what the pulsewidth). The size (in ground plane feet) represented by this square is dependent on the distance of the target from the aircraft. At long distances,

this is much larger than the 50 ft range resolution of the P^3I, and at small distances this is less than the 50 ft range resolution of the P^3I, as depicted in Figure 8. By combining the P^3I and CBRS techniques, it is possible to maximize the accuracy of the display presentation, with the 50 ft range resolution being the worst displayed. The display resulting from the combination of these two methods is depicted in Figure 9.

The transition from P^3I to CBRS is dependent on distance from the aircraft. Assuming a flat earth, this can be defined as occuring at a particular angle (θ') down from the horizontal for any given altitude (A). This transition angle (θ') is the angle at which both the P^3I and the CBRS have the same 50-ft range resolution for a particular altitude. For angles down from the horizontal (θ) less than θ', the P^3I will have the better resolution; for θ greater than θ', the CBRS will have the better resolution. The ideal transition angle θ' as a function of aircraft altitude is determined using Figure 10. The results for BW = 1° and ΔR = 50 ft are plotted in Figure 11. For example, if A = 100 ft, then $\frac{\Delta R}{A} = \frac{50}{100} = 0.5$. Using Figure 10 for BW = 1° and $\frac{\Delta R}{A} = 0.5$ results in $\theta' = 10.5$ degrees. Thus, the curve of Figure 11 passes through the point A = 100 ft, $\theta' = 10.5$ degrees.

The ideal range "resolution improvement" (R.I.) obtained by this combination of P^3I and CBRS techniques is defined in several manners:
For:

$$0° < \theta < \theta' \ (P^3I) \tag{1}$$

$$\text{R.I.} = \frac{\text{Distance represented by 1 degree beam (ft)}}{50 \text{ (ft)}}$$

This represents the advantage of using the P^3I instead of the CBRS for this angular range.

For:

$$\theta = \theta' \text{ (transition)}, \tag{2}$$

$$\text{R.I.} = 1,$$

because the range resolution of both techniques is the same (50 ft) at the transition angle, θ'

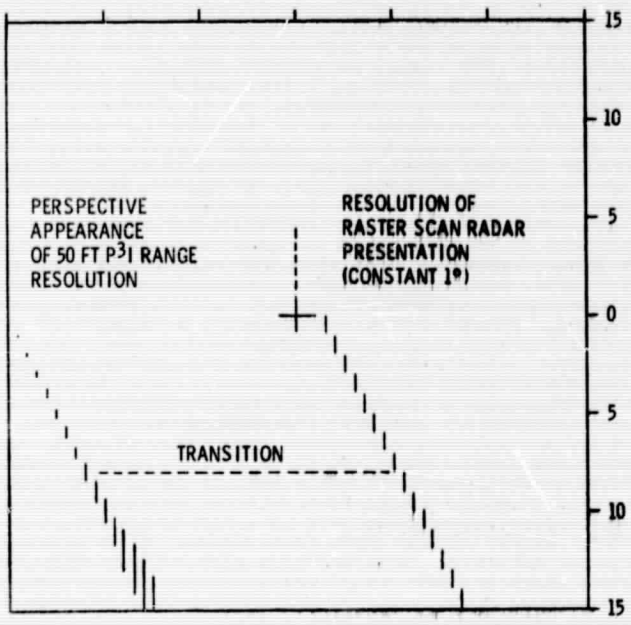

Figure 8. Graphical Representation of Resolution Improvement Concept.

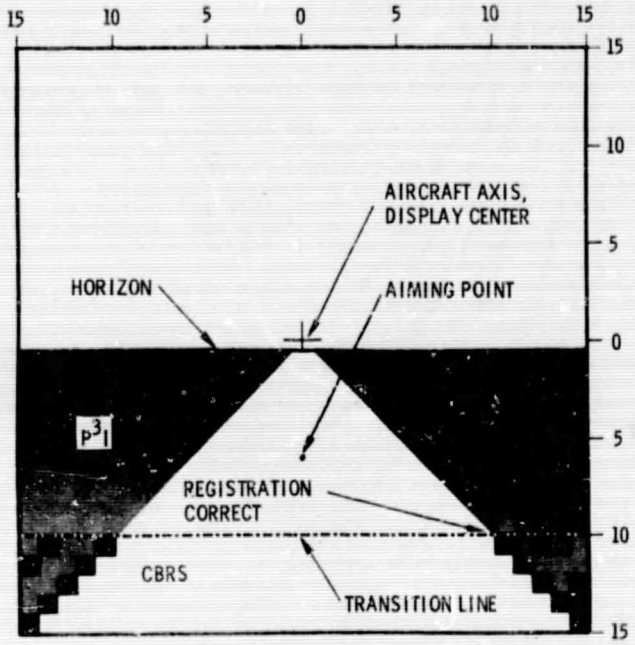

RUNWAY = 10,000 FT X 200 FT, 1000 FT
THRESHOLD TO AIMING POINT

RADAR RANGE ≈ 10,000 FT

AIRCRAFT AT 100 FT ALTITUDE
6° GLIDE SLOPE
ZERO PITCH AND ROLL
HEADING ALONG RUNWAY CENTERLINE

Figure 9. Display with Combination of P^3I and CBRS Presentation

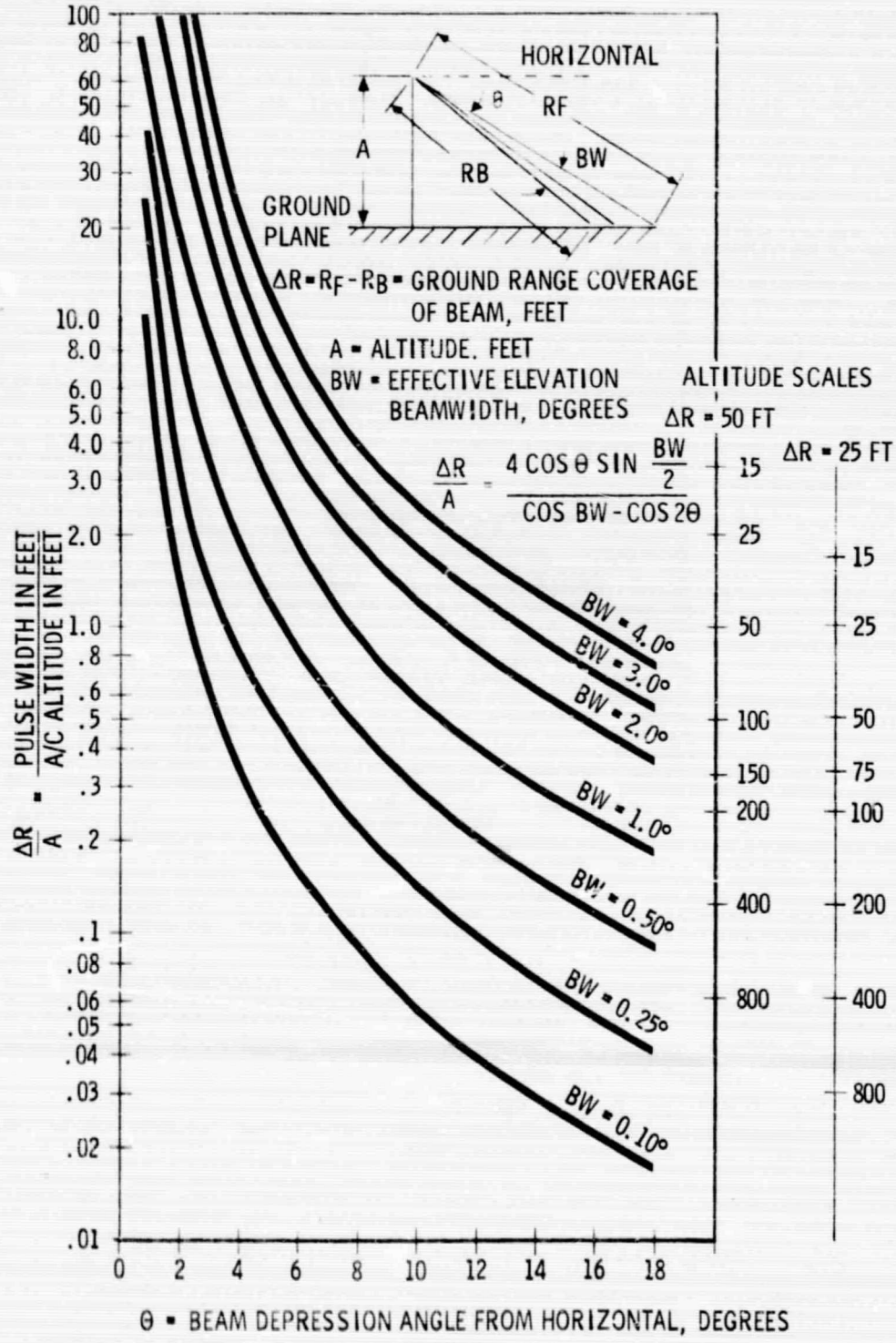

Figure 10. Derivation of Ideal Transition Angle

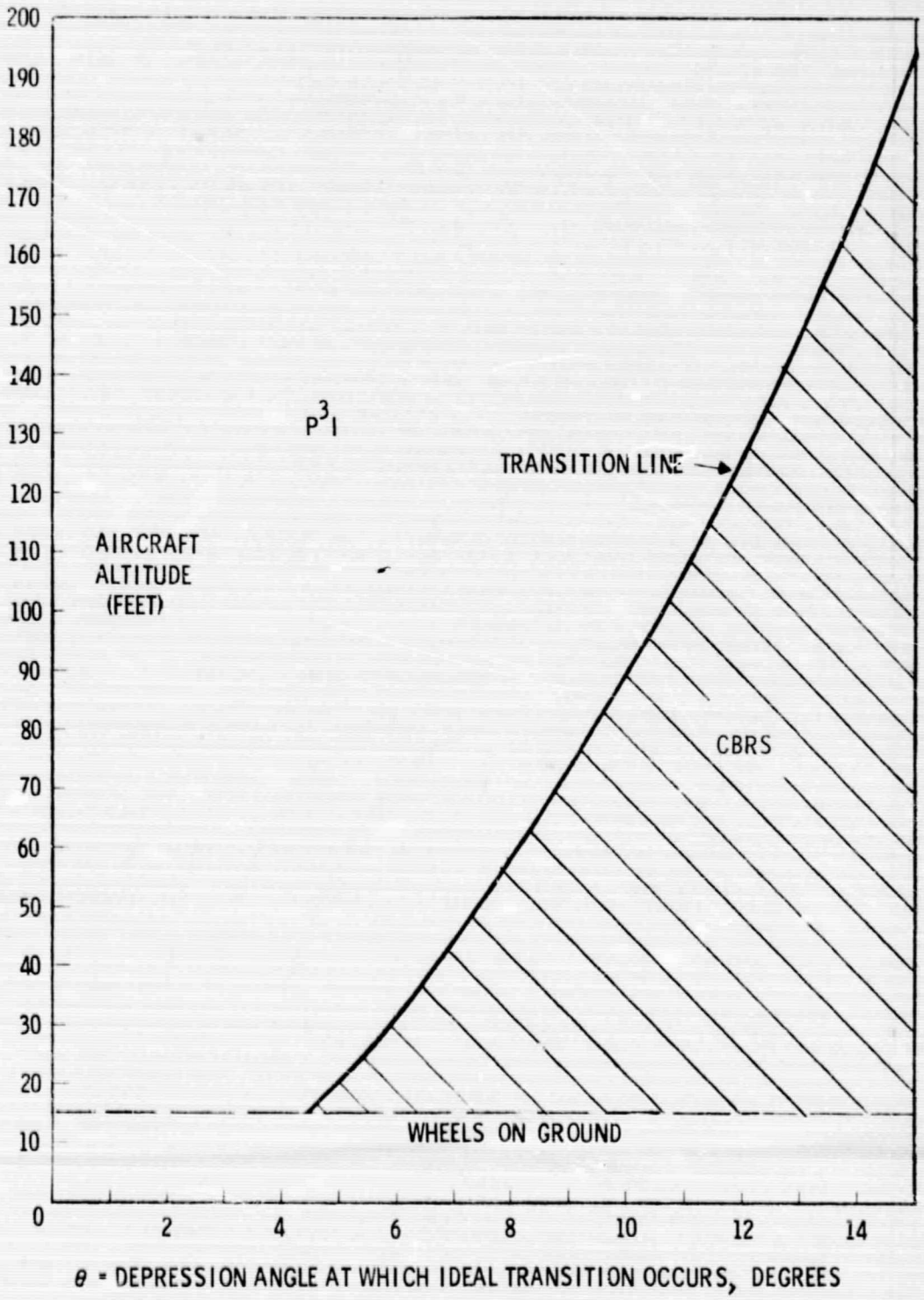

Figure 11. Ideal Transition Angle as a Function of Altitude

For:

$$\theta' < \theta < 90^\circ \text{ (CBRS)} \tag{3}$$

$$\text{R.I.} = \frac{50 \text{ (ft)}}{\text{Distance represented by 1 degree beam (ft)}}$$

This represents the advantage of using the CBRS rather than the P^3I in this angular range.

This ideal resolution improvement, due to its dependence on θ, is dependent on aircraft altitude; samples are graphed in Figure 12. The angle θ' as defined above is the angular depression from the earth-referenced horizontal. Since the pitch attitude (θ_P) of the aircraft coming down the glide slope is fairly constant, a good approximation of the ideal θ' can be obtained by relating some transition angle (θ_0) as an angle from the aircraft longitudinal axis. The transition would then occur at an angle $\theta_0 = \theta' - \theta_P$ from the aircraft axis (θ_P is positive for pitch down), and would appear on the display at θ_0. θ_P can be set in as a constant for the desired glide slope, resulting in θ_0 being dependent only on altitude. Since the CBRS samples in 1-degree sectors, θ_0 should change at 1-degree increments as a function of altitude. If the altitude increments are made constant, the location of the transition line on the display becomes an index of altitude, and its movement becomes an index of altitude rate. By accurately coupling a radar altimeter to trigger the transition angle changes, a scale can be provided on the display for the direct readout of altitude, permitting the pilot to save much of the time that would otherwise have to be spent in switching his vision between the VSD and the radar altitude indicator. The position of this transition line is not critical, and this usage of altitude as the defining variable for its location may provide a very valuable cue.

The requirement for azimuth resolution may be considerably different from that for elevation resolution, since it is believed that the required azimuth resolution for a particular aircraft position is linear, i.e., is the same at the extreme left, center, and extreme right of the display, for any particular depression angle. This is because the range to the intersection of that line of sight with a flat, horizontal earth-surface does not change. However, the required elevation resolution is nonlinear, i.e., greater resolution is required nearer the horizon than at larger depression angles (for a particular

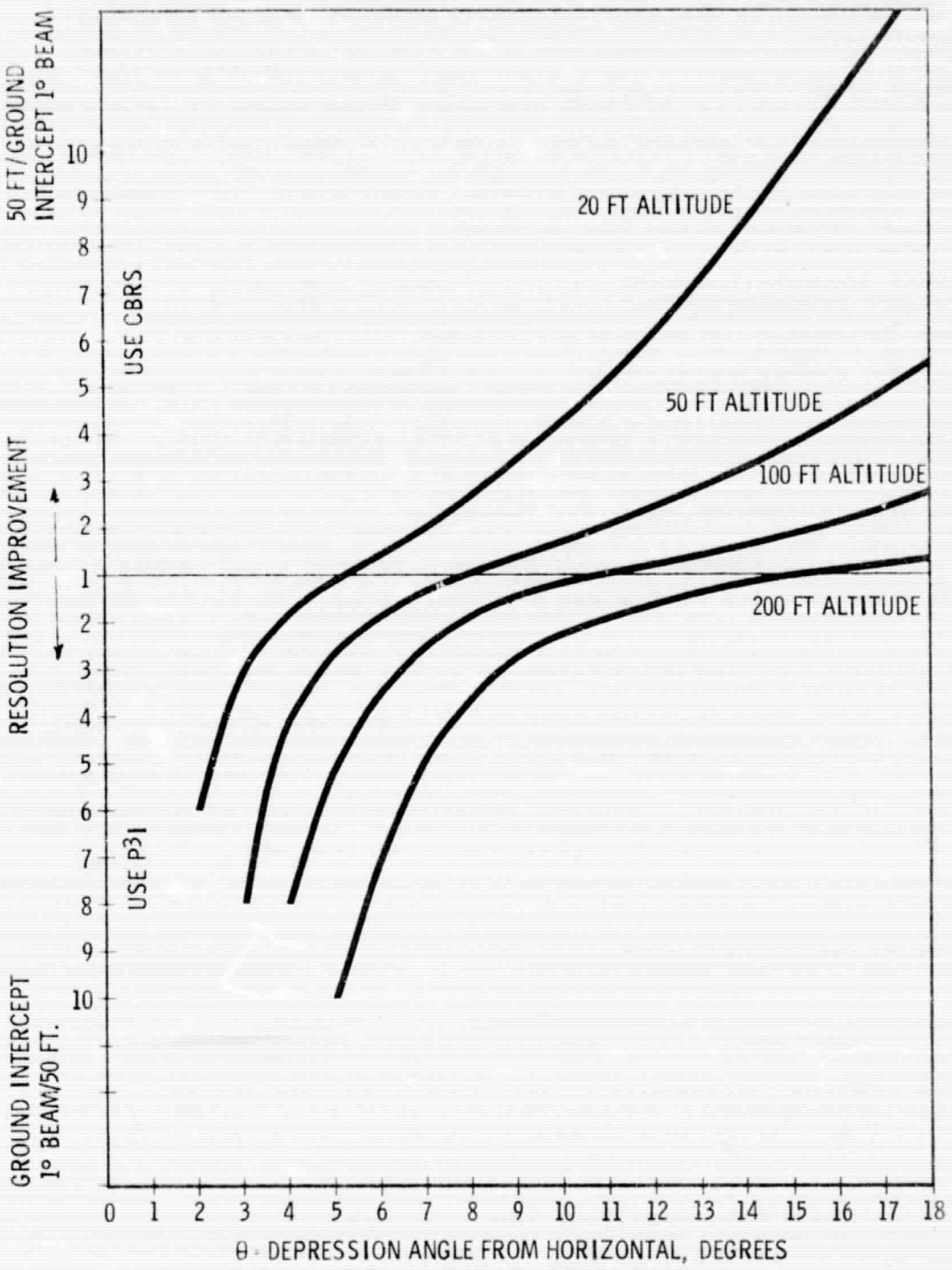

Figure 12. Ideal Resolution Improvement

azimuth angle) because the earth-range encompassed by an angular resolution element changes greatly. For example, at an altitude of 100 ft and a depression angle below the horizon of 3.5 degrees, an elevation resolution of 1 degree corresponds to a range resolution swath on the ground of about 475 ft while a 1 degree azimuth resolution corresponds to a swath on the ground of only 57 ft, a nearly 10:1 ratio of resolution in the ground plane. It is important to consider resolution in the plane of the earth's surface because the air field facilities, such as runway, runway lights, buildings, etc., are laid out in the ground plane.

4.4 P^3I REGISTRATION USING CROSS-BEAM ANTENNA

The P^3I technique is based on two assumptions: the terrain over which the P^3I system will be used during a landing approach is relatively flat and horizontal, and the roll, pitch, and altitude inputs to the P^3I system are correct. Deviations from the P^3I assumptions might present a display which is not properly aligned with the real world. The result would be that the pilot views improper cues concerning his approach status.

The previous section has mentioned that the P^3I might be compared against the CBRS to result in adjustment or "registration" of the P^3I display. This section presents an interim registration technique that would use a single passive antenna instead of the CBRS. (Other registration techniques are being considered; an example is presented in Addendum II.)

LEC, under its IRAD Helicopter Radar Program, has developed a concept known as the "Cross-Beam Scan."[26, 36] The PPI antenna, using microwave energy, illuminates the terrain. The cross-beam antenna is a passive device which receives a 1° horizontal swath of the terrain illuminated by the PPI antenna. This antenna is placed at a known depression angle from the aircraft axis, so that the returns received by the cross-beam antenna can be placed in their proper depression angle location on the P^3I display, regardless of terrain characteristics. By combining the 1° horizontal beam information with the P^3I display, a display is generated containing exact (1° beam) information against which derived (P^3I) information can be compared and adjusted to obtain a suitable derivation. This is the process termed "registration," and the 1° horizontal beam has been termed the "registration beam."

The registration analysis is included below, beginning with a definition of terms which are depicted in Figure 13.

Definition of terms:

A_A = Actual Altitude, the projected altitude above the runway, obtained by triangulation of the registration beam with the terrain

A_{MR} = Measured Altitude, obtained by Radar altimetry

θ_R = The depression angle of the Registration beam from the horizon to the actual intersection of the registration beam with the actual ground plane

θ_O = The Observed registration beam angle as seen on the P^3I display, which is the depression angle from the horizon to the projected intersection of the registration beam with the assumed ground plane at the same range as the ground returns for θ_R

R = The Range to the intersection of the actual registration beam with the actual ground plane (as above, it is also the range to the intersection of the observed registration beam with the assumed ground plane)

i. Altitude Registration Using Registration Beam Position

For small values of θ,

$$\theta_R = \frac{KA_A}{R} \quad , \quad \theta_O = \frac{KA_{MR}}{R}$$

Therefore,

$$\frac{\theta_R}{\theta_O} = \frac{A_A}{A_{MR}}$$

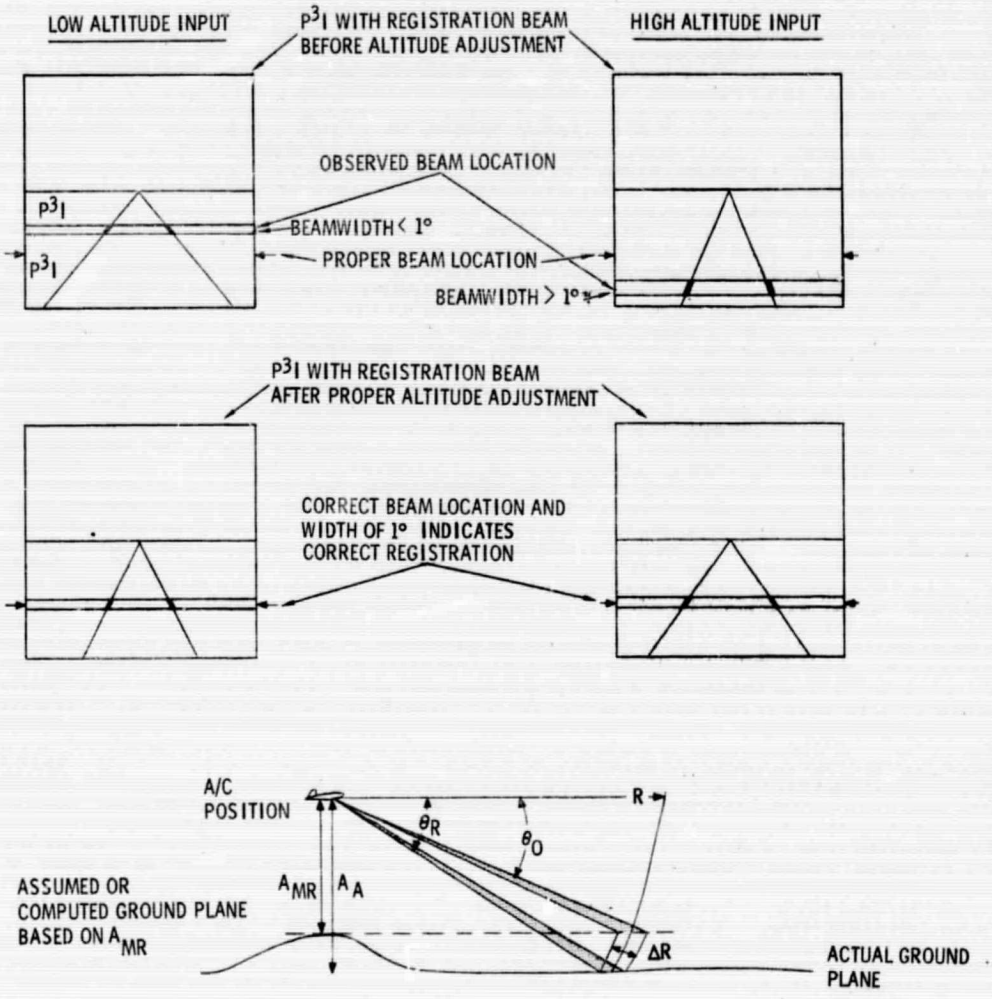

Figure 13. P^{3}I Altitude Registration

$$\theta_R = \frac{A_A}{A_{MR}} \theta_O$$

$$\theta_R - \theta_O = \frac{A_A}{A_{MR}} \theta_O - \theta_O = \theta_O \left(\frac{A_A}{A_{MR}} - 1 \right)$$

or,

$$\theta_O - \theta_R = \theta_R \left(\frac{A_{MR}}{A_A} - 1 \right)$$

for example:

(1) If A_{MR} = 500 ft, A_A = 600 ft, and θ_O = 10°, then

$$\theta_R - \theta_O = 10° \left(\frac{600}{500} - 1 \right) = 10° (.2) = 2°$$

(2) If A_{MR} = 500 ft, A_A = 600 ft, and θ_O = glide slope = 3°,

then $\theta_R - \theta_O = 3° (.2) = .6°$

This is a small error when we consider the aircraft is 12,000 ft from the aiming point for these conditions.

Figure 13 shows the usage of registration beam position for altitude registration.

From the above, the following conclusions may be drawn:

(1) Rather large errors in altitude must occur to effect a substantial error in the P^3I display.

(2) An adjustment in P^3I function generator gain corresponding to only a few degrees is expected.

(3) Altitude registration is independent of attitude, since the horizon is the reference.

(4) A check on the P^3I horizon can be achieved by manually scanning the registration beam to the horizon; as the

horizon is reached, the registration angle (θ_R) and the observed registration angle (θ_O) approach the same angle as a limit.

ii. Altitude Registration Using Registration Beam Width

BW_A = Actual registration beam width (nominally 1°)

BW_O = Registration beam width Observed on P^3I display

$$\frac{\Delta R}{A_A} = \frac{4 \cos \theta_R \sin \left(\frac{BW_A}{2} \right)}{\cos BW_A - \cos 2\theta_R}$$

$$\frac{\Delta R}{A_{MR}} = \frac{4 \cos \theta_O \sin \left(\frac{BW_O}{2} \right)}{\cos BW_O - \cos 2\theta_O}$$

(Refer to Figure 10)

$$\frac{A_{MR}}{A_A} = \left(\frac{\cos BW_O - \cos 2\theta_O}{\cos BW_A - \cos 2\theta_R} \right) \left(\frac{\cos \theta_R \sin \frac{BW_A}{2}}{\cos \theta_O \sin \frac{BW_O}{2}} \right)$$

Assuming the beam width is very small, and θ is small,

$$\frac{A_{MR}}{A_A} \approx \frac{BW_A (1 - \cos 2\theta_O)}{BW_O (1 - \cos 2\theta_R)}$$

Since $\sin^2 \theta = 1/2 (1 - \cos 2\theta)$ and θ is small,

$$\frac{A_{MR}}{A_A} \approx \left(\frac{BW_A}{BW_O} \right) \left(\frac{\theta^2_O}{\theta^2_R} \right)$$

as previously shown,

$$\frac{\theta_R}{\theta_O} = \frac{A_A}{A_{MR}}$$

therefore,

$$\frac{BW_A}{BW_O} \approx \left(\frac{A_{MR}}{A_A}\right)\left(\frac{\theta_R}{\theta_O}\right)^2 = \left(\frac{A_{MR}}{A_A}\right)\left(\frac{A_A}{A_{MR}}\right)^2$$

and

$$\frac{BW_A}{BW_O} \approx \frac{A_A}{A_{MR}} = \frac{\theta_R}{\theta_O}$$

for example:

If $A_{MR} = 500$ ft, $A_A = 600$ ft, $\theta_O = 10°$ and $\theta_R = 12°$
(from previous example 1.)

$$\frac{BW_A}{BW_O} = \frac{600}{500} = 1.2, \text{ or } \frac{BW_A}{BW_O} = \frac{12}{10} = 1.2$$

for

$$BW_A = 1°, \; BW_O = 5/6°$$

It is noticed that if $A_{MR} < A_A$ then $BW_O < BW_A$, and if $A_{MR} > A_A$ then $BW_O > BW_A$. This is shown in Figure 13, where a $BW_A = 1°$ is depicted.

Thus, the observed registration beam width can be compared to the actual beam width to obtain a check on the accuracy of altitude inputs to the P^3I system. Again, fairly large altitude errors are required to produce any noticeable change in the registration beam width as observed on the P^3I display.

iii. Attitude Registration

A pitch error is displayed as an improper location of the registration beam. This would appear parallel to the bottom of the display and, because attitude does not affect observed beam width, it would be discriminated from an altitude error by maintaining a constant width. Since pitch is a bias input to the P^3I system, a pitch error is corrected by simply adjusting this bias.

A roll error is displayed as a registration beam that is not parallel to the bottom of the display, with the angular difference from parallel equalling the roll error. This is depicted in Figure 14. Roll error is corrected by adjusting the roll input to the P^3I system until the registration beam is parallel to the display bottom.

Based on the different cues available for detecting the different types of errors, it is recommended that the order of adjustment be as follows:

(1) Correct roll errors (roll input adjustment)

(2) Correct pitch errors (pitch bias adjustment)

(3) Correct altitude errors (gain adjustment in P^3I sweep function generator)

This is initially envisioned as an adjustment process which can be performed by a flight engineer or technician. However, the basic concept is such that automatic registration techniques can be implemented, and should be considered during a follow-up research phase.

The P^3I display cross-beam registration techniques are capable of correcting for errors in altitude and attitude. Given this capability, it is possible to account for many of the orientation problems which can occur during landing. This includes those problems which can result while approaching runways which are inclined or declined from the horizontal. The result is a P^3I display which maintains a one-to-one relation with the visual landing situation and can provide the pilot accurate information on his approach status when visual contact is unavailable. Thus, the concept of using a 1° horizontal beam for registration of the P^3I system is recommended as a step toward the achievement of "better than visual" landings with an aircraft-contained radar landing system.

4.5 RADAR RANGE AS A FUNCTION OF SIGNAL TO NOISE RATIO

The performance capability of the radar utilized in the P^3I system is readily established from the range equation. This is easily identified for an optimum (coherent detector) and constant (non-fluctuating) reflection coefficient.

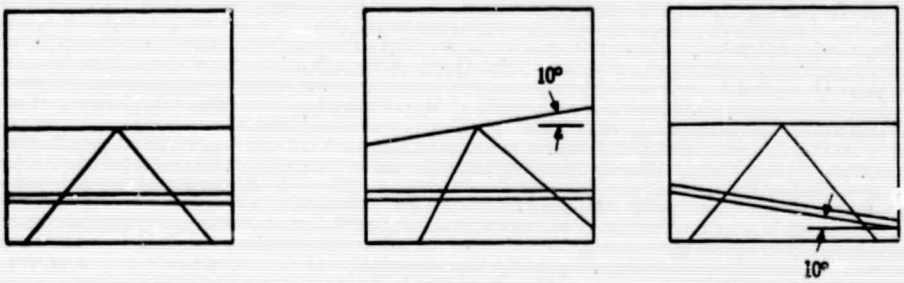

ROLL = 0°
ROLL REGISTRATION CORRECT

ROLL = 10° RIGHT
ROLL REGISTRATION CORRECT

ROLL = 10° RIGHT
ROLL REGISTRATION
REQUIRES 10° RIGHT
ROLL CORRECTION

Figure 14. P^3I Roll Registration

In this case, the output signal-to-noise ratio is given by:

$$\eta_0 = \frac{P_r}{N_r} = \frac{E}{N_0} \tag{1}$$

where: η_0 = output signal-to-noise ratio

E = received signal energy (joules)

N_0 = noise power density (watts/cps)

P_r = received signal power

N_r = input receiver noise

For a pulsed carrier radar signal, equation (1) becomes:

$$\frac{E}{N_0} = \frac{P_r \tau N}{FKT\ L_a} \tag{2}$$

where:

τ = pulse width

N = number of pulses integrated

FKT = N_0 = noise power density

L_a = system losses

Finally, combining equation (2) with the basic radar range equation results in:

$$\eta_0 = \frac{P_t\ \tau \sigma A_r\ G_t\ N}{(4\pi)^2\ R^4\ FKT\ L_a} \tag{3}$$

where:

P_t = peak transmitter power

σ = radar reflective coefficient

A_r = effective area of receiving antenna

G_t = gain of transmitting antenna

R = range

Equation (3) is readily utilized to predict a radar's performance since there is much literature available to identify the value of η_0 which corresponds to

any required probability of detection and false alarm rate. Physically, η_0 corresponds to the final output signal-to-noise power ratio and η_0/N represents the input carrier signal-to-noise power ratio. This is illustrated in the sketch below.

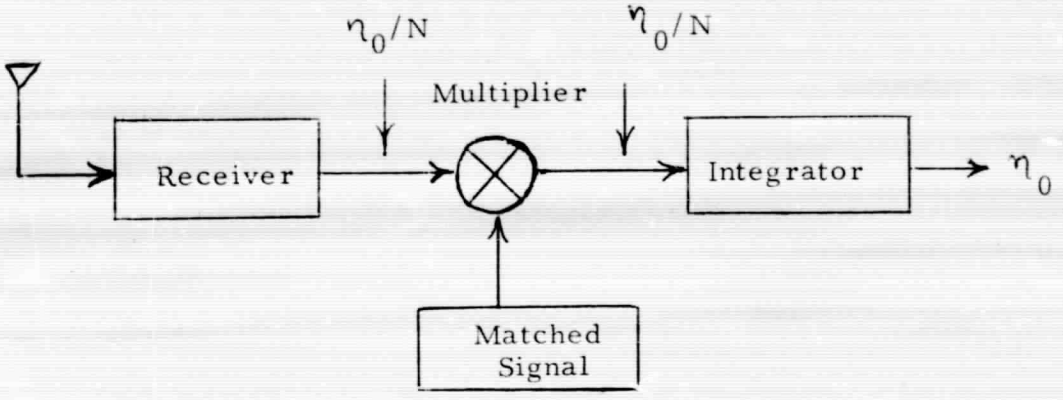

In essence, the input signal-to-noise power ratio is improved by the number of pulses integrated, and this condition is independent of the input signal-to-noise level. When the input signal is video detected prior to integration, the nonlinear operation of a square law or linear detector degrades the signal-to-noise level before it is improved by the process of integration. The amount of degradation is a function of the input signal-to-noise ratio and, therefore, cannot be treated as a constant loss factor in the range equation. The exact effect the detector law has on realizing a specified probability of detection and false alarm rate has been rigorously treated by J. I. Marcum.[33] The results of his work have been summarized by Merrill I. Skolnik as a set of curves which identifies the degradation introduced due to a linear or square law detector. In using these results, it is only necessary to replace N by NL_i in equation (3). L_i is essentially an efficiency factor and is a comparatively insensitive function of probability of detection and false alarm number η_f. The set of curves in Skolnik's text are for a system which ideally integrates (the system is matched at video) the video pulses following video detection. If the integration is accomplished using a display and operator, the integration process adds an additional amount of degradation.

It has been experimentally established by many in the radar field that the integration improvement factor NL_i varies as $\sqrt{N}$ when the system employs a viewed display. This is due to the losses introduced by the nonlinear processes associated with eyeball integration. A reasonably good estimate of radar performance for a system using an operator for visual detection is therefore, obtained by simply replacing N by $\sqrt{N}$ in equation (3).

The total number of pulses integrated will now be determined in order to obtain η_0 as a function of only σ and R. This corresponds to the number of times the same portion of the display is illuminated for the duration of time the eye can effectively integrate.

A reasonable quantity to use for this integration time, which we will identify as τ_η, is 1/30 second.

Expressed mathematically:

$$N = \text{hits/scan} \frac{\tau_\eta}{T_s} \tag{4}$$

where:

τ_η = total integration time

T_s = scan time

Now the hits/scan is given by:

$$\frac{T_s}{\text{Number of lines on display} \times t_r}$$

Where:

t_r = pulse repetition period

Hence:

$$N = \frac{\tau_\eta}{\text{Number of lines} \times t_r} \tag{5}$$

We can now incorporate the basic parameters of the radar which are tabulated in Appendix B into equations (5) and (3) to get $\eta_0 = f(\sigma, R)$.

This results in:

$$N = \frac{(1/30)\ 24\ (10^3)}{26}$$

$$N = 31$$

And:

$$N_O = 1.66\ (10^{15})\ \frac{\sigma}{R^4} \tag{6}$$

For our purposes, the output signal-to-noise ratio is best presented as a function of the depression angle for various altitudes of interest. Also, since the available empirical data on ground return for the frequency of interest is in terms of the back-scattering coefficient, σ must be solved for in terms of the incidence area.

$$\sigma = \gamma A_i \tag{7}$$

Where:

γ = back-scattering coefficient

A_i = incidence area

Referring to figure 15:

$$A_i = \ell S = \ell R \phi_b \tag{8}$$

Where:

ϕ_b = azimuth beamwidth

$$\ell = C\tau/2 \tan \theta \tag{9}$$

Combining equations (7), (8) and (9) gives σ in terms of the geometry and radar parameters.

$$\sigma = \gamma A_i = \gamma R \phi_b C\tau/2 \tan \theta \tag{10}$$

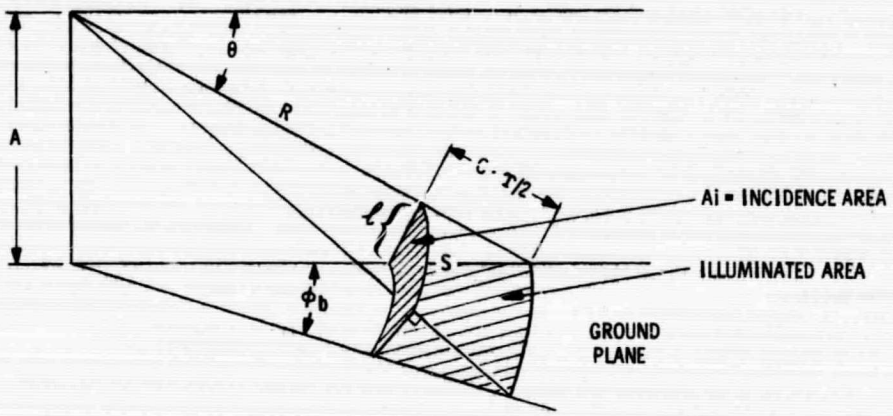

Figure 15. Area Contributing to Radar Return

Also:

$$R = \frac{\Lambda}{\sin \theta} \tag{11}$$

Substituting for σ and R in equation (6) yields the desired result, which enables identifying the detection characteristics of the radar system.

$$\eta_0 = 5.2\,(10^{14})\,\frac{\sin^4 \theta}{\cos \theta\, A^3}\,\gamma \tag{12}$$

Values for the back-scattering coefficient as a function of incidence angle for scrub pine and unbroken grass and grain are available in an internal memo for file.[35] Utilizing this empirical data enables computing η_0 from equation (12) for various altitudes. The results are shown plotted in Figure 16. Equation (11) is plotted in Figure 17 to facilitate identifying the radar range that corresponds to the data presented in Figure 16. The maximum required slant range was tentatively established as 10,000 feet in order to fully utilize the motion cues displayed. Referring to Figure 17, we see that this corresponds to an incidence angle of 2.9 degrees at an altitude of 500 ft. Referring to Figure 16, an incidence angle of 2.9 degrees at an altitude of 500 feet results in an output signal-to-noise ratio of 9 dB for terrain consisting of unbroken grass and grain and 17 dB for a 3 to 5 foot scrub pine. A 17 dB signal-to-noise ratio yields a probability of detection greater than .996 for a probability of false alarm as low as 10^{-12}. Although 9 dB is somewhat low, it is sufficient for obtaining a probability of detection greater than .50 when a probability of false alarm equal to 10^{-3} is acceptable.

The detection capability of the identified radar system may be improved by about 4 dB by simply utilizing a tunnel diode amplifier front end. This increase alone would provide a probability of detection greater than .995 for an allowable false alarm probability of 10^{-3}. In addition, a larger aperture antenna is contemplated. The azimuth beamwidth may be reduced to 0.6 degrees, resulting in a still larger output signal-to-noise ratio.

From equation (3) we see that:

$$\eta_0 = K_1 A_r G_t \sigma \tag{13}$$

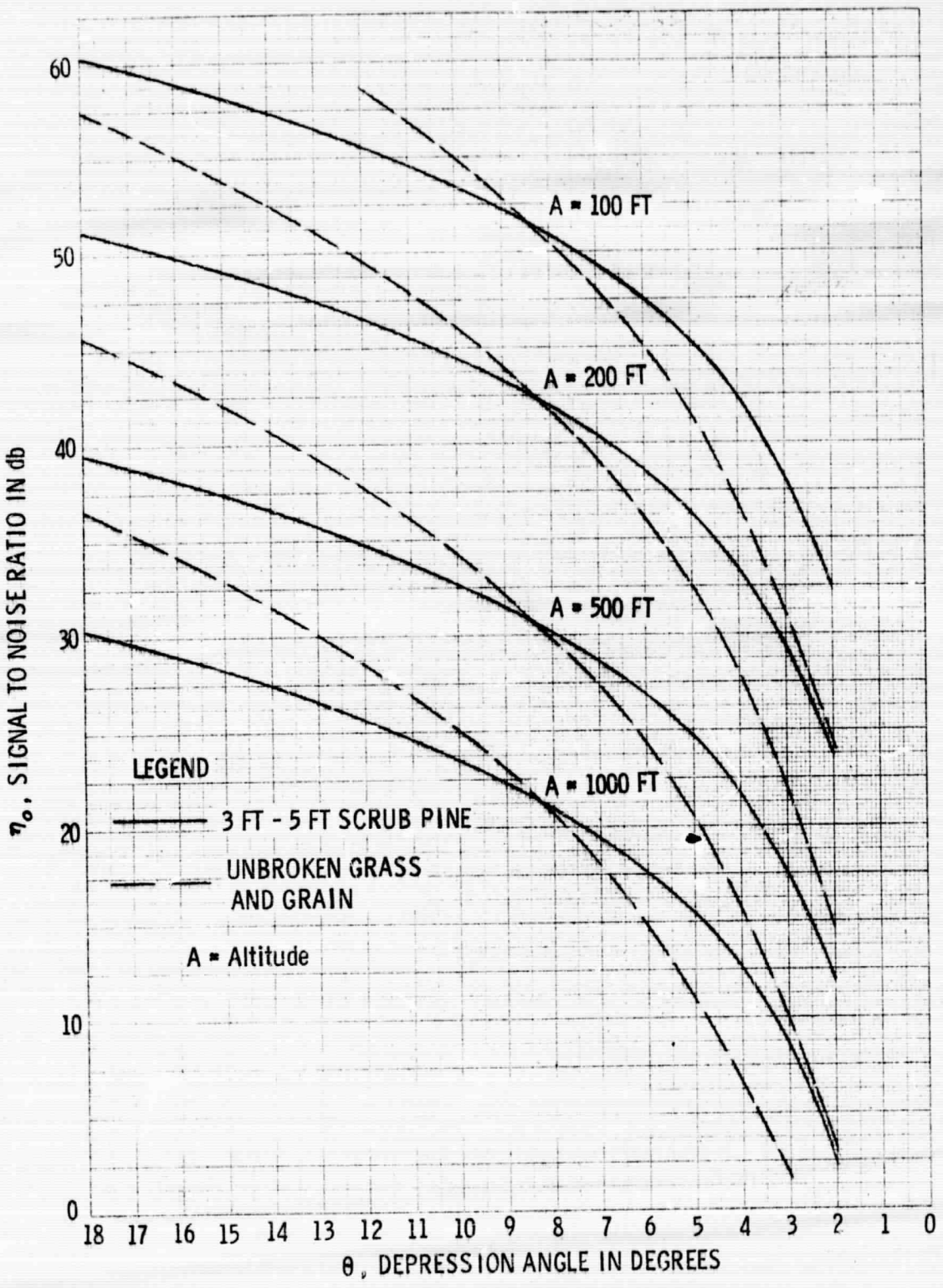

Figure 16. Output Signal to Noise Ratio vs Depression Angle for P3I System

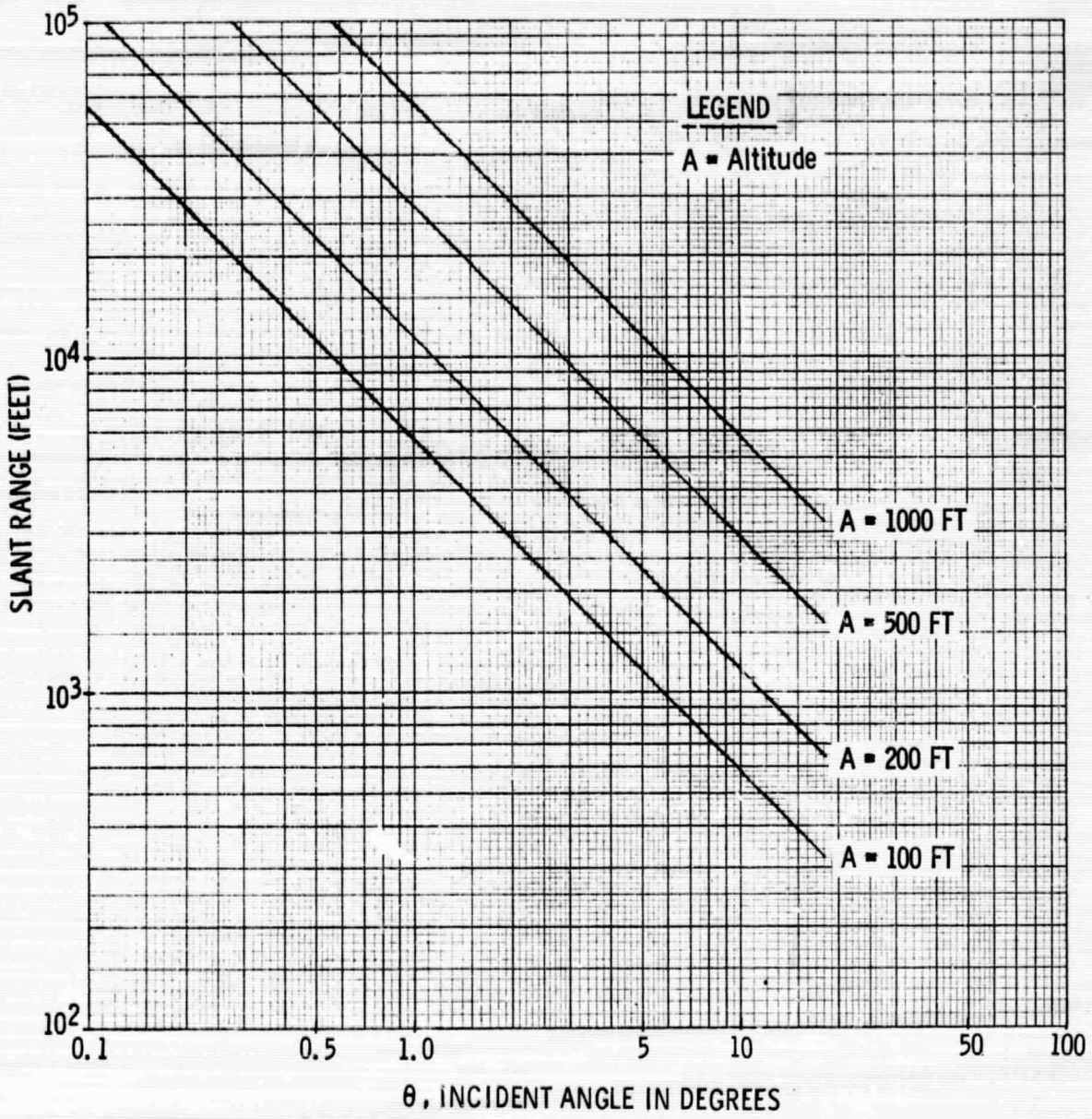

Figure 17. Slant Range vs. Incident Angle

Where:

A_r, G_t and σ are the only parameters involving the antenna aperture or equivalently the antenna beamwidths.

Now since:

$$A = \frac{G\lambda^2}{4\pi} \tag{14}$$

$$G = \frac{27000}{\theta_b \phi_b} \tag{15}$$

Where:

θ_b = elevation beamwidth

ϕ_b = azimuth beamwidth

By combining equations (13), (14), and (15), we get:

$$\eta_0 = K_2 \frac{\sigma}{(\phi_b)^2} \tag{16}$$

Utilizing the expression for σ in equation (10) results in:

$$\eta_0 = K_3 \left(\frac{1}{\phi_b} \right) \tag{17}$$

Equation (17) establishes that the output signal-to-noise ratio is inversely proportional to the azimuth beamwidth. Hence, reducing this by $\frac{.6}{1.2} = 1/2$ would improve the output signal-to-noise ratio by an additional 3 dB.

5. MOTION CUE GUIDANCE

5.1 INTRODUCTION

The vertical situation display identified as the P^3I system (Processed Plan Position Indicator) provides a perspective view of the earth equivalent to the view that would be visually seen by the pilot. All of the natural cues associated with a visual approach are, therefore, present in the P^3I system to aid in guidance of the aircraft. Several prior studies [6, 8, 11, 23, 24] have been concerned with the information contained in the visual data available during a landing and its detection and value. A general conclusion which may be inferred from the referenced reports is that velocity cues, i.e., the cues resulting from movement of terrain texture with respect to the pilot, are perhaps the most valuable. They enable estimating the center of an expansion pattern of terrain movement (commonly referred to as the sunburst effect) which corresponds to the impact point. How accurately this impact point may be estimated and what total guidance information this conveys is best established from plots of isovelocity and isoacceleration curves. An isovelocity curve is a continuous line on the earth, all points of which are moving radially out from the impact point with the same angular velocity. Similarly, an isoacceleration curve is a continuous line on the earth, all points of which are moving radially out from the impact point with the same angular acceleration. The sensitivity with which these angular rates may be perceived identifies how well the pilot can utilize the motion cues to establish the flight path and aircraft velocity. These constitute the most critical parameters for a pilot to identify in order to make a safe landing. In the course of a job analysis based on reports of 185 airline accidents and 519 critical incidents, Gordon (quoted in Reference 8) found:

"The most critical component of the pilot's job, as determined from all sources is that involving the skills of establishing and maintaining a proper angle of glide, rate of descent, and speed of glide on the approach. Failure

to perform this part of the job adequately was found to result in three times as many accidents as does failure to perform any other part of the job."

5.2 ANALYSIS

An equation for the isovelocity curves was derived in Reference 11 which relates the radial angular velocity to ground coordinates. This is repeated below using the notation of Havron.

$$K = \frac{V\sqrt{X^2 + Y^2 \sin^2 \alpha}}{X^2 + Y^2 + D^2 + 2\,DY \cos \alpha} \qquad (1)$$

where:

- K = radial angular velocity with respect to the aircraft of any point on the ground with coordinates X, Y = $\frac{d\beta}{dt}$
- X = distance perpendicular to the aircraft's flight path, with the flight path representing X = 0, to the left of the flight path being negative and to the right being positive
- Y = distance along the aircraft's flight path, with the aiming point representing Y = 0; Y from the a.p. to the aircraft is negative and Y from the a.p. to the horizon is positive
- D = slant range distance from the a.p. to the aircraft
- V = velocity of the aircraft along its glide slope
- α = glide slope angle, between the aircraft's velocity vector and the negative Y axis

These terms are represented in Figure 18. For our calculations it was assumed that the aiming point was on the centerline and 1000 ft beyond the threshold of a runway 200 ft x 10,000 ft; this is compatible with the zero-zero landing study work currently performed by NASA-Ames Research Center at Moffett Field.

In order to convert the X, Y coordinates to those of a perspective display, it is necessary to obtain the depression angle θ and the azimuth angle ϕ

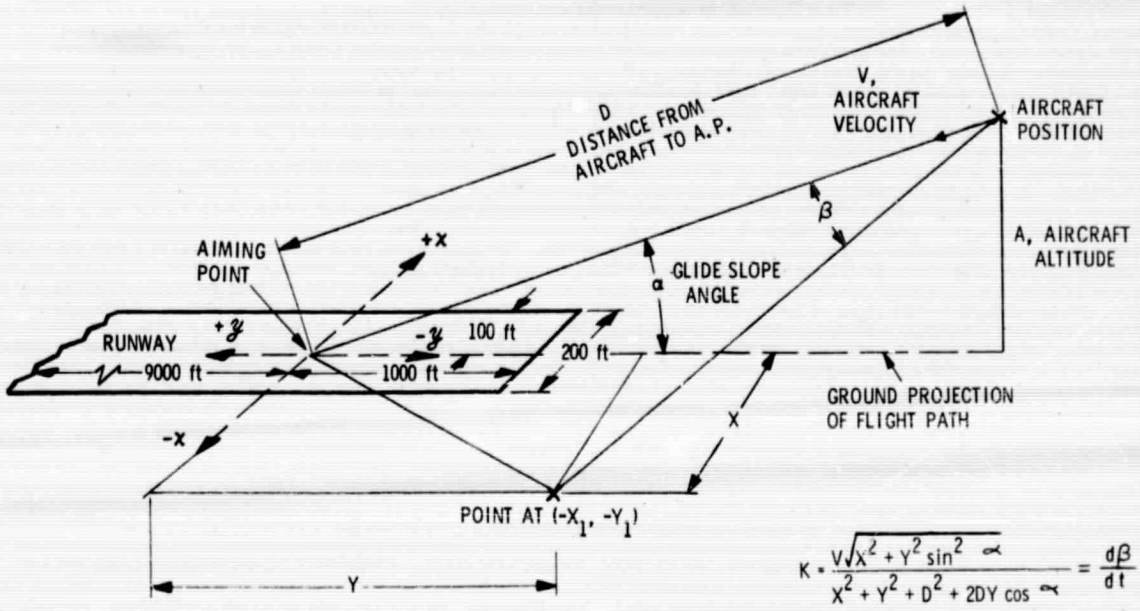

Figure 18. Geometry Identifying Parameters
Associated with Radial Angular Velocity

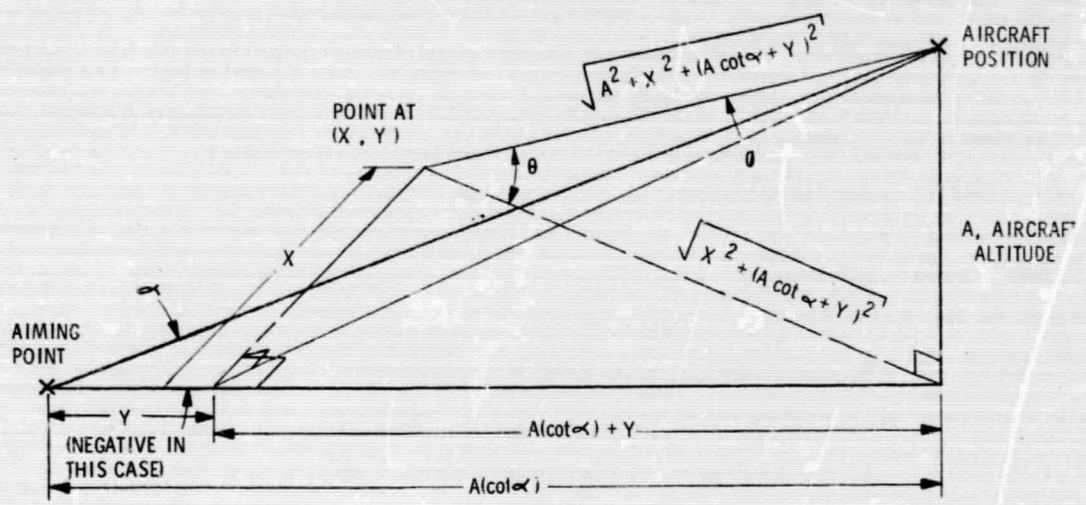

$$\theta = \arctan \frac{A}{\sqrt{X^2 + (A \cot \alpha + Y)^2}}$$

$$\emptyset = \arcsin \frac{X}{\sqrt{A^2 + X^2 + (A \cot \alpha + Y)^2}}$$

Figure 19. Transformation from (X, Y) to (θ, ∅) Coordinates

most aircraft landing speeds including the Convair 340. A simple multiplying factor would present the data for any other velocity which might be considered. The results are shown in Figures 20 through 39. Figures 20 through 29 present the isovelocity curves at the above-mentioned altitudes for a 3° glide slope and Figures 30 through 39 present the isovelocity curves at the same altitudes for a 6° glide slope. Similar data have also been obtained for a 9° glide slope but were omitted since the results for 3° and 6° was considered sufficient for identifying the effect different glide slopes have on isovelocity curves. Isovelocity curves were also obtained with a descent slope of 1/10 degree at an altitude of 15 feet (this corresponds to the wheels touching the ground) for velocities of 120 and 60 knots. This was done to identify the motion cue existing at touchdown and during taxiing. The results are illustrated in Figures 40 and 41.

Before establishing the significance of the results presented thus far, let us determine an expression for constant radial acceleration curves. An equation for the rate of change of the radial velocity was not found in the literature. Since this had to be derived, it seemed desirable to exploit the possibility of obtaining one of the perspective display coordinates in terms of the radial angular rates and the other perspective display coordinate. That is, it would be worthwhile to solve for $\phi = f(K, \theta, D, \alpha \text{ and } V)$ or $\theta = f(K, \phi, D, \alpha \text{ and } V)$ in order to compute constant K curves directly. Also, obtaining $\phi = f(\dot{K}, \theta\ D, \alpha \text{ and } V)$ or $\theta = f(\dot{K}, \phi, D, \alpha \text{ and } V)$ would facilitate computing constant $\dot{K}$ curves directly.

These results were realized by first obtaining $K = f(\theta, \phi, D, \alpha \text{ and } V)$ and $\dot{K} = f(\theta, \phi, D, \alpha \text{ and } V)$. Utilizing the approximation $[\cos^2 \theta - \sin^2 \phi \approx \cos^2 \theta]$ then enabled rearranging the equations for K and $\dot{K}$ to achieve the desired results. The indicated approximation was considered quite reasonable since the maximum value of concern for both θ and ϕ is $\pm 15°$ for normal flight conditions. Details of the derivation are contained in Appendix A where we obtained:

$$\sin^2 \phi = \left(\frac{DK}{V}\right)^2 \frac{\sin^2 \alpha}{\sin^2 \theta} - \sin^2 (\alpha - \theta) \qquad (4)$$

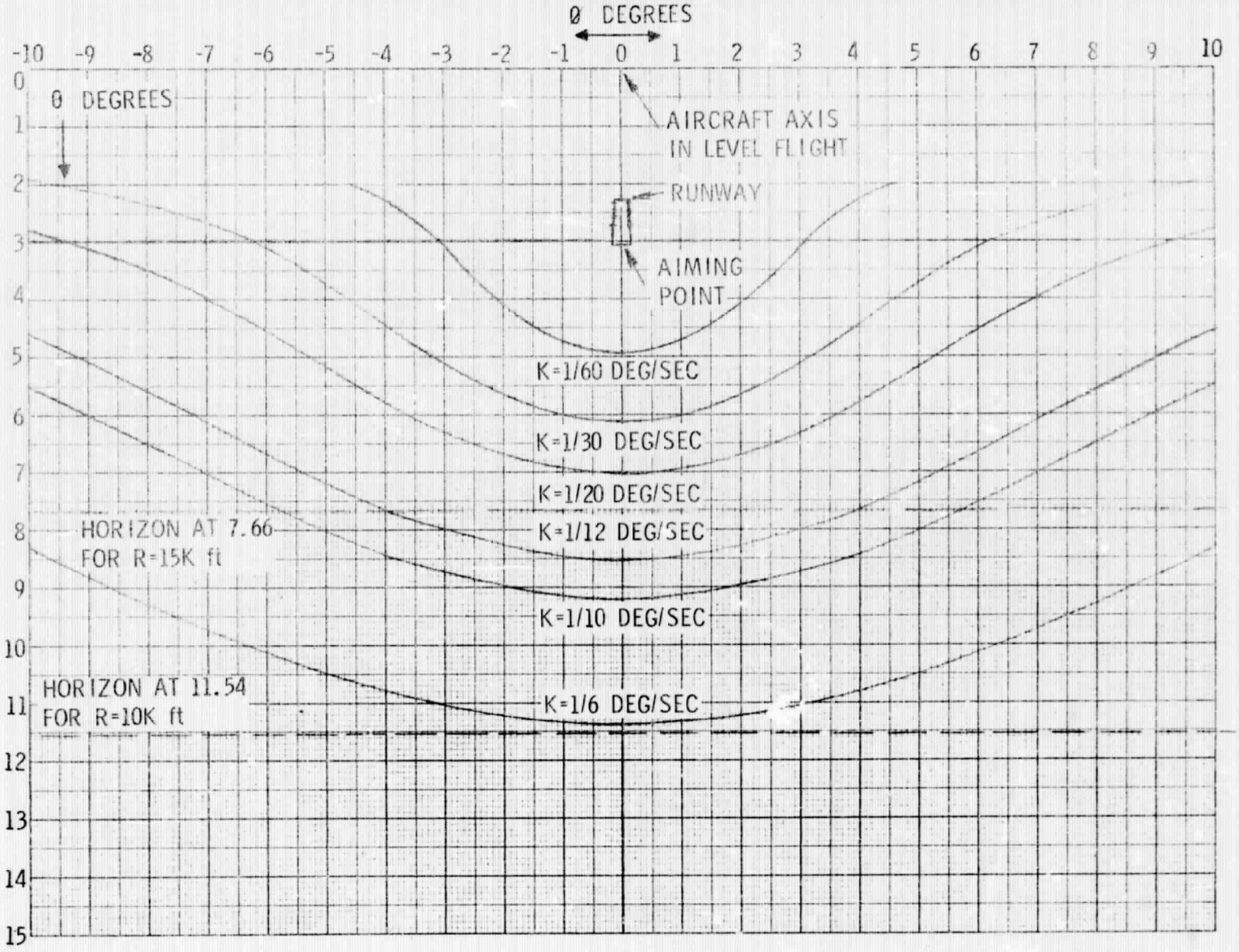

Figure 20. K-Curves for A=2000 Ft, $\alpha = 3°$

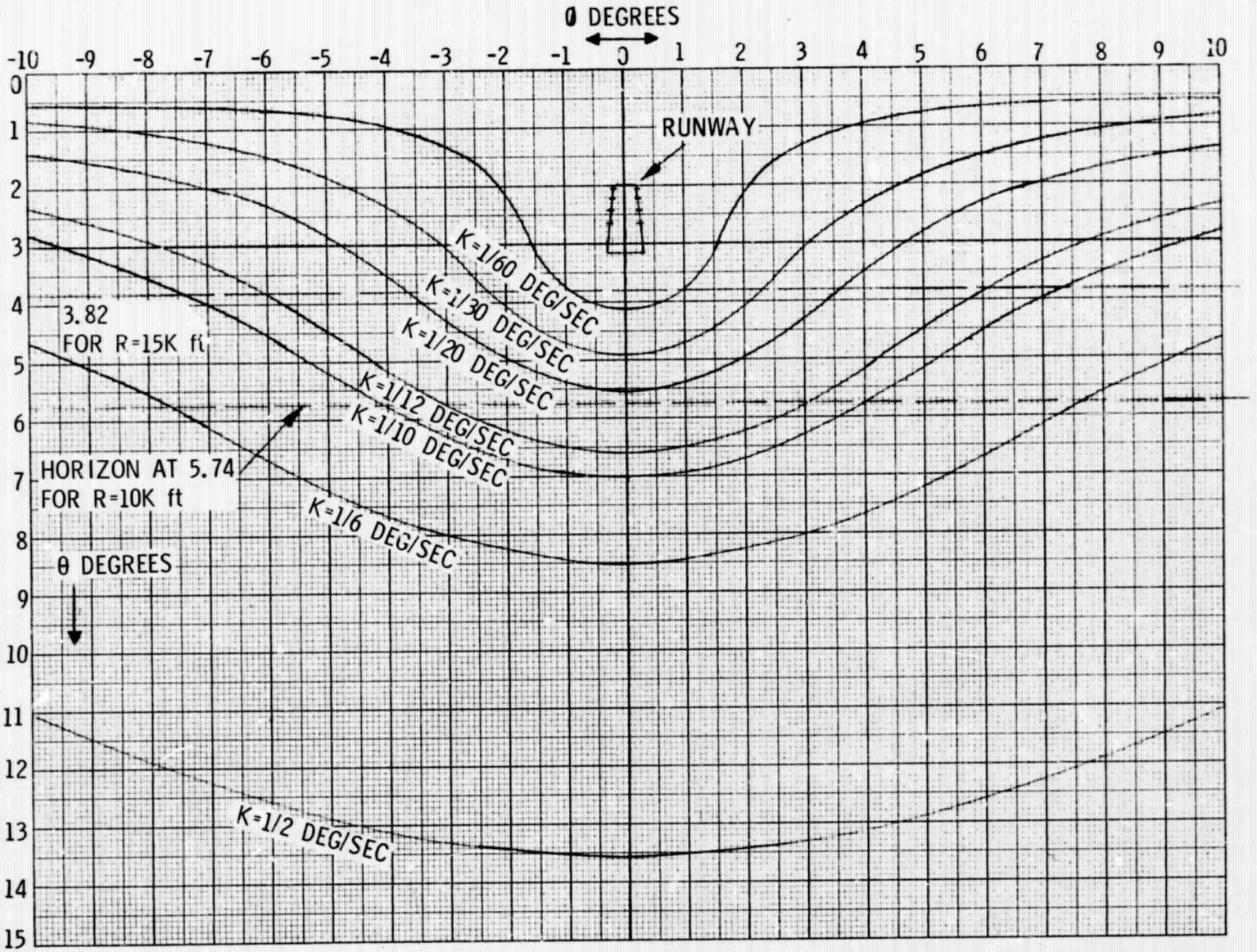

Figure 21. K-Curves for A = 1000 ft, α = 3°

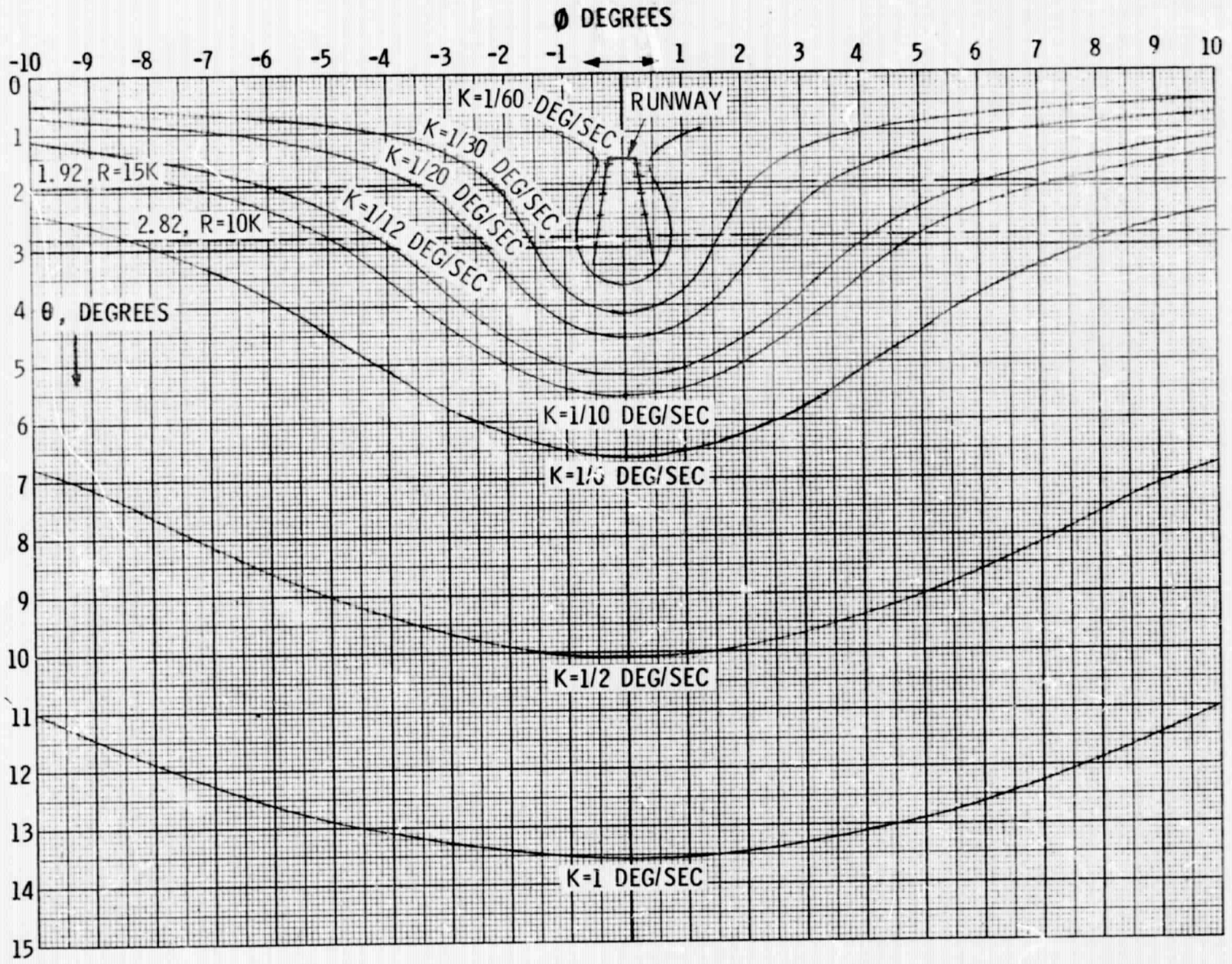

Figure 22. K-Curves for A = 500 ft, γ = 3°

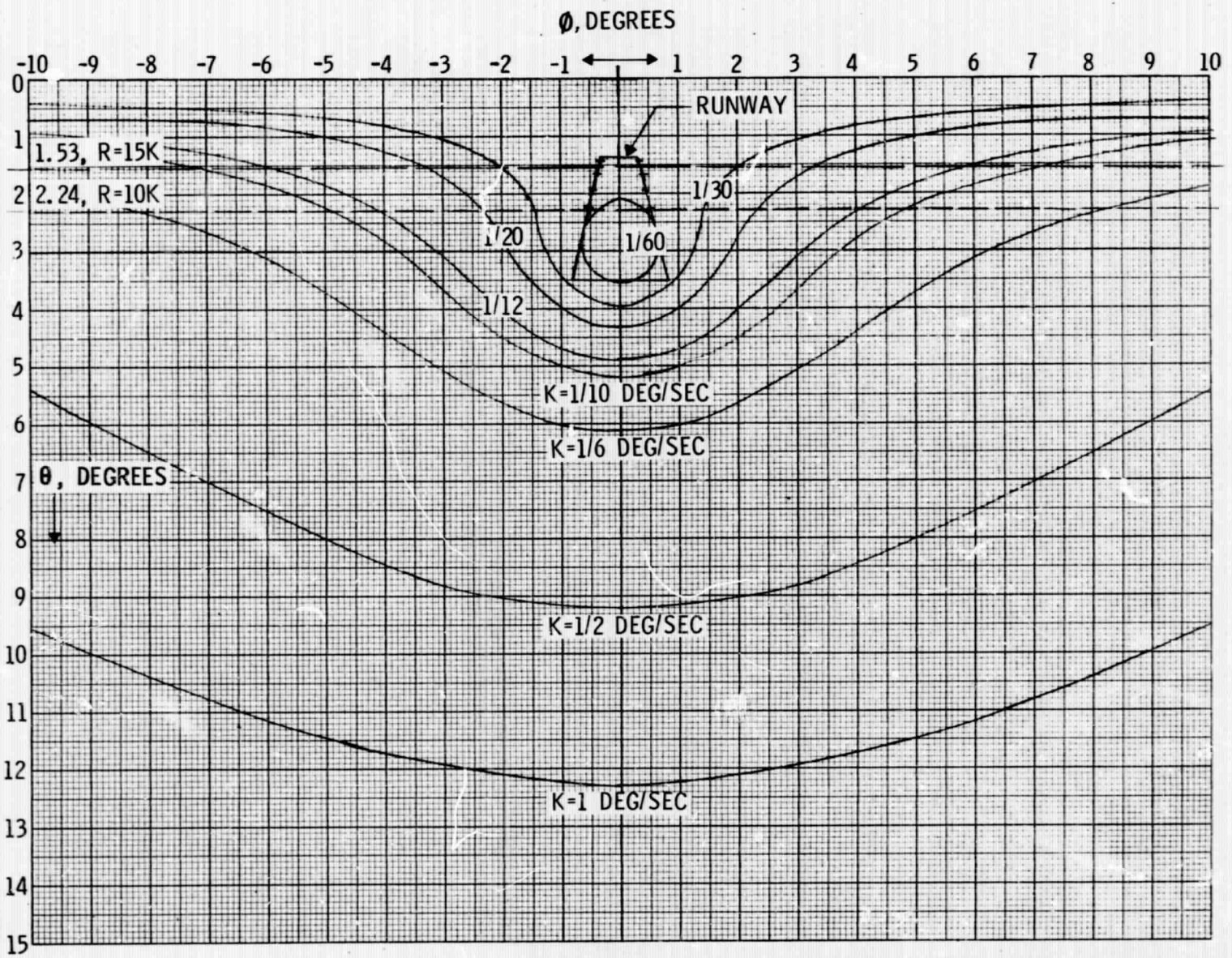

Figure 23. K-Curves for A = 400 ft, α = 3°

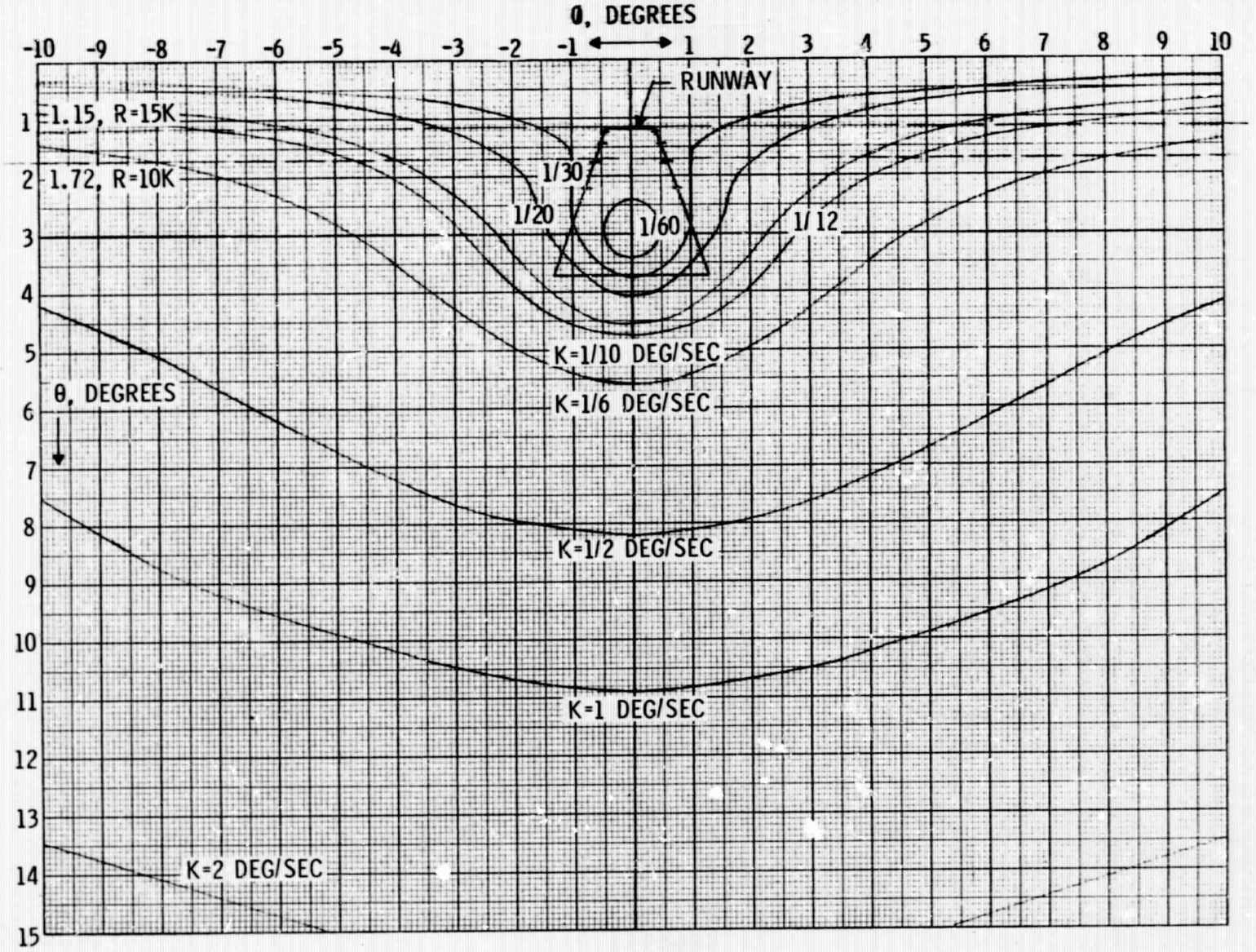

Figure 24. K-Curves for A = 300 ft, α = 3°

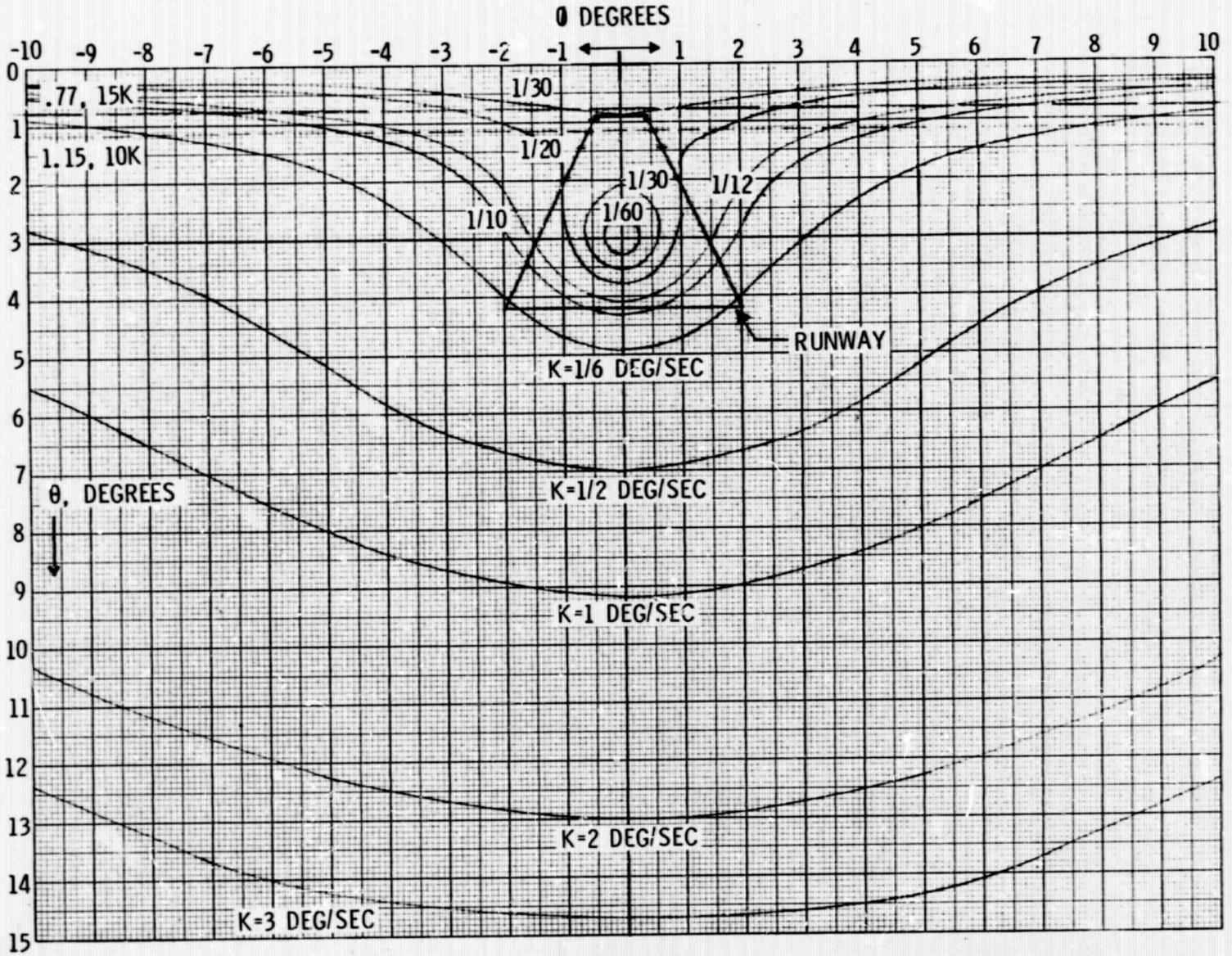

Figure 25. K-Curves for A = 200 ft, α = 3°

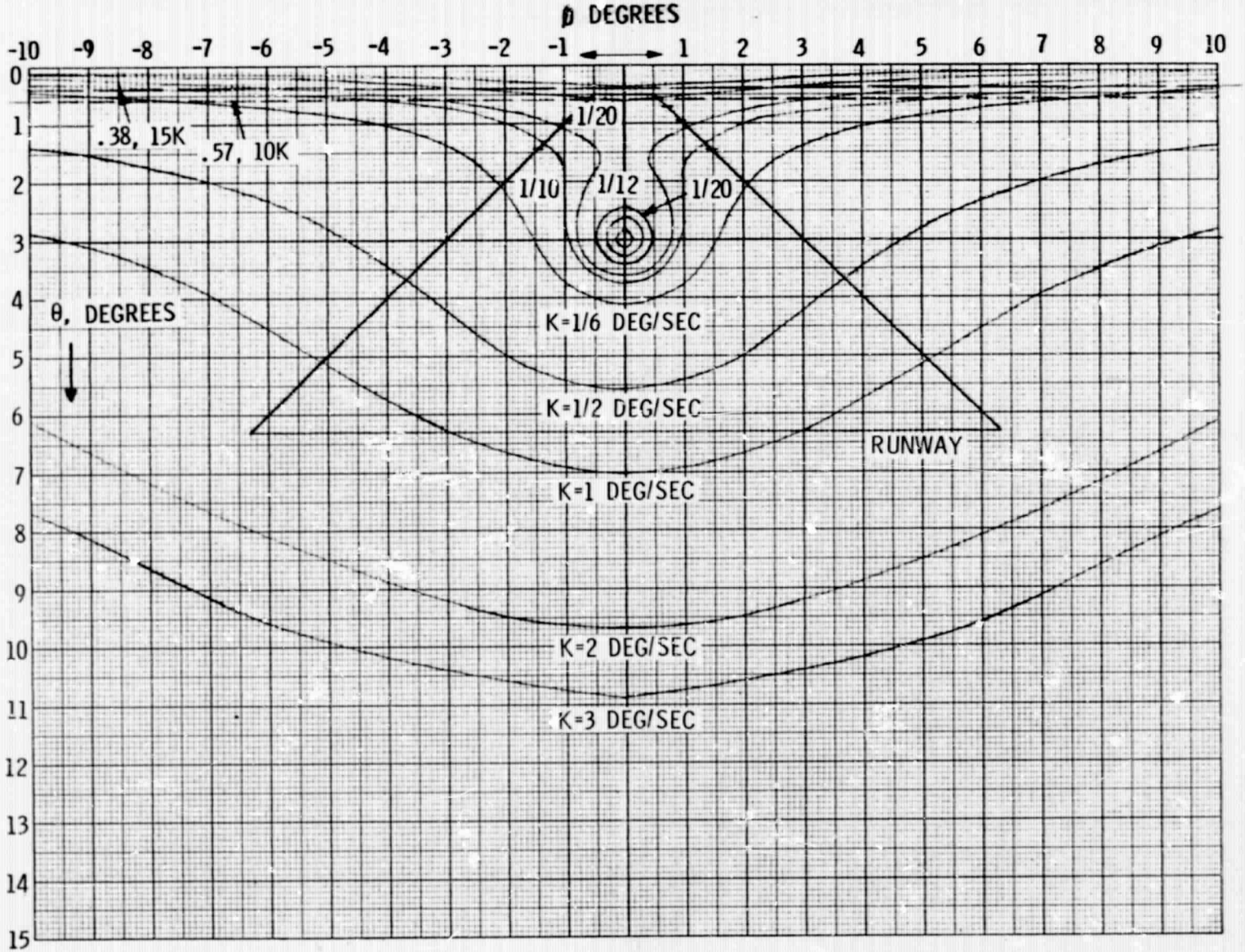

Figure 26. K-Curves for A=100 Ft, $\alpha = 3°$

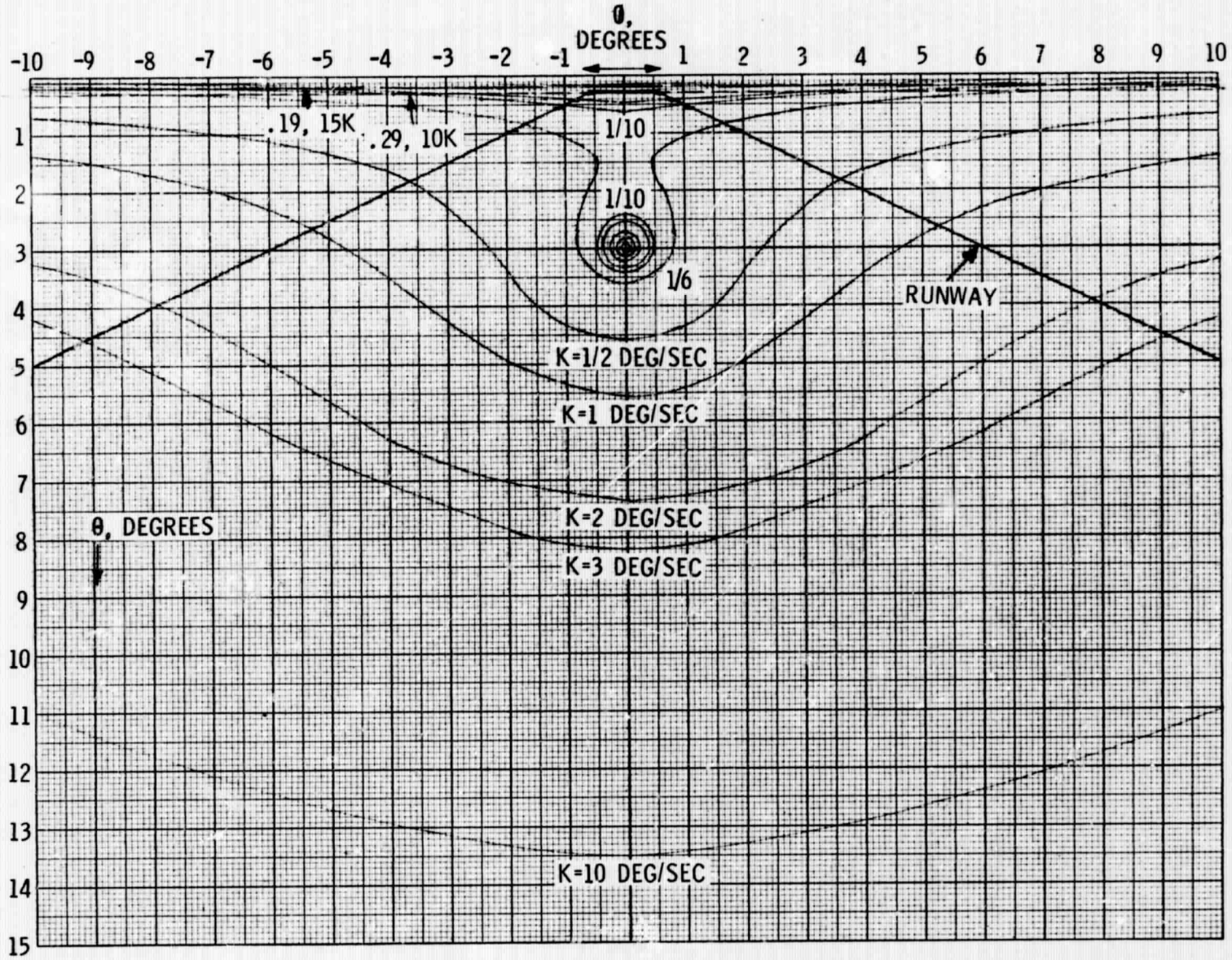

Figure 27. K-Curves for A=50 Ft, $\alpha = 3°$

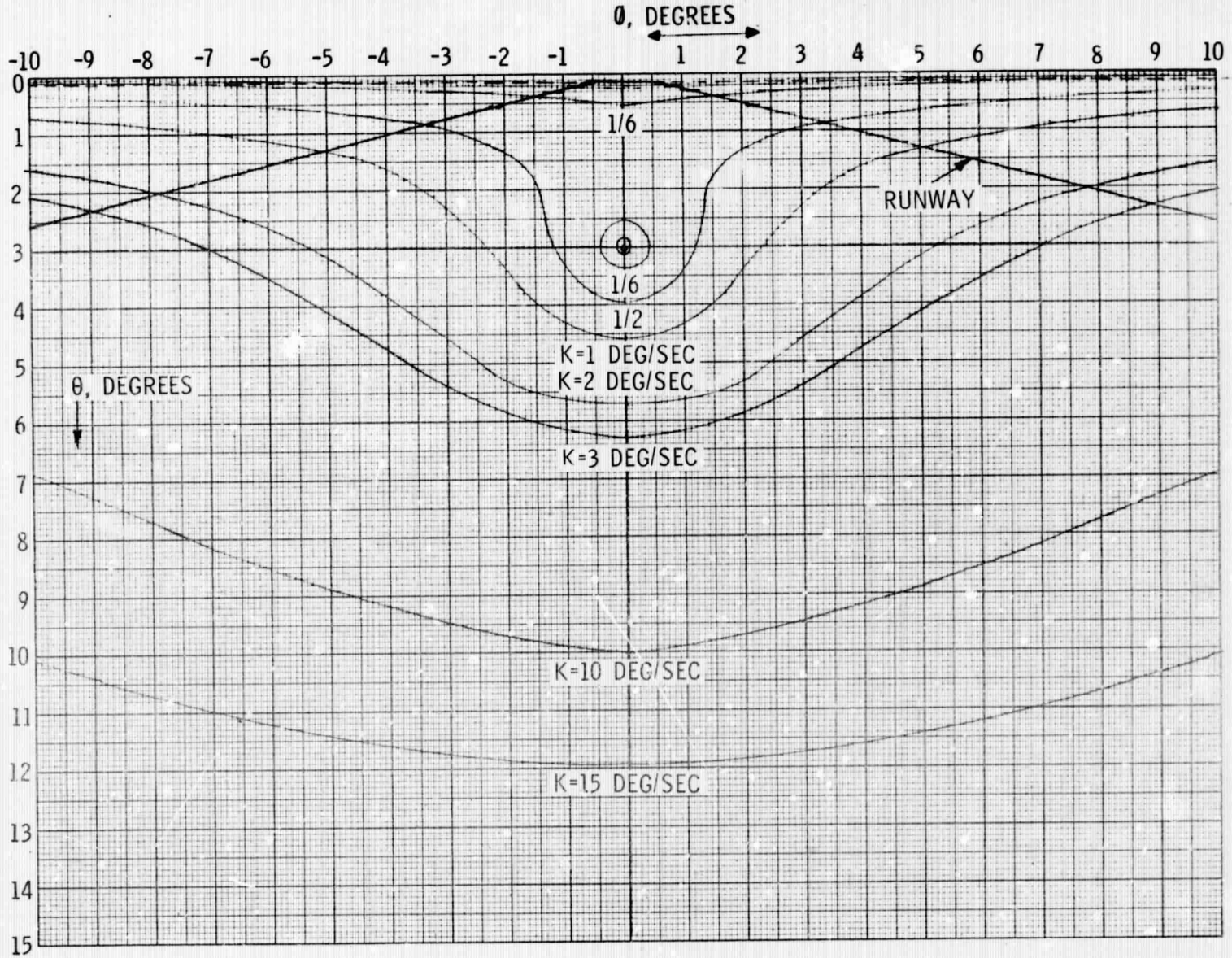

Figure 28. K-Curves for A=25 Ft, $\alpha = 3°$

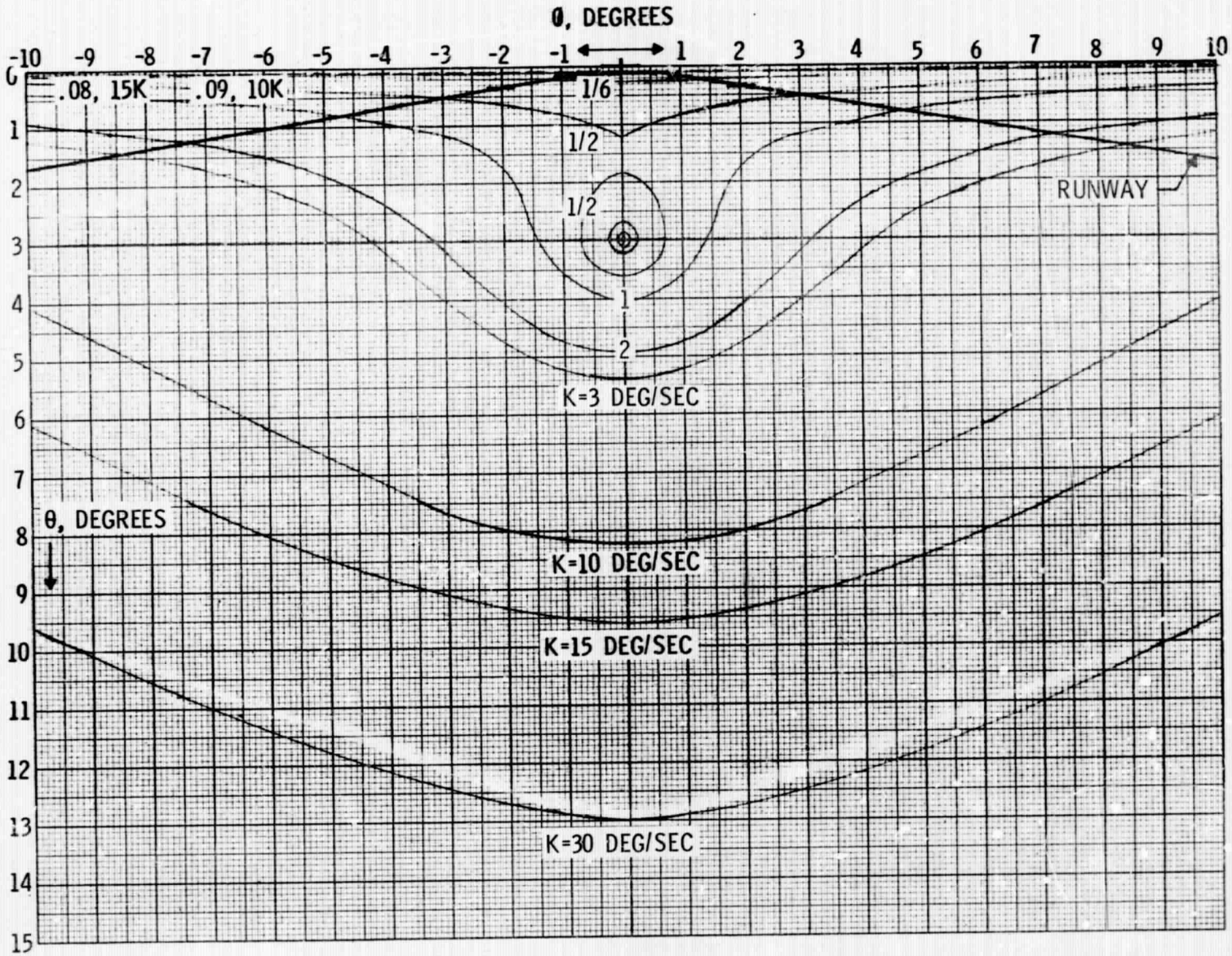

Figure 29. K-Curves for A = 15 ft, α = 3°

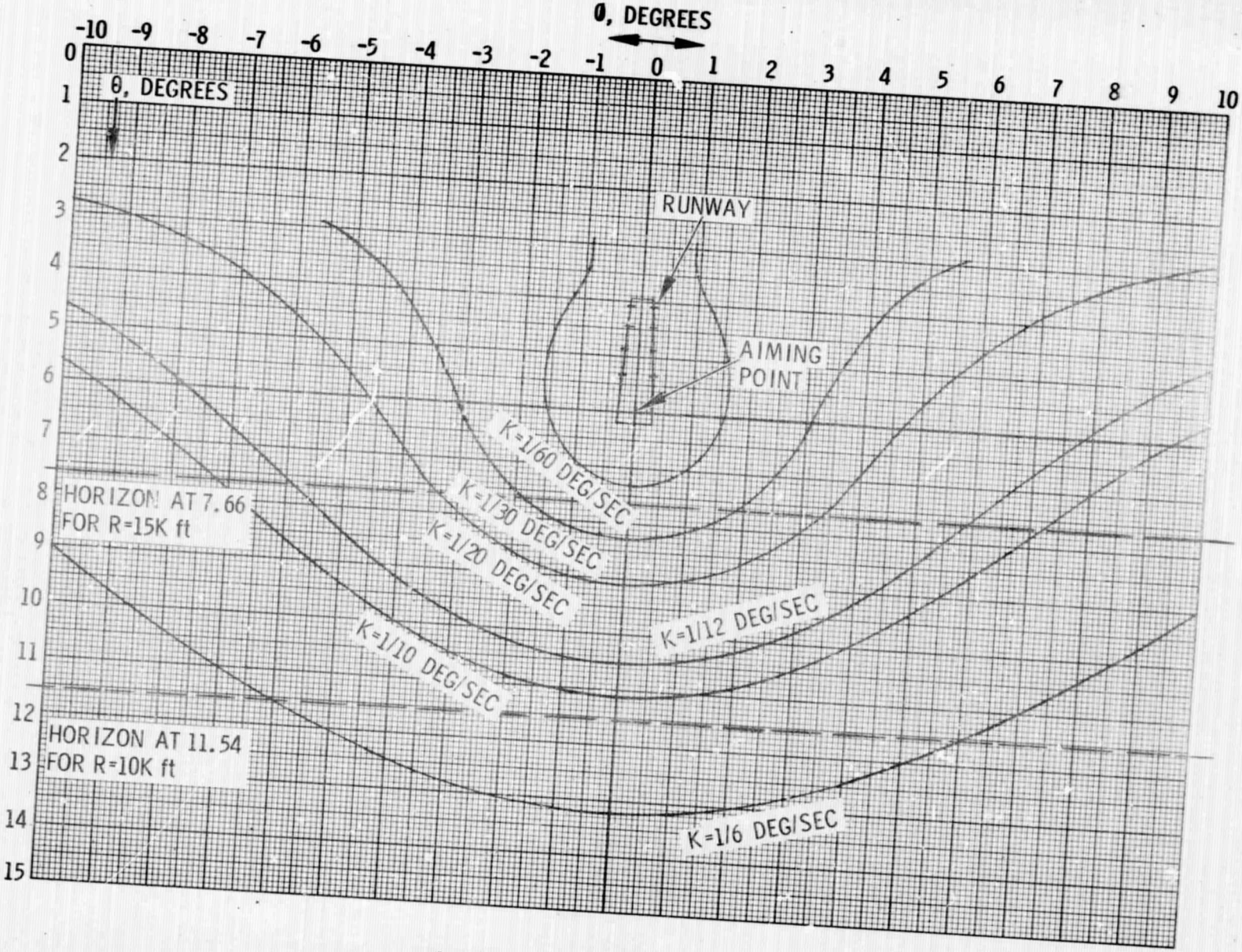

Figure 30 K-Curves for A = 2000 ft, α = 6°

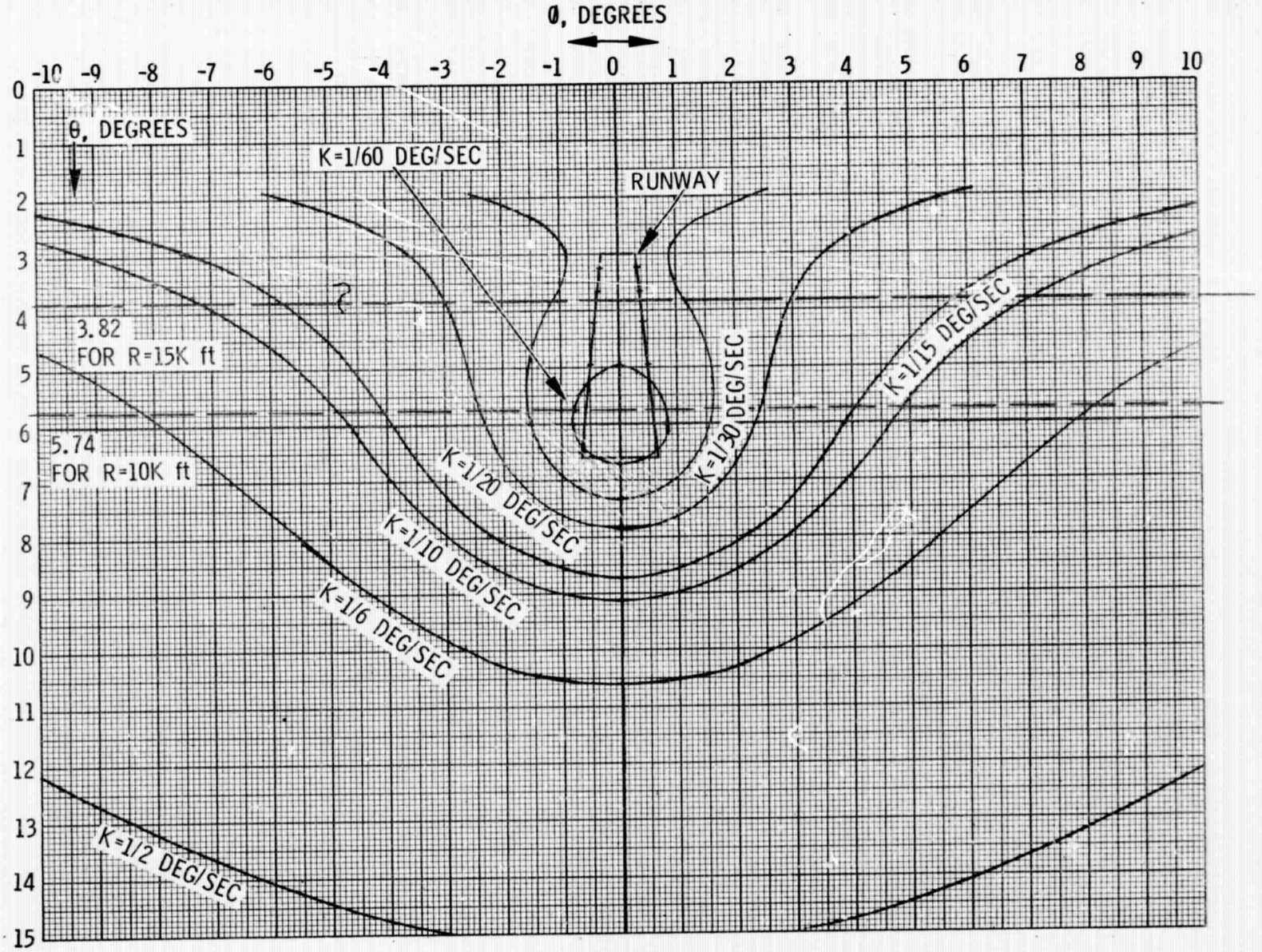

Figure 31. K-Curves for A = 1000 ft, $\alpha = 6°$

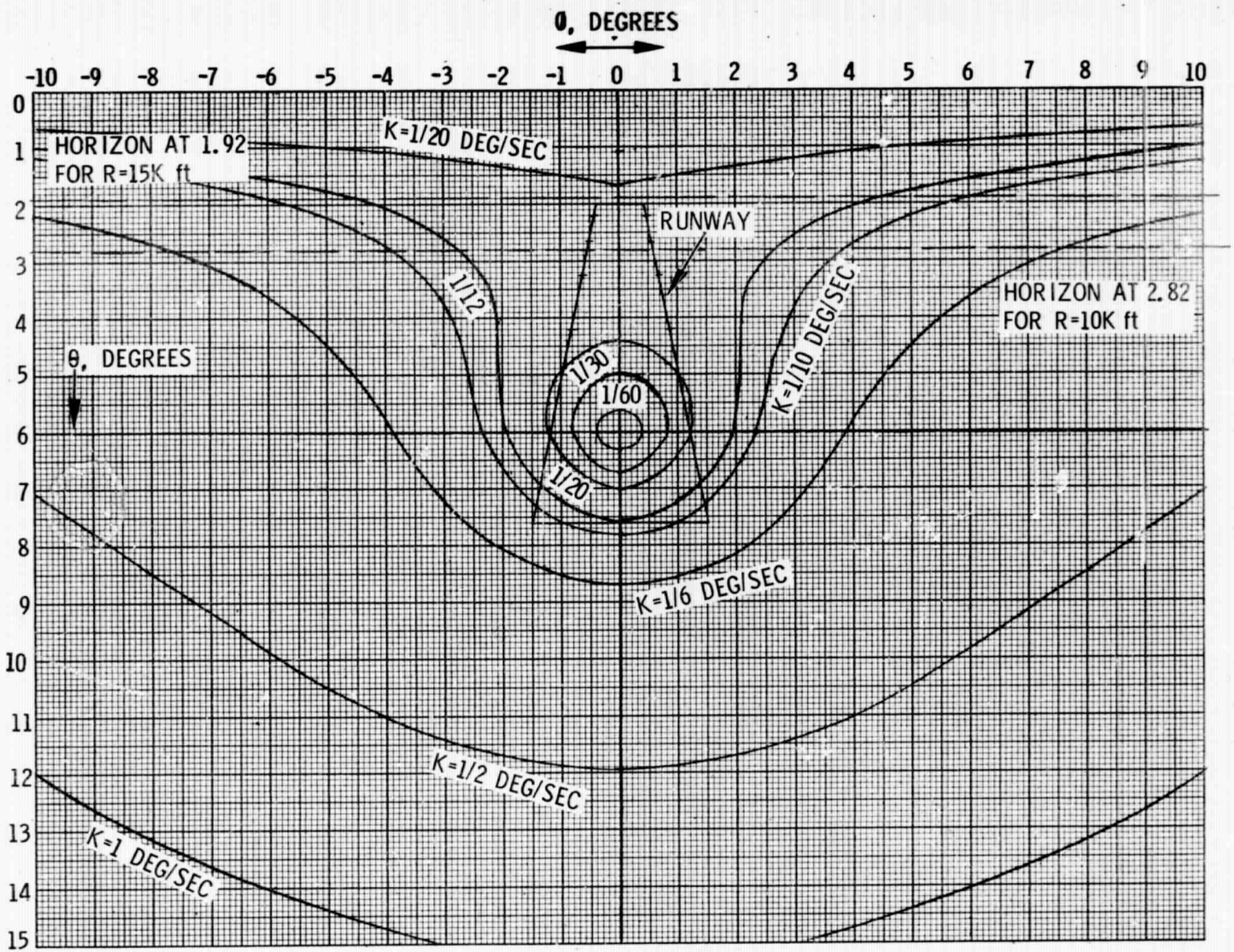

Figure 32. K-Curves for A = 500 ft, $\alpha = 6°$

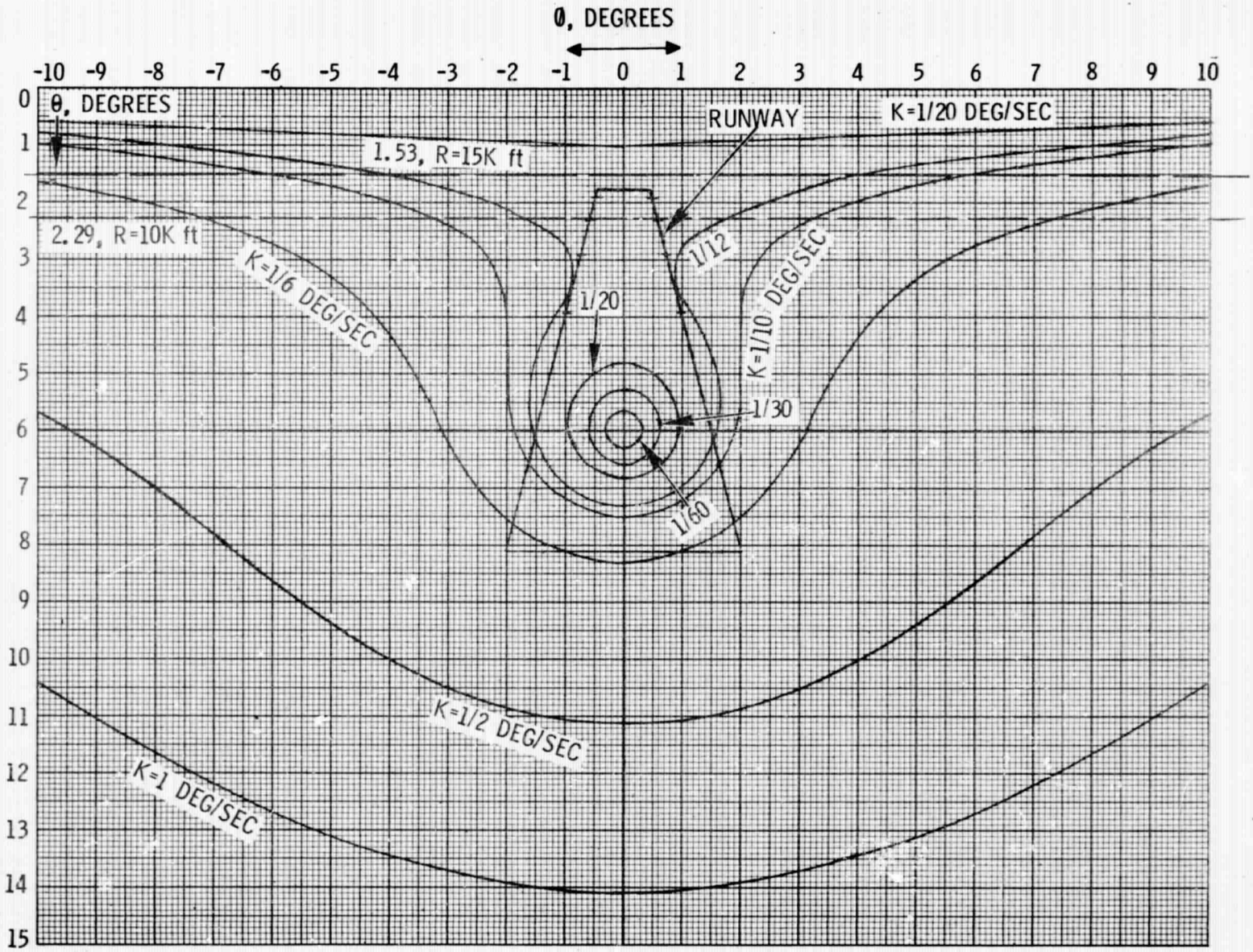

Figure 33. K-Curves for A = 400 ft, α = 6°

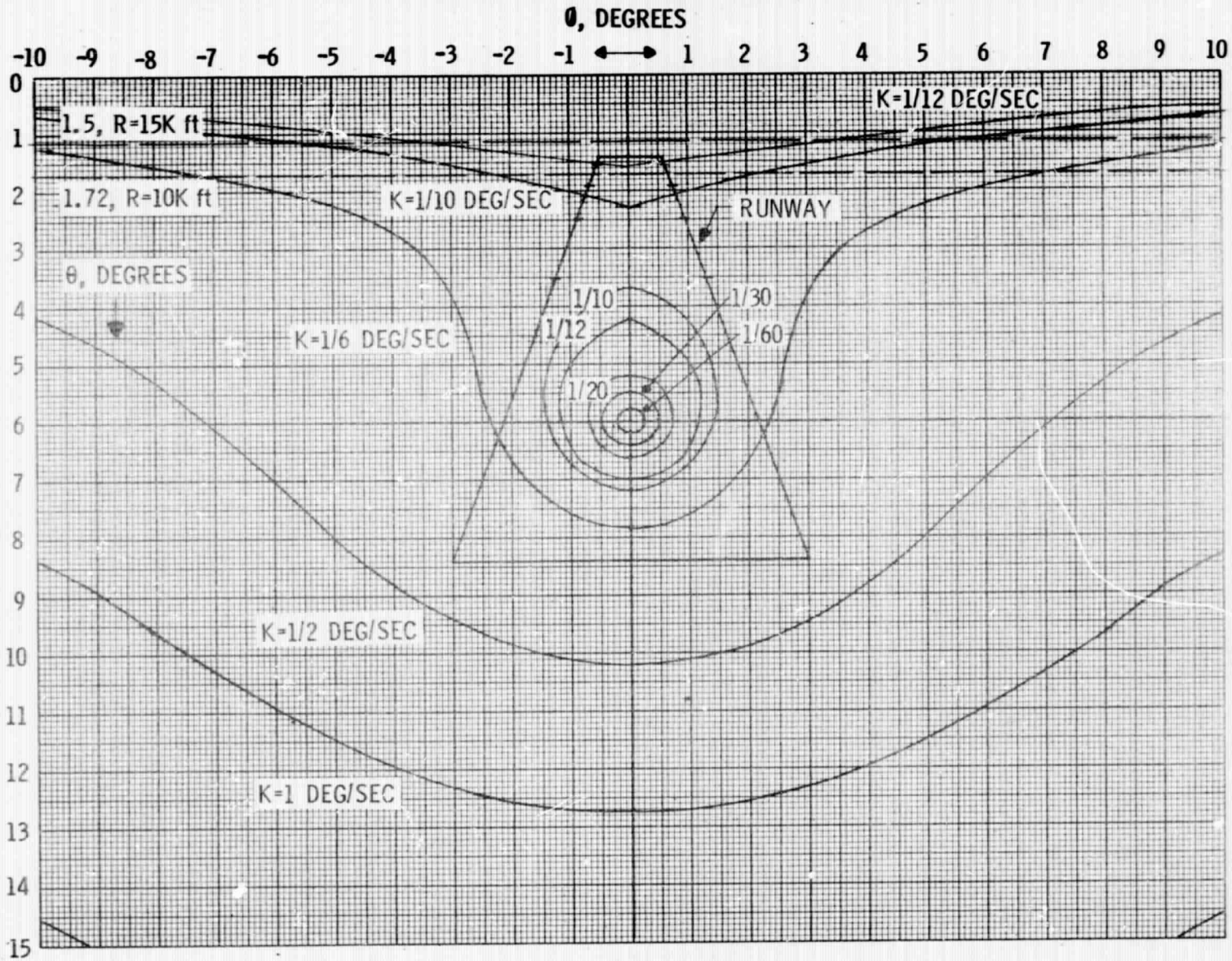

Figure 34. K-Curves for A = 300 ft, $\alpha = 6°$

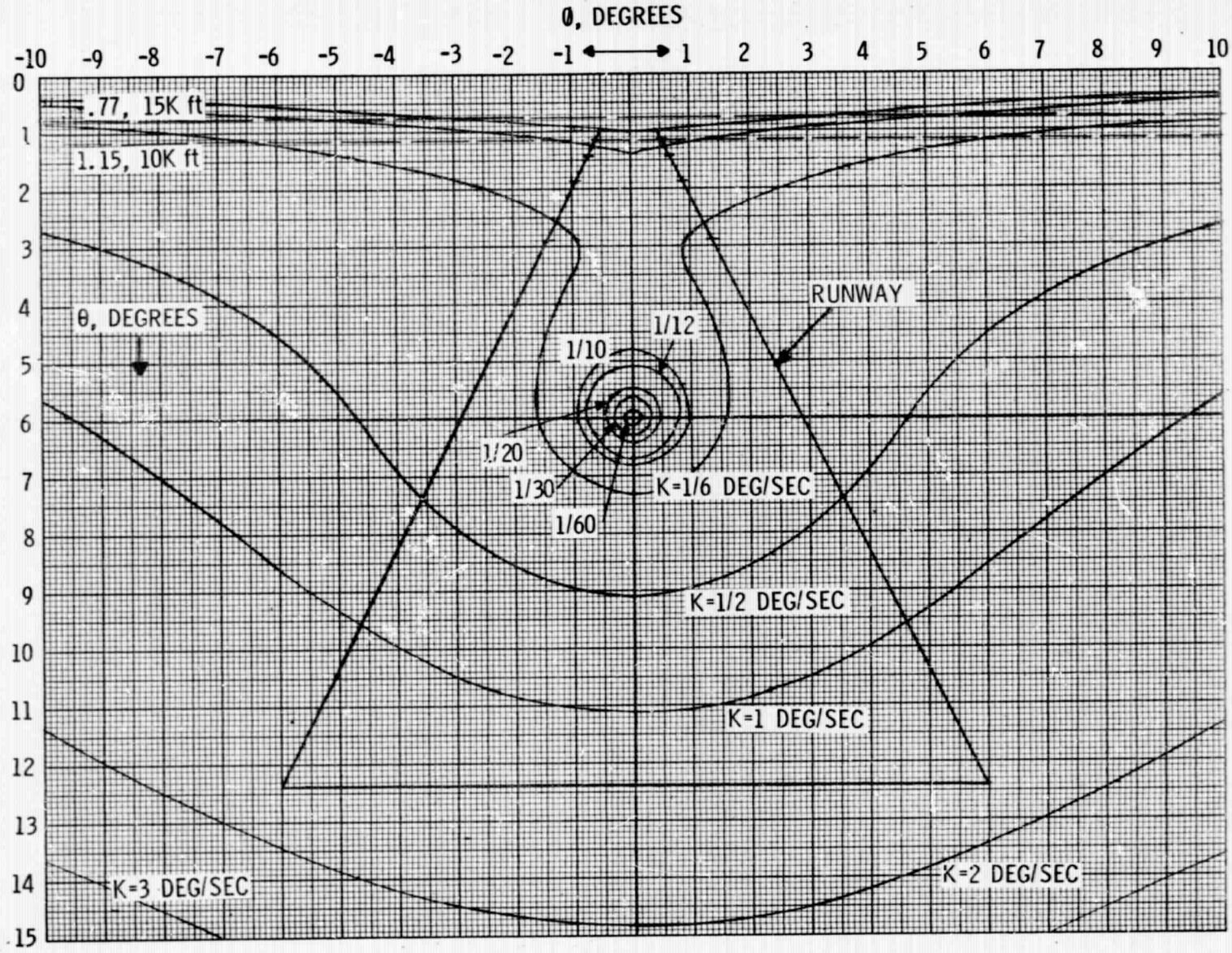

Figure 35. K-Curves for A = 200 ft, α = 6°

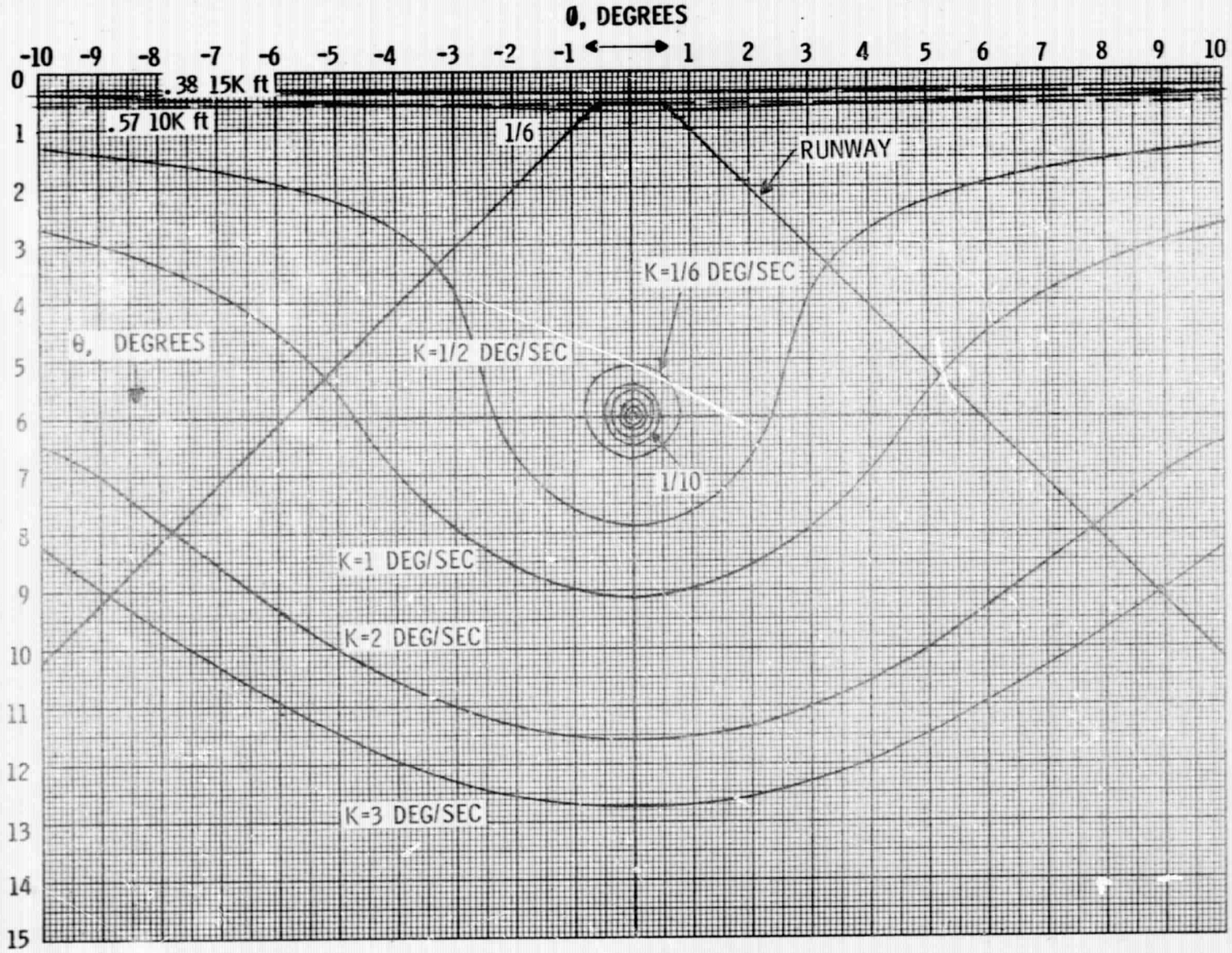

Figure 36. K-Curves for A = 100 ft, $\alpha = 6°$

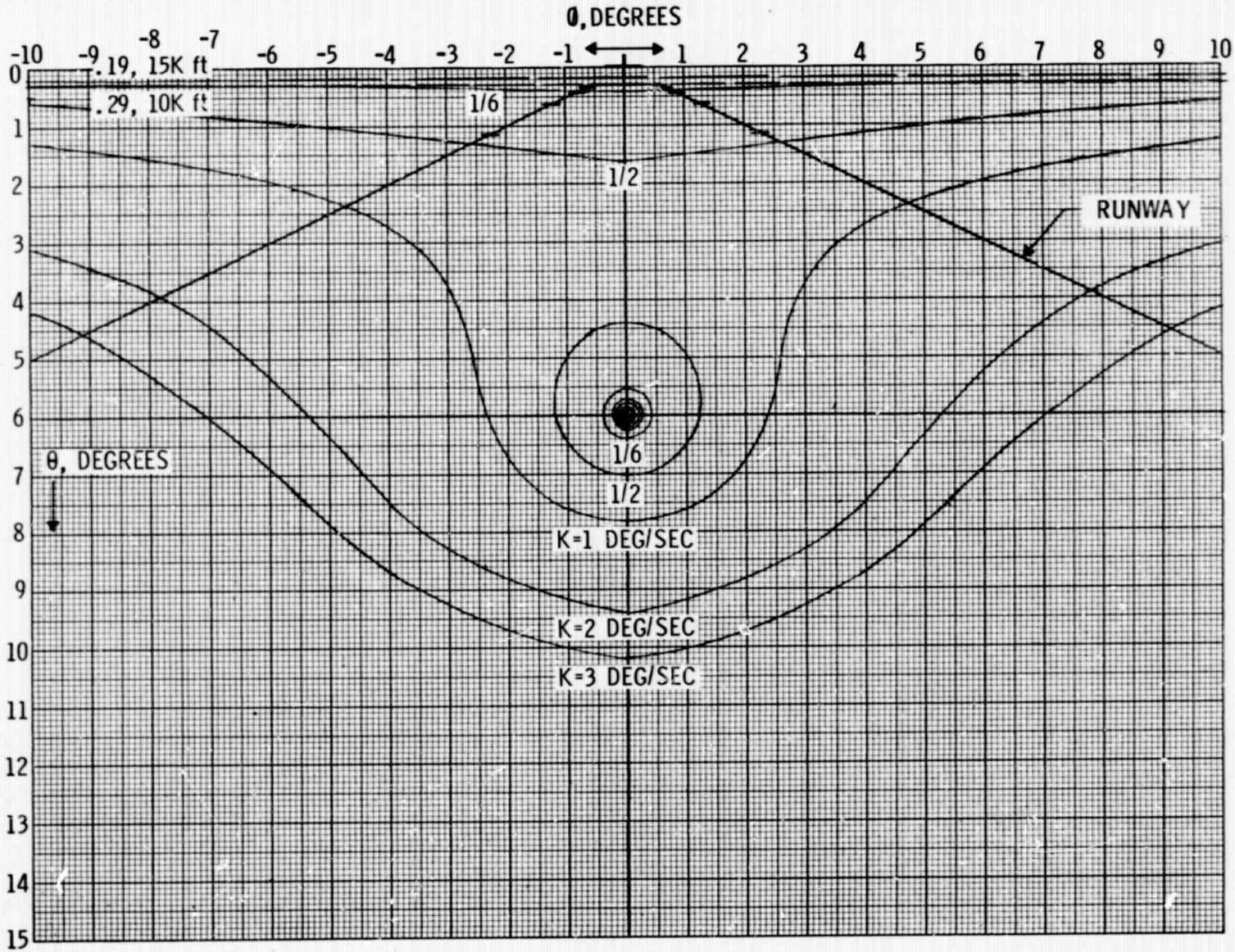

Figure 37. K-Curves for A = 50 ft, α = 6°

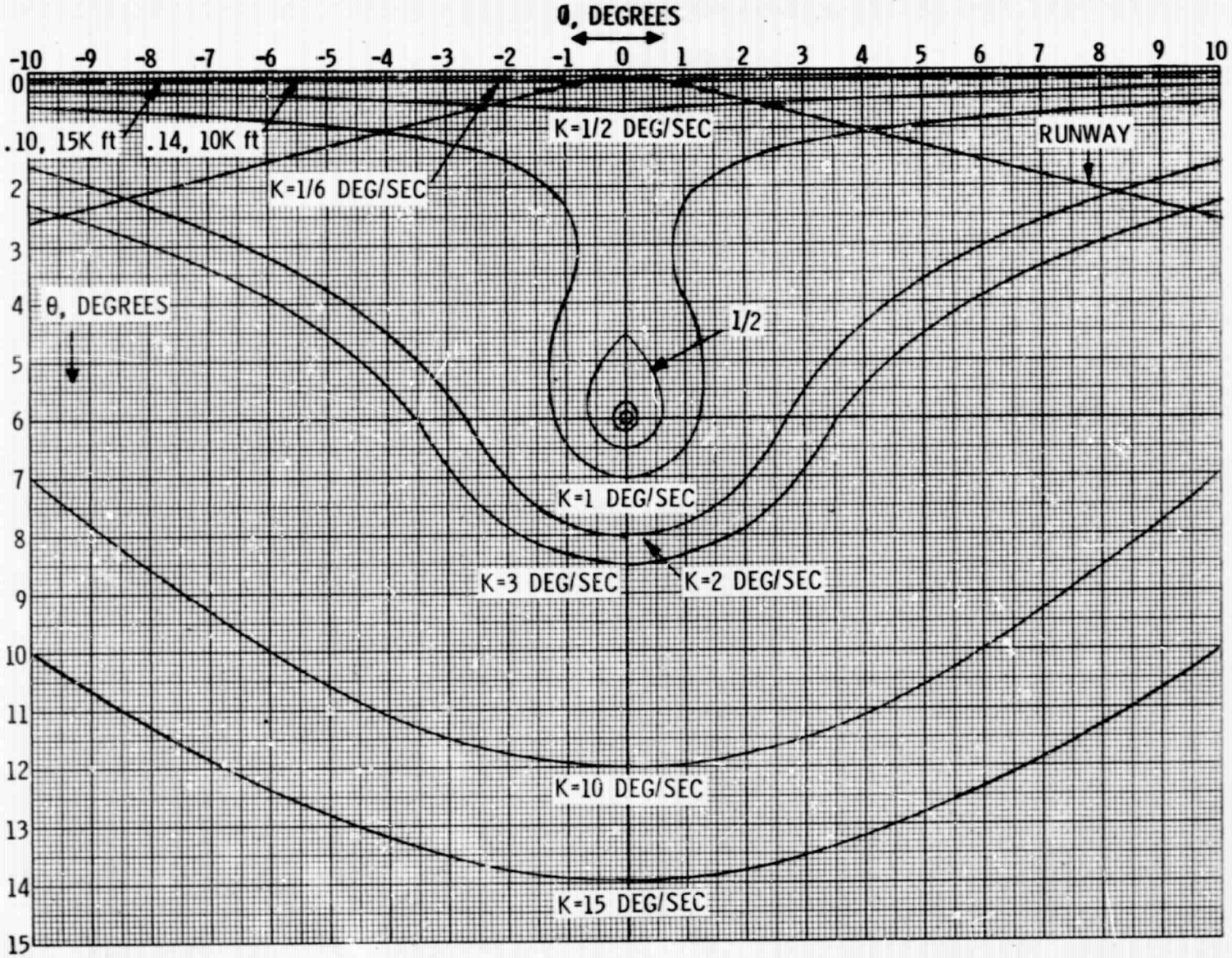

Figure 38. K-Curves for A=25 Ft, $\alpha = 6°$

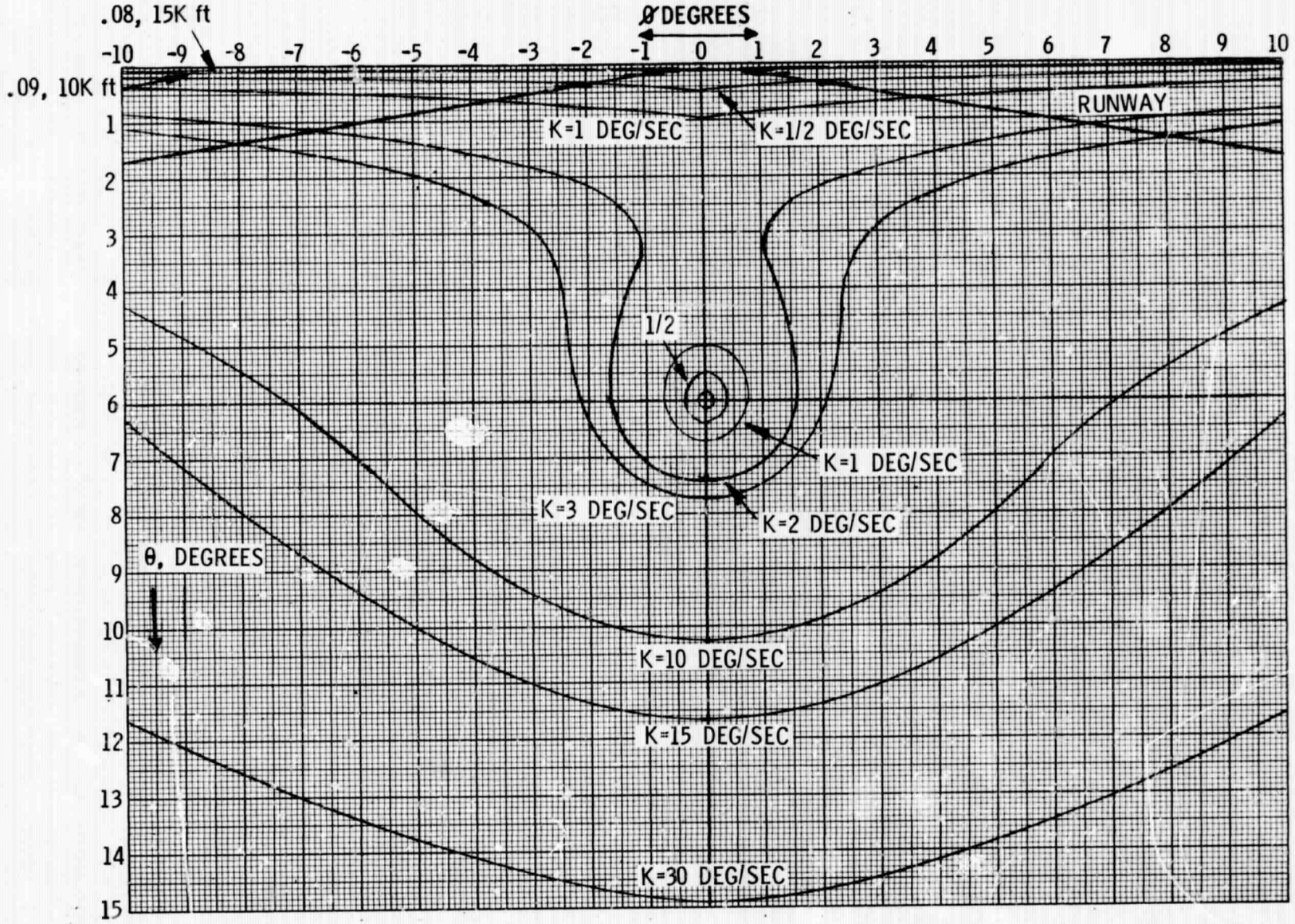

Figure 39. K-Curves for A=15 Ft, $\alpha = 6°$

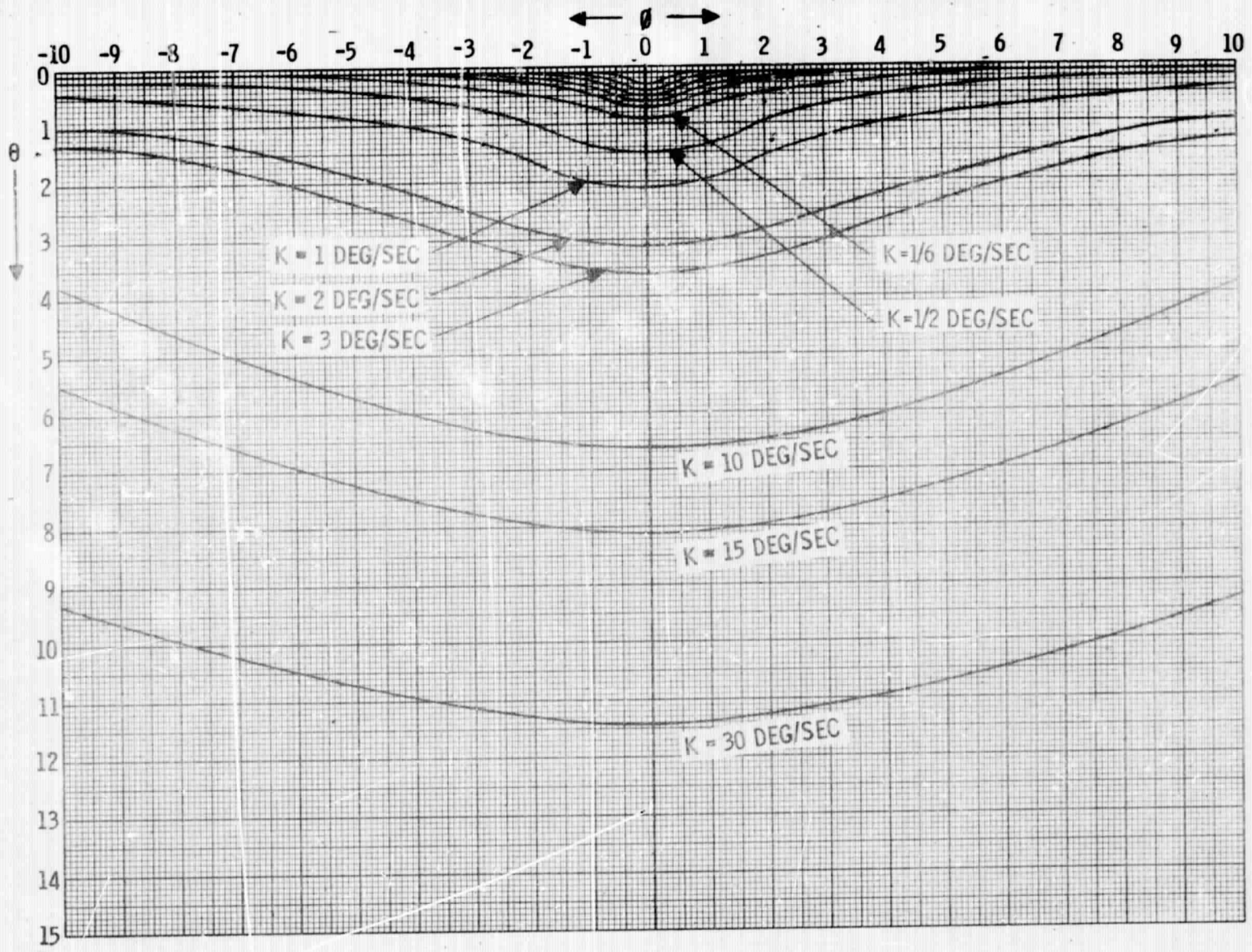

Figure 40. K-Curves for A=15 Ft, α = 0.1°, V = 120 Kts

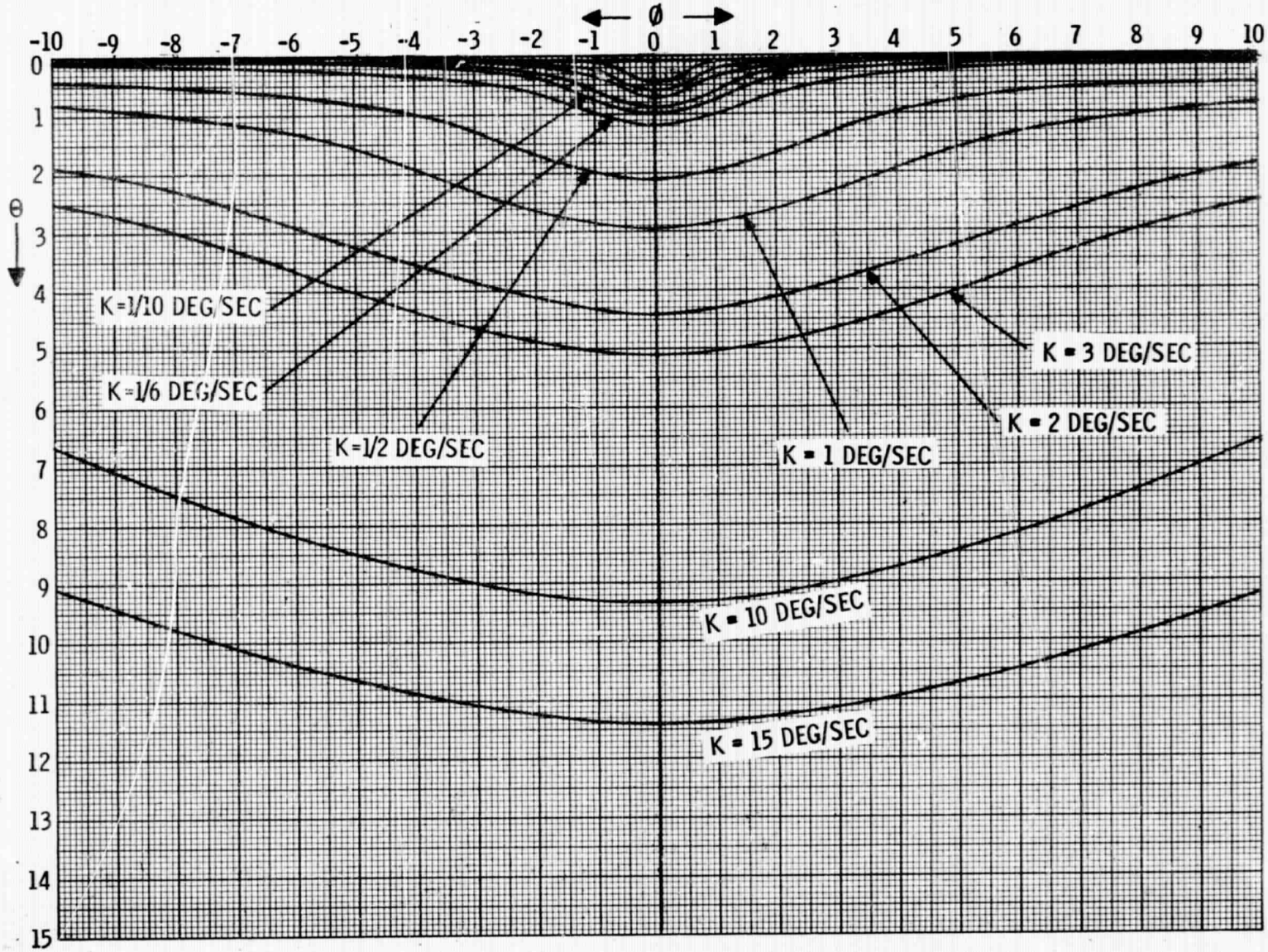

Figure 41. K-Curves for A=15 Ft, $\alpha = 0.1°$, V = 60 Kts

And

$$\sin^2 \phi = \left(\frac{\dot{K} D^2 \sin^2 \alpha}{2V^2 \sin^2 \theta \cos (\alpha - \theta)} \right) - \sin^2 (\alpha - \theta) \qquad (5)$$

Where:

$$\dot{K} = \frac{d^2 \beta}{dt^2} = \frac{dK}{dt}$$

= radial angular acceleration

The remaining parameters are all as previously defined.

Equations (4) and (5) are surprisingly simple and easily programmed to obtain isovelocity and isoacceleration curves for any set of conditions desired. The loss of accuracy introduced by the approximation used in the derivation appears to be negligible. Referring to tables 1, 2 and 3 in Appendix A, we see that the largest difference between the computer solution and the derived equation is .05 degrees, or less than 1%. Lack of time prevented setting up a program for equations (4) and (5) to investigate more completely the variations of the constant velocity contours with altitude and descent slope in addition to identifying the shapes of the isoacceleration curves.

5.3 MOTION DETECTION AND SIGNIFICANCE

The value of the motion cues depends on their physical character in combination with the perceptual abilities of the pilot. Physically, the ground points move radially away from the impact point which itself has no movement. The constant angular velocity contours encircle the impact point, then expand and open up into a horseshoe shape as the values increase. Further increase in the angular velocity results in the horseshoe opening up. An examination of Figures 20 through 39 reveals that for a constant glide slope the K-curves move in toward the aiming point as the aircraft descends. This means that the lower the aircraft is on its approach path, the faster the movement in the pilot's visual field, which would be expected.

These changes help to identify the altitude, rate of descent and velocity vector. By comparing the 3° and 6° approaches for the same altitudes, it is seen that the glide slope angle modifies both the shape of the curves and the centering of the curves; i.e., the curves change with respect to the runway. It is these cues which inform the pilot of his glide slope, changes of his glide slope and the instantaneous aiming point. An approach with a proper glide slope but an incorrect aiming point would be noticed by a shift of the runway with respect to the K-curves. These graphs help to illustrate the value of the motion cues which the pilot uses, often unconsciously, when making a visual landing. It is thought that this type of analysis can lead to greater awareness among pilots of the cues available for their use, to better utilization of these cues, and to better, more efficient, pilot training techniques.

These general comments pertaining to the physical phenomena which exist tacitly assume that the pilot can observe or detect the various contours. In actuality he does, but not the lower angular rates which were plotted. The lowest angular velocity which can be perceived is identified as 1/6 degree/second in Reference 11. This conclusion was established as a threshold value for daylight conditions by interpreting the data in Figure 42. It is assumed that pilots can reliably detect (essentially detectable in all cases) movement of this rate under most conditions encountered in flight. A study of the K-curves reveals that this threshold is not nearly as good as one would desire (at least from the point of view of accurately identifying the impact point). The impact point is not completely encircled until the aircraft is as low as 25 feet for the 3° descent slope and 100 feet for the 6° descent slope. This is illustrated more clearly in Figures 43 and 44 which presents the K curves for 1/6 degree/second for various altitudes ranging from 2000 feet down to 15 feet at a descent slope of 3° and 6°, respectively. Any accuracy achieved in determining the impact point from the isovelocity effect is probably the result of employing triangulation. If the pilot can estimate the direction of the angular velocity for several ground points on the left and right sides of the display, he can then establish their point of intersection, which would correspond to the impact point.

The data in Figures 45 and 46 presents the K-curves for 1/20 degree per second at various altitudes and descent slopes of 3° and 6° respectively.

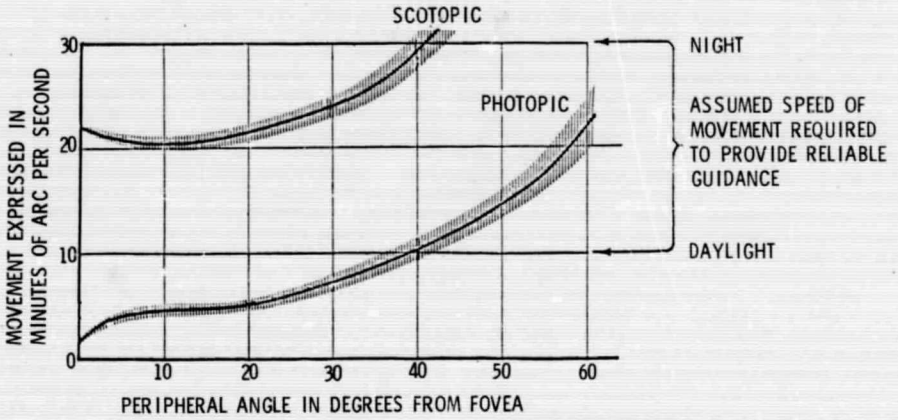

Figure 42. Estimated Photopic and Scotopic Movement Detection Thresholds

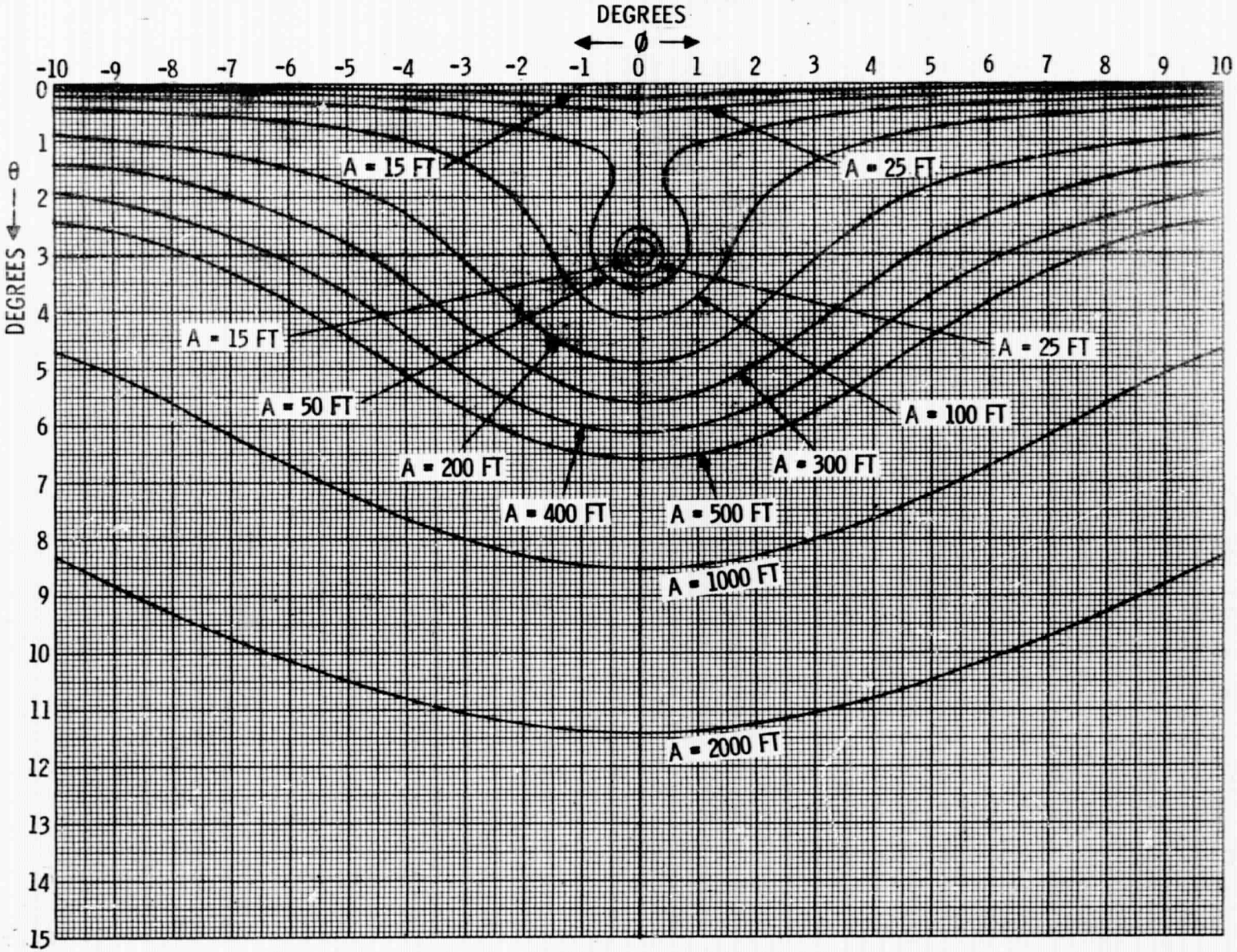

Figure 43. K-Curves for K=1/6 Deg/Sec, α = 3°

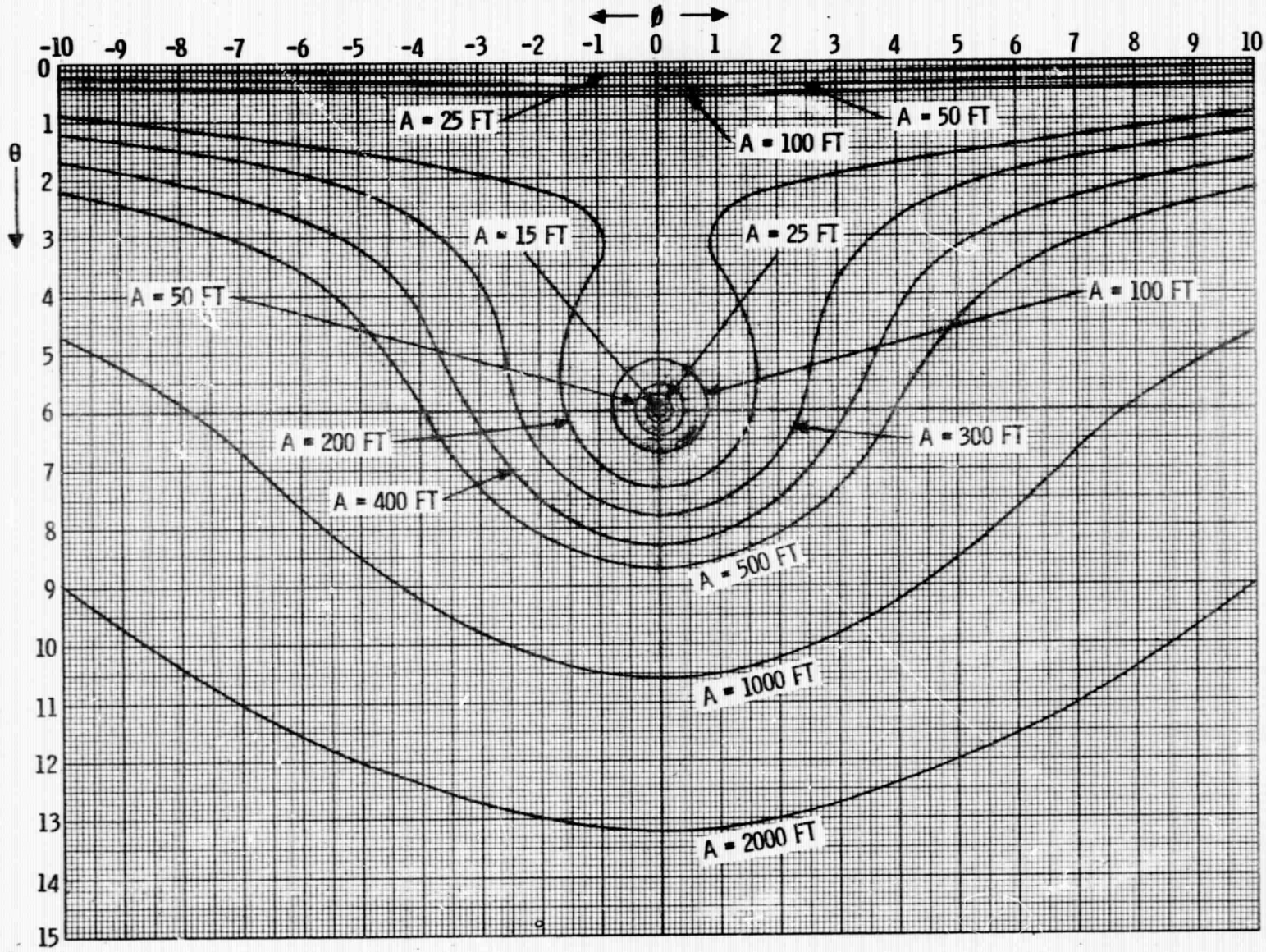

Figure 44. K-Curves for K=1/6 Deg/Sec, $\alpha = 6°$

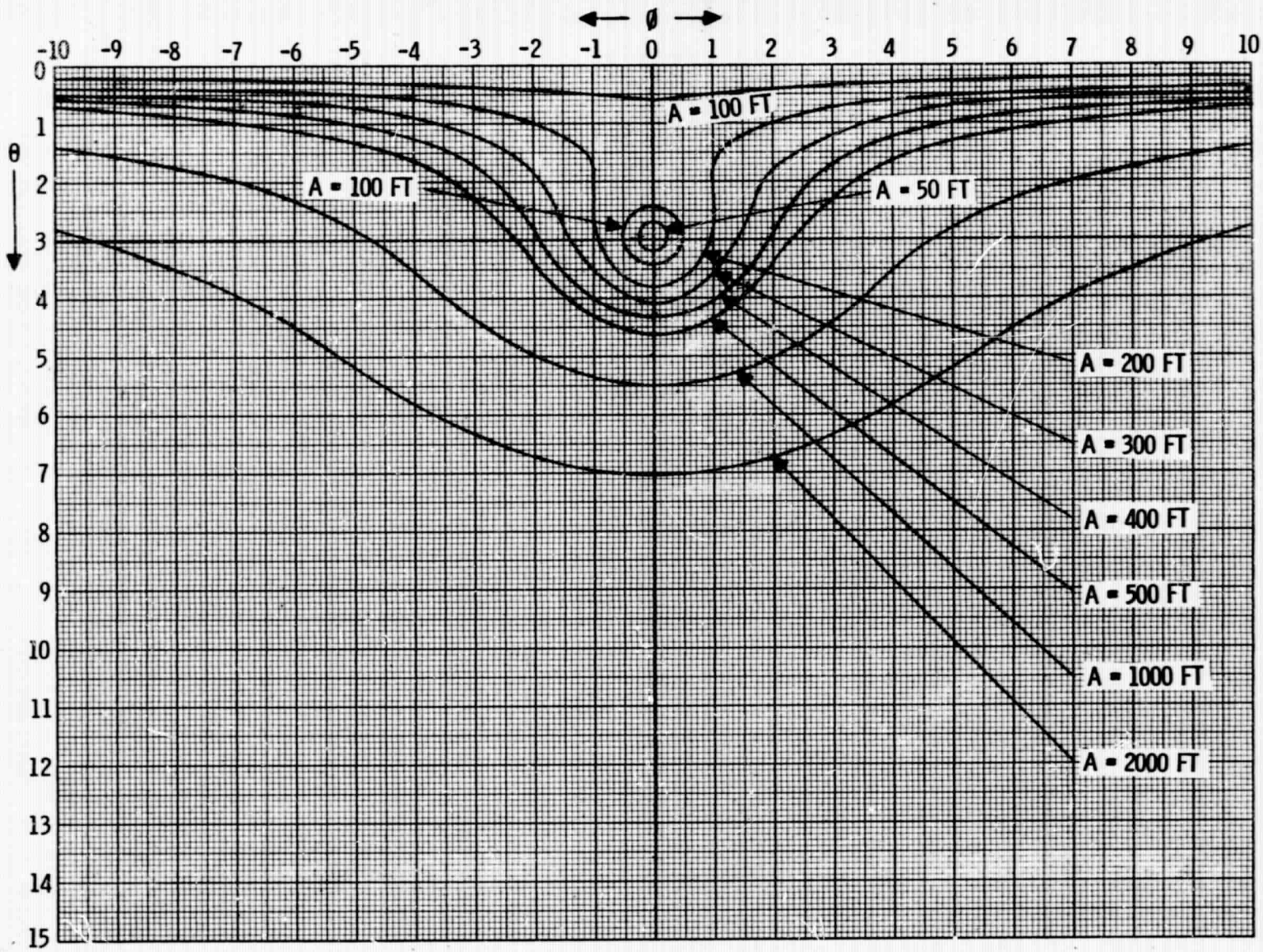

Figure 45. K-Curves for K=1/20 Deg/Sec, $\alpha = 3°$

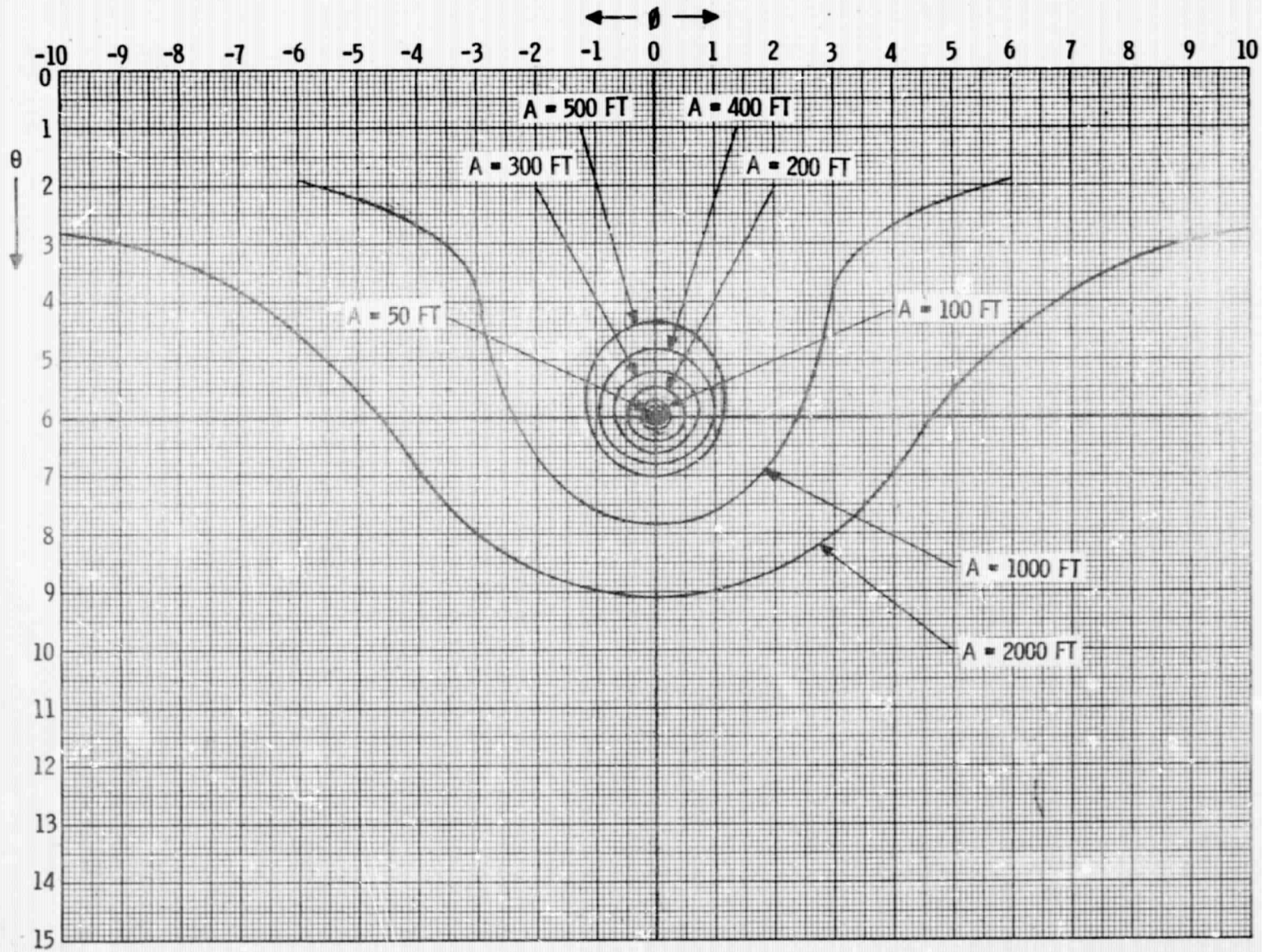

Figure 46. K-Curves for K=1/20 Deg/Sec, $\alpha = 6°$

Figures 47 and 48 are for K = 1/60 degree per second. The degree of improvement in accuracy associated with better detection thresholds is evident from the results presented in Figures 43 through 48. Note in particular that if an angular rate of 1/60 degree/second (this is a 10/1 improvement over the visual threshold) could be determined, then the impact point would be completely encircled at an altitude of 400 feet for a 3° descent slope or 1000 feet for a 6° descent slope. A reasonable method of estimating the impact point position from the distorted circle is to determine the intersection of the two lines which bisect the maximum and minimum depression angle and azimuth angle. This procedure would result in an error of 0.2° in the depression angle for a 3° descent slope at an altitude of 400 ft. For a 6° descent slope, this error would only be .05° at an altitude of 400 ft. These errors are quite small and become much less as the altitude becomes smaller. There would be essentially no error for altitudes $\leq$ 100 ft for the 3° descent and for altitudes $\leq$ 200 ft for the 6° descent. It would appear that some method of detecting these lower angular rates would be of considerable value and provide a better than visual landing capability.

5.4 MOTION CUE GUIDANCE HYPOTHESIS FOR MAXIMUM RADAR RANGE

An additional use of the isovelocity curves is in the determination of the maximum radar slant range required for an adequate presentation of the real-world situation. This maximum radar range would become the horizon of the vertical display. Our studies lead us to propose the concept that what the pilot requires as the horizon is not the earth-horizon but actually a line on the earth that is moving at his threshold for angular rate perception. We have termed this the "perceptual horizon," and it is approximated by the K-curve moving at 1/6 degree/second (as previously mentioned). It must be pointed out that this K = 1/6 degree/second curve is not a firm value for the angular rate perceptual threshold and therefore the perceptual horizon. Under some conditions, lower rates of motion may be detected, but it is probable that, under most conditions encountered in flight, the perceptual threshold for angular rate detection will be larger than 1/6 degree/second. For this reason, it is not necessary that the maximum radar range

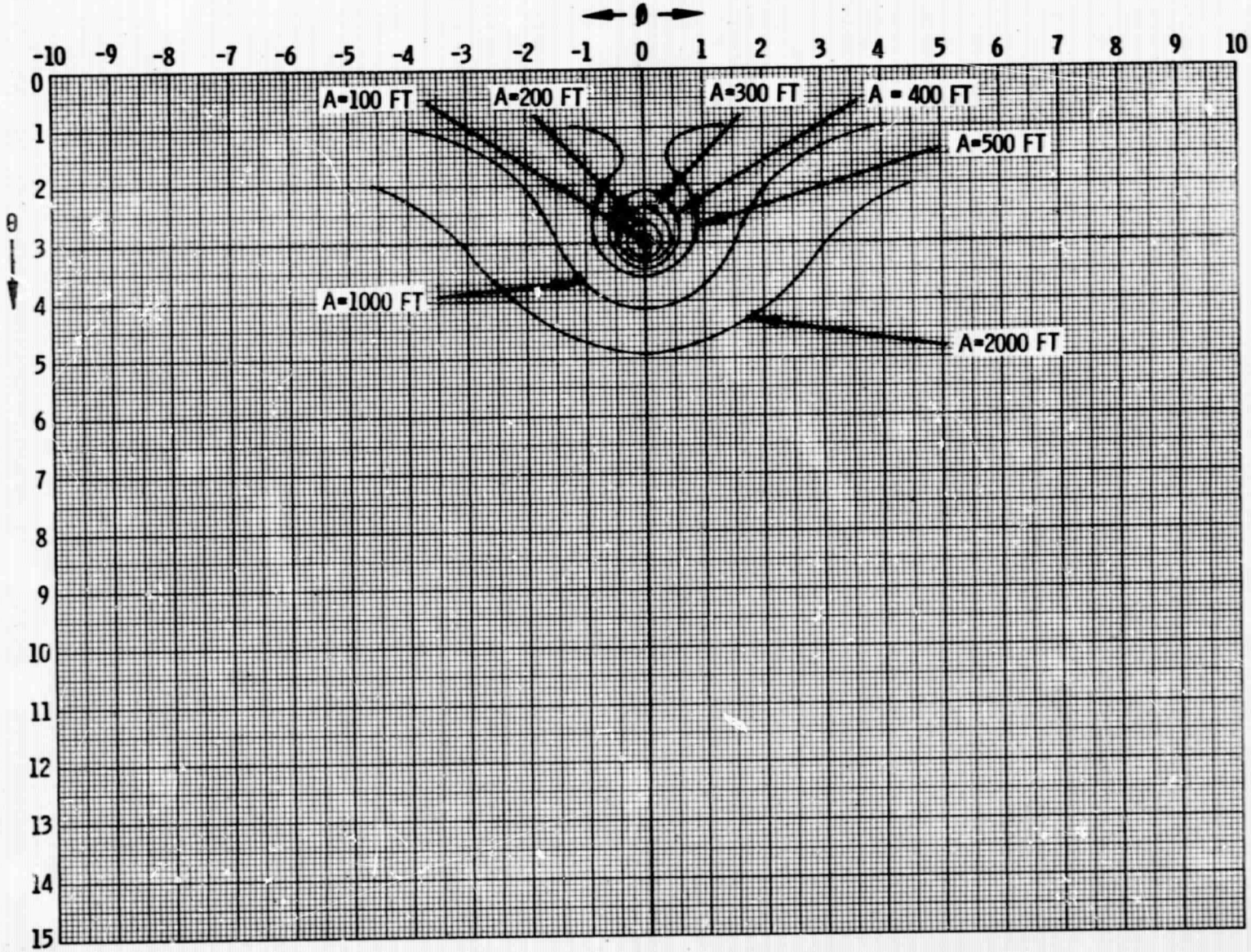

Figure 47. K-Curves for K=1/60 Deg/Sec, $\alpha = 3°$

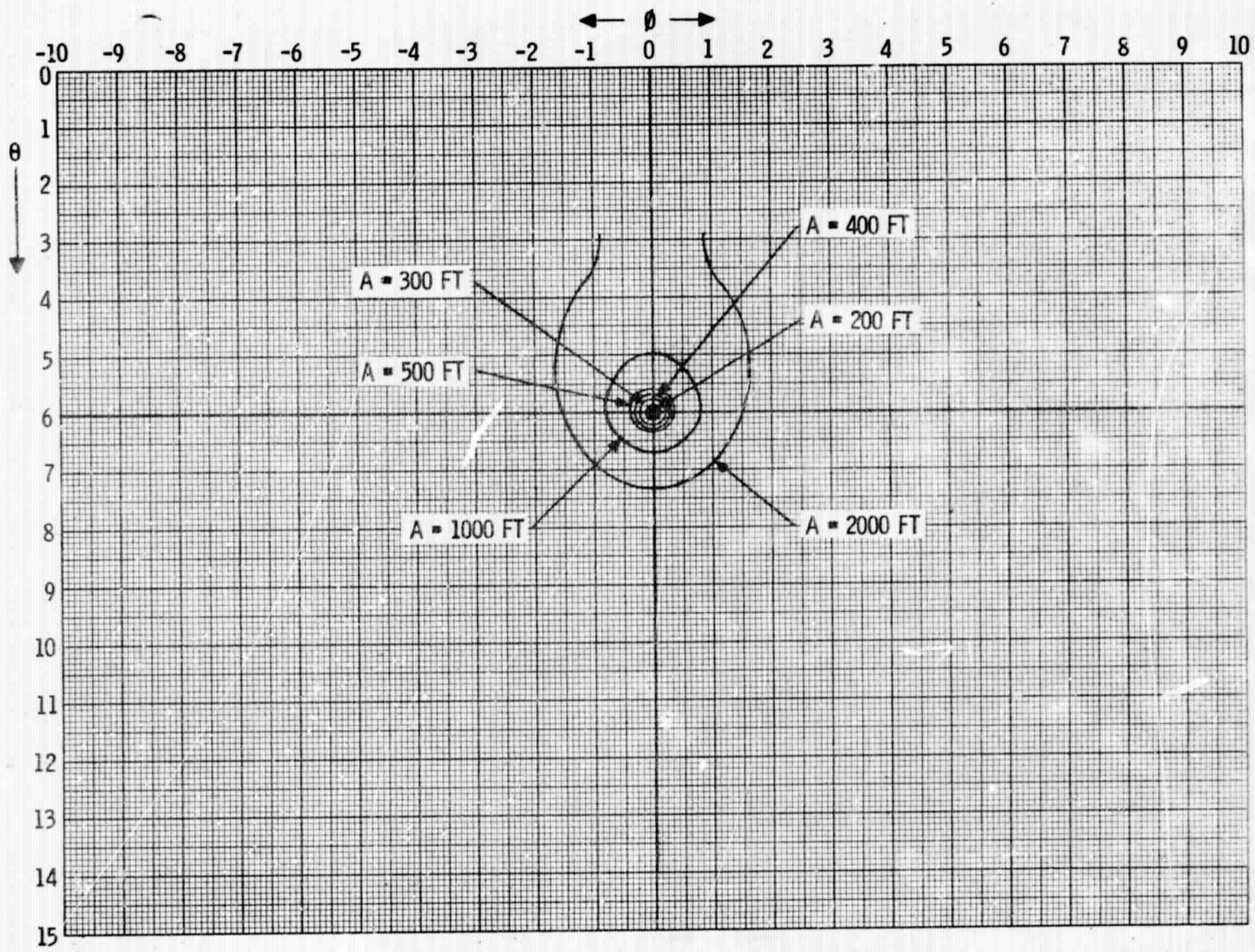

Figure 48. K-Curves for K=1/60 Deg/Sec, α = 6°

completely encompass the K = 1/6 degree/second isovelocity curve, but instead provide coverage of the ground which includes a portion of this curve and approximates the remainder by the "horizon."

Two horizon lines have been presented in each of Figures 20 through 39. The lower corresponds to the horizon that could result from use of a 10,000-ft maximum radar slant range and the upper represents the horizon that could result from use of a 15,000-ft maximum radar slant range. It is seen that the 10,000-ft slant range encompasses a large enough portion of the K = 1/6 degree/second curve to be considered the perceptual horizon by the above definition. The horizon for a 15,000-ft slant range provides a larger view of the earth and the runway, and goes beyond the K = 1/6 degree/second curve in the field of view. However, this goes beyond the hypothesis that all that is necessary is the perceptual horizon, and it cannot be assumed that the additional information gained will be worth the additional expense of the increase in maximum slant range required. For this reason, the maximum radar slant range required has been set at 10,000 ft. For a 3° glide slope, the 1/6 degree/second perceptual threshold along the runway centerline occurs at ranges of 10,000 ft and 5,000 ft for altitudes of 2,000 and 600 ft, respectively.

The FAA Visual Flight Rules visibility requirements are somewhat similar. FAR 91[22] implies that only one mile visibility is required when the pilot's primary function is landing and other air traffic is light or under special control. The FAA's one mile visibility "horizon" for a pilot flying a 3° glide slope, 120 kt velocity at a pattern altitude of 1000 ft would correspond with a motion threshold of approximately 1/3 degree/second. Thus, FAR 91 appears to support the technique.

5.5 MOTION CUE DETERMINATION OF DISPLAY/ANTENNA SCAN RATES

The display frame rate, which determines the scan rate of the antenna, is another display parameter which is determined using motion cues. To provide smooth motion of the runway outline, centerline, and surrounding terrain, it is necessary that during one frame period no terrain feature should pass through more than one angular resolution cell. Although the P^3I has much greater resolution than 1 degree near the horizon, the motion

rates occur at larger angles from the horizon and at the low altitudes where the CBRS is required.

The blur rate is as high as 30 degrees/second, with the exact magnitude dependent on visual factors. This velocity of terrain movement will be observed for a 120 knots approach at altitudes below 50 ft and after the aircraft has flared to the final approach angle of approximately 1/4 to 1/2 degree. (This was determined using the equation below, which is a simplification of Equation 15 of Appendix A for motion along the runway centerline:

$$K \approx \frac{V\theta\,(\alpha - \theta)}{57.3A} \quad \text{degrees/second}$$

Therefore, if a nominal 1-degree beam is used to scan a 30-degree field of view, the scan period should equal or be less than 1/30 second to ensure smooth motion up to the blur rate of 30 degree/second. Thus, an antenna should be provided with a scan rate of at least 30 frames/second.

6. P^3I IMPLEMENTATION

6.1 INTRODUCTION

The purpose of the circuit combination described in this section is to generate a pictorial representation of the forward view from the aircraft using video from an azimuth scanning antenna. The technique for generating this view uses a velocity-modulated fast vertical scan to provide a P^3I (Processed PPI) display. The vertical deflection waveform is a hyperbola whose exact shape is dependent on aircraft altitude. Use of this shape gives rise to a perspective representation in one-to-one geometric aspect to that which would appear in the normal forward view.

6.2 BLOCK DIAGRAM

The discussion will be presented in terms of the block diagram of Figure 49. This diagram shows the major elements required to present the desired display. The video amplifier is conventional and poses no special requirements for P^3I use. The horizontal sweep generator provides an output proportional to the azimuth angle of the antenna, at a suitable scale factor for the basic scope; it also provides an auxiliary output for the roll portion of the attitude correction circuit. Attitude insertion accepts one signal from each axis of a conventional attitude gyro, and operates only with slow waveforms. The vertical sweep generator accepts an altitude input and the transmitter trigger and generates the fast, nonlinear sweep that is the heart of the P^3I system. The shading amplifier developes compensation for the changes in velocity (writing rate) of the sweep.

The vertical sweep has been described as the heart of the P^3I system. The equation and some of the properties are presented in Appendix C, along with plots of typical cases.

The present program included an evaluation and experimental study of several ways of synthesizing, to suitable accuracy, the required family of curves.

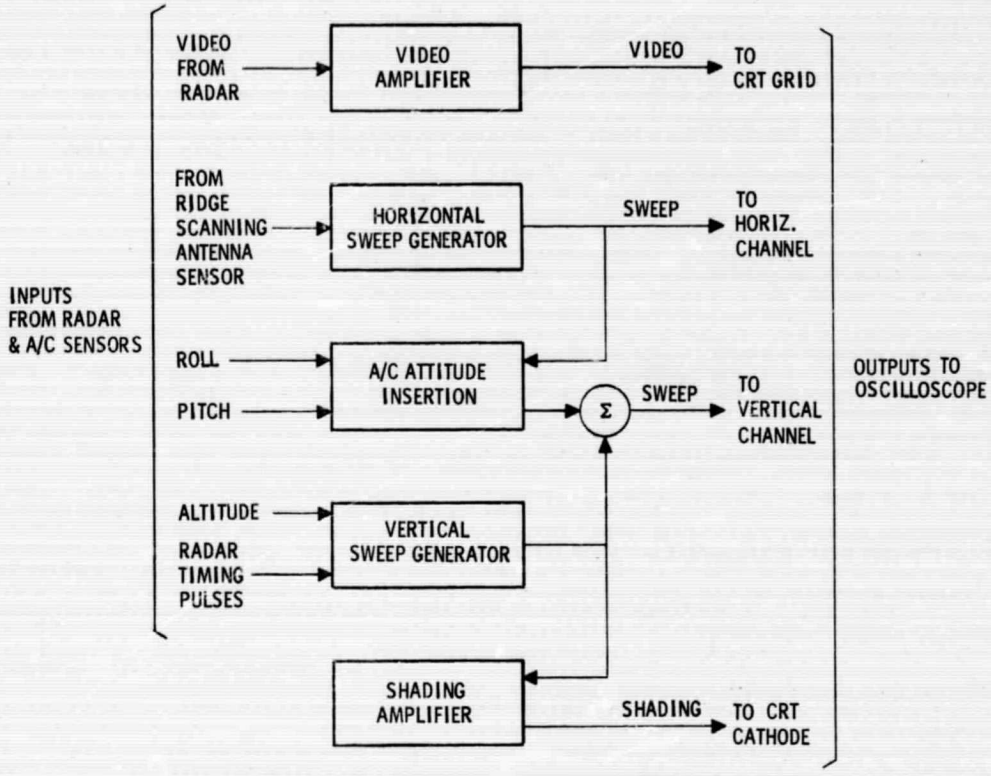

Figure 49. P^{3}I Display Block Diagram

The method selected, both for the experimental program and for later flight hardware, uses a sum of exponentials. This choice is justified in Appendix D.

6.3 EXPERIMENTAL ELECTRONICS

The overall block diagram of the P^3I display unit is shown in Figure 49. The basic indicator is a Fairchild 765 MH oscilloscope, which is militarized and uses a 5-inch CRT. It has cavities for plug-in amplifiers in both horizontal and vertical deflection channels. A video amplifier, following the schematic of Figure 50, was added to the scope. A one-volt positive pulse input causes full spot unblanking. Frequency response is in excess of 5 MHz.

The horizontal sweep generator supplies to the horizontal channel of the scope a signal which is a replica of the horizontal scan pattern of the antenna.

Referring back to Figure 49, the A/C Attitude Insertion block inserts roll and pitch information into the display, in accordance with equation C-2 of Appendix C. The circuitry used to accomplish this with manual roll and pitch inputs is described below. In order to use electrical roll and pitch inputs, different circuitry, discussed in Appendix E, must be used.

The shading amplifier differentiates the hyperbolic sweep waveform, amplifies the result, and applies it to the CRT cathode to vary the intensity. This compensates for intensity variations due to the nonlinear writing rate. In this circuit, given in Figure 51, the input network, consisting of two capacitors, one resistor, and three diodes, performs the necessary differentiation. The remaining circuitry is simply linear amplification.

For the P^3I system testing described in Section 7, a single exponential-waveform generator was used to approximate the hyperbolic waveform required for vertical scan. This signal was then added to the required functions of roll and pitch to produce the signal for driving a Fairchild Type 74-19 amplifier plugged into the left cavity of the 765 MH scope.

The circuit used is given in Figure 52. The value of C_1 was 150 pF; C_2 and C_3 were not used. The input pulse came from a pulse generator triggered by the radar timing generator. Altitude control was a 50 kilohm potentiometer. A field-effect transistor (FET) was used to provide a low impedance for driving

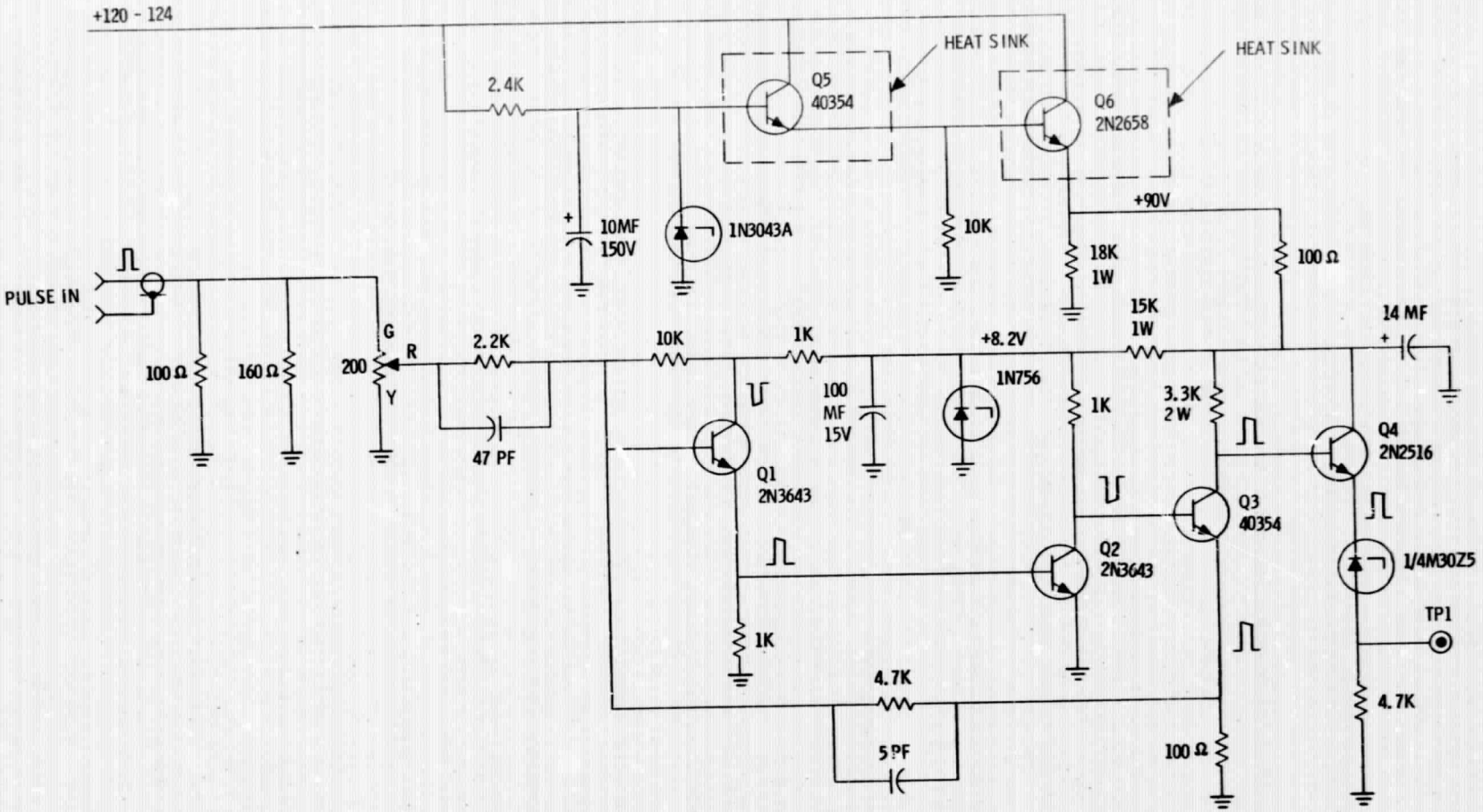

Figure 50. Video Amplifier Schematic

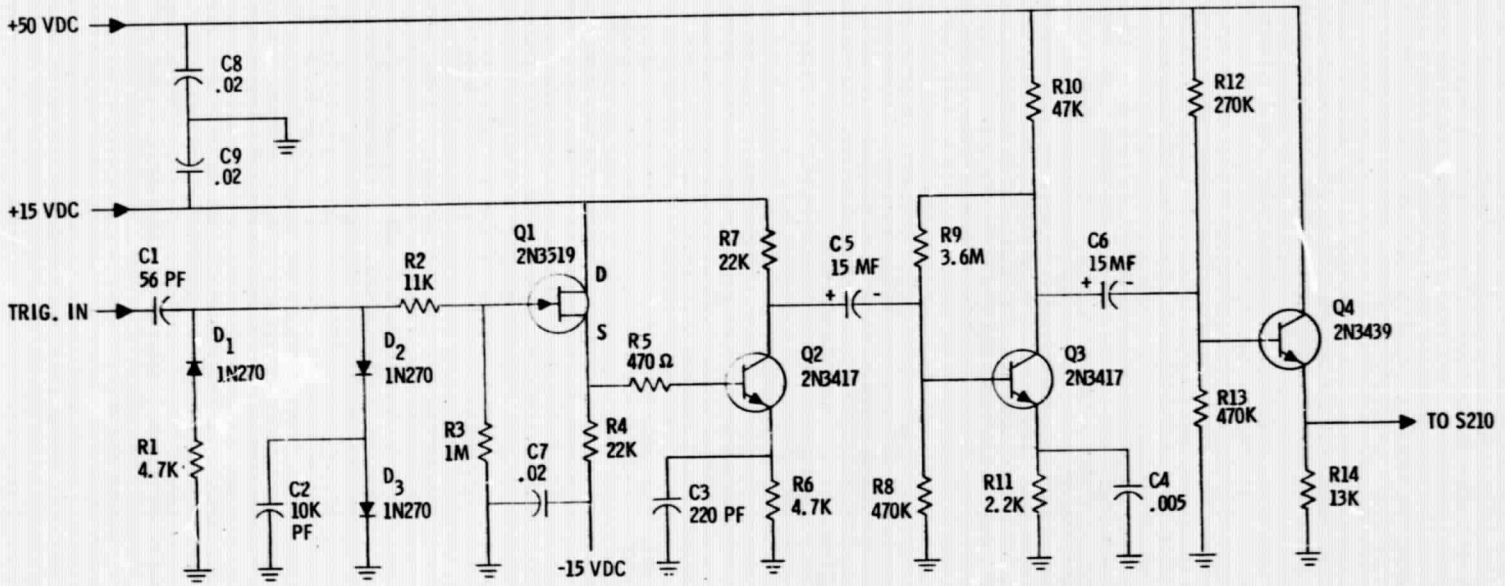

Figure 51. Shading Amplifier Schematic

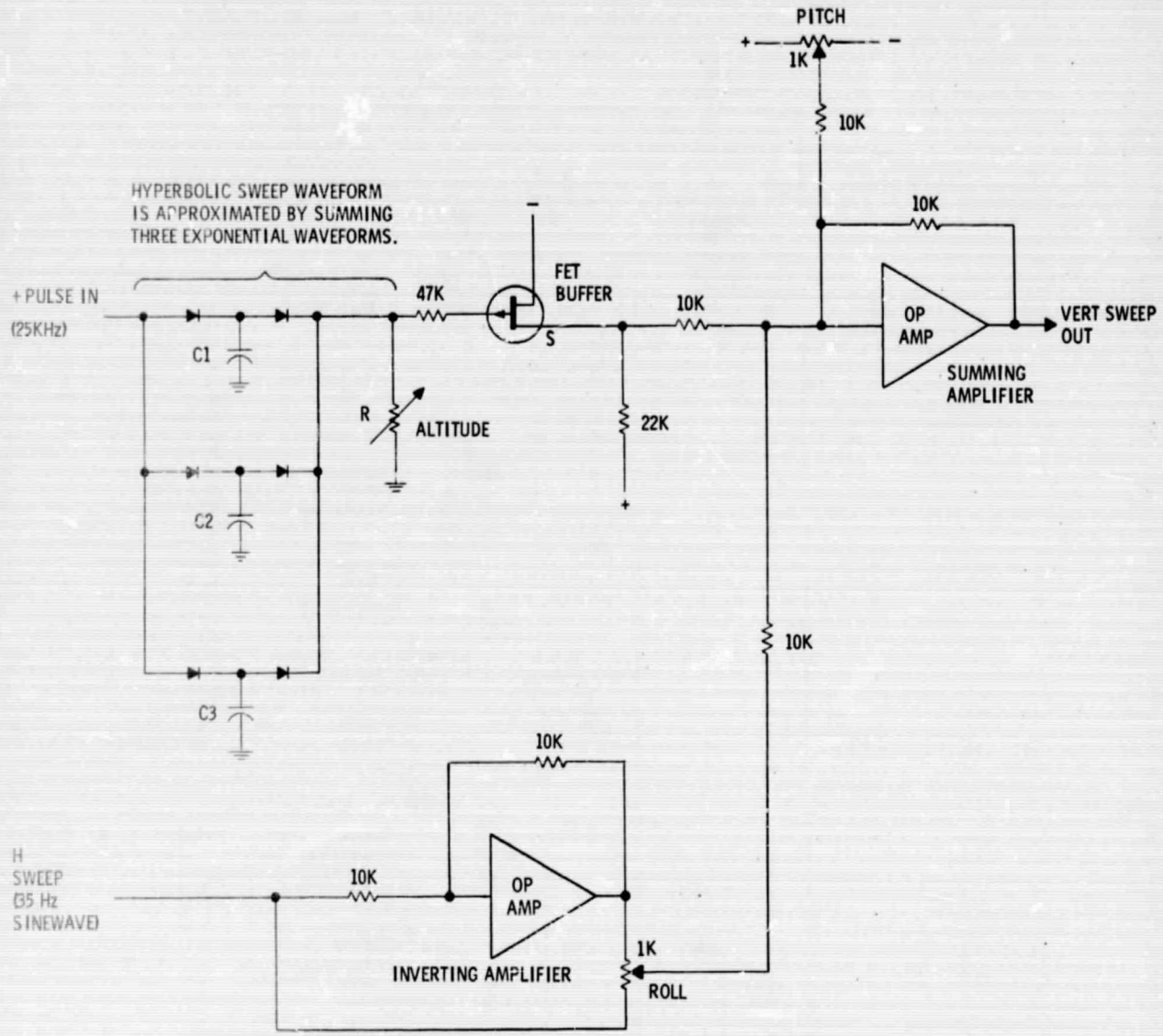

Figure 52. Circuitry for P^{3}I Vertical Sweep Generator Using Manual Altitude, Roll, and Pitch Inputs

the following stage without loading the exponential-waveform generator. The output from the FET is the exponential sweep waveform. Subsequent attitude processing is accomplished by adding roll and pitch voltages to that waveform.

The pitch voltage comes from a 1000-ohm potentiometer acting as a voltage divider across the +15 and -15 volt power supplies, as shown. The setting of the potentiometer is proportional to the pitch angle; a setting of mid-scale provides zero volts, which corresponds to zero pitch.

The roll signal must be multiplied by the horizontal sweep signal. This is accomplished by applying a push-pull horizontal sweep signal across a 1000-ohm potentiometer. The setting of this potentiometer is proportional to the tangent of the roll angle; a mid-scale setting provides zero signal corresponding to zero roll angle.

A positive 15-volt and a negative 15-volt power supply was used to supply power to the vertical and horizontal sweep circuitry. Diagrams of these power supplies are shown in Figure 53. All other power required was taken from the 765 MH scope.

6.4 RESULTS

In addition to the system test results described elsewhere in this report, the experiments using the circuits described above gave rise to a clearer notion of what hardware might be suitable for flight use. Considerable study effort was also devoted to elaboration of these notions. The results, presented in Appendix E, are techniques chosen to make use of components within the state-of-the-art and to emphasize simplicity and ease of test.

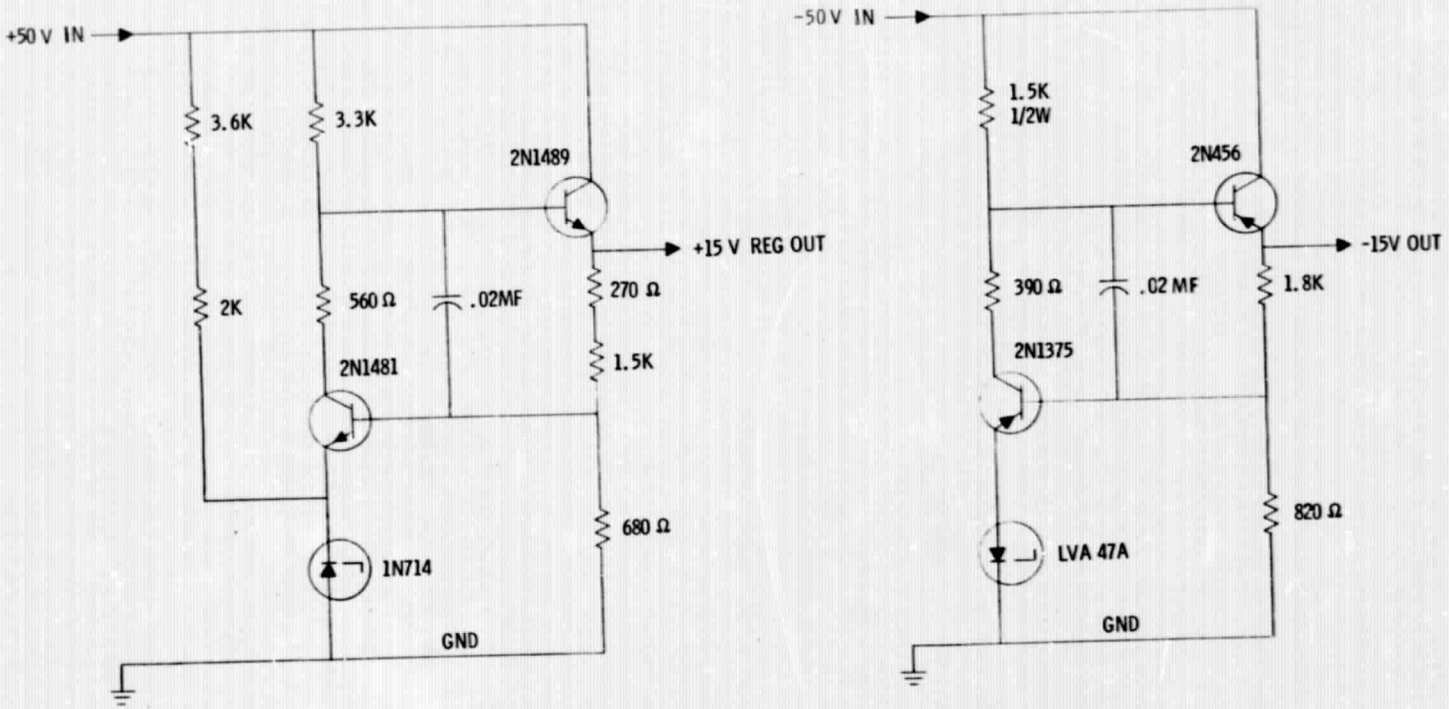

Figure 53. Positive and Negative 15-Volt Power Supplies

7. P^3I SYSTEM TEST

In October and November of 1967, testing of the first P^3I system/display was performed at the Plainfield facility of Lockheed Electronics Company. This testing was intended, (1) to demonstrate the feasibility of electronically (rather than optically) producing such a display, and (2) to demonstrate the ridge scanning antenna. The excellent results obtained are self-evident in Figures 58 and 59.

7.1 SYSTEM DESCRIPTION

A breadboard system was assembled, consisting of a vacuum tube transmitter and receiver, ridge scanning antenna, and P^3I display. Also included were control circuits, power supplies, and other test components intended to provide the flexibility required for system evaluation. The P^3I display subsystem used during testing was described in Section 6. The following sections describe the radar subsystem and the antenna used for testing.

a) Radar Subsystem. - Figure 54 shows the block diagram of the laboratory breadboard radar subsystem. The Ku band RF output pulse from the transmitter has a pulse width of 0.1 microsecond and a peak power of 2 kW. Radar pulse repetition frequency (approximately 24 kHz) and the transmitter input trigger are generated by a laboratory pulse generator. Primary power required for the transmitter is 115V AC at 400 Hz. The transmitter RF output is isolated from the load VSWR by a load isolator. A circulator is utilized for transmit and receive signal switching. The RF transmit signal output from the circulator is connected to the ridge scanning antenna through a directional coupler used for test purposes.

The Ku band RF signal received from the ridge scanning antenna passes through the test directional coupler and receive ports of the circulator to the TR tube. The TR tube functions to limit the peak leakage power of the RF transmitted pulse, which couples through the circulator to the receiver. The received signal out of the TR tube is mixed to a 60 MHz IF and amplified

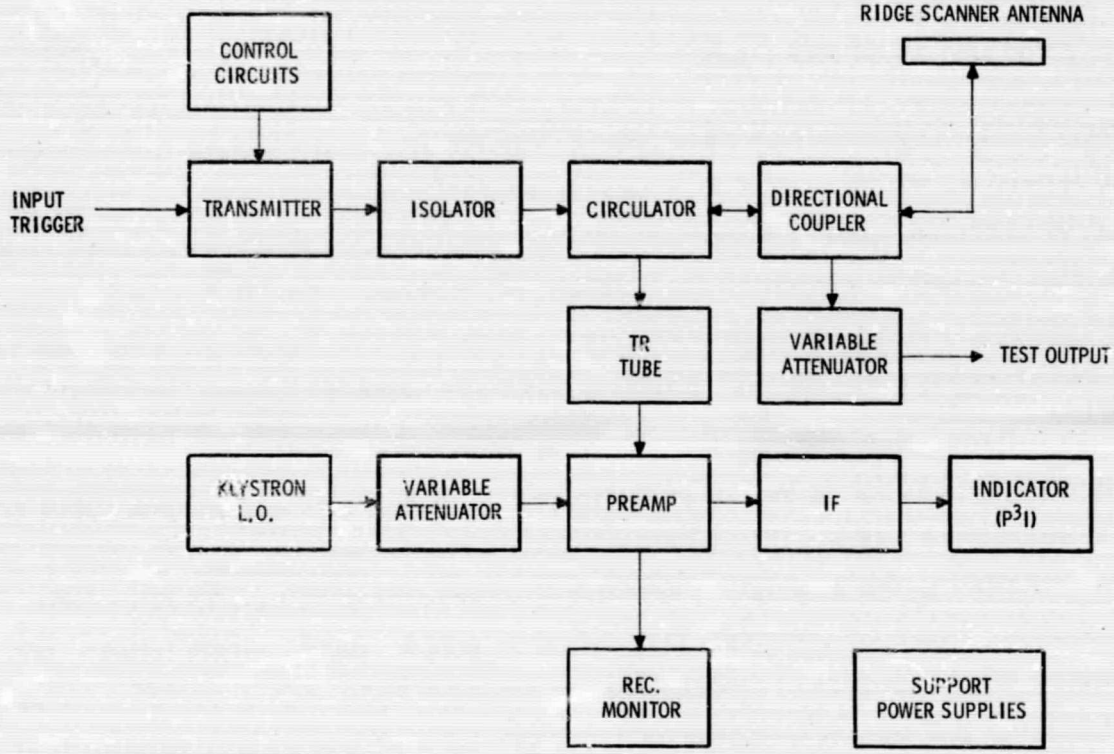

Figure 54. General Block Diagram of Laboratory Breadboard Radar Subsystem

at IF by the preamplifier following the mixer. The Ku band local oscillator power required for mixing is generated by a manually tuned klystron oscillator whose output is connected to the mixer through a variable attenuator. The IF signal out of the preamplifier is further amplified logarithmically and detected in the log IF amplifier. The detected output video from the log IF amplifier is connected to the P^3I display where it is further processed.

b) Variable Ridge Scanning Antenna. - An experimental electromechanical variable ridge scanning antenna, similar to the one reported in References 29 and 30, was designed and fabricated as the antenna to be used in testing. This antenna, shown in Figures 55 and 56, consists of a radiating array with a ridged transmission line. The depth to which this ridge may be inserted into the array is variable and changes the length of the wave in the transmission line. This, in turn, will change the scanning angle. Variation of the ridge insertion depth is accomplished by a series of seven scotch yokes driven by an eccentric shaft.

Azimuth scan angle is determined by a pick-off consisting of a magnet attached to the end of one of the scotch yokes moving through a coil. This movement produces a sinusoidal output that must be phase-shifted 90° to provide a properly phased output to the display. The output from the phase-shifting network gives a voltage which is directly proportional to the scan angle of the antenna. Azimuth beamwidth is approximately 1.2 degrees.

The antenna is driven by a variable speed motor. Testing was performed at a reduced scan speed of 6 revolutions (12 frames) per second, compatible with the filming technique used. In order to provide a flickerless display for in-flight use, the antenna can be driven at 30-35 revolutions (60-70 frames) per second.

7.2 TEST DESCRIPTION AND RESULTS

Testing was performed in a 100 foot high tower at the Lockheed Electronics Company Plainfield facility. All equipment was housed in the upper part of the tower, shown in relation to the surrounding terrain in Figure 57. The P^3I display had a 26° azimuth field of view and a 15° depression (25° total vertical) angle field of view, with vertical sweep waveform corresponding to a 100 feet altitude. Radar data was obtained with 1.2° azimuth resolution and

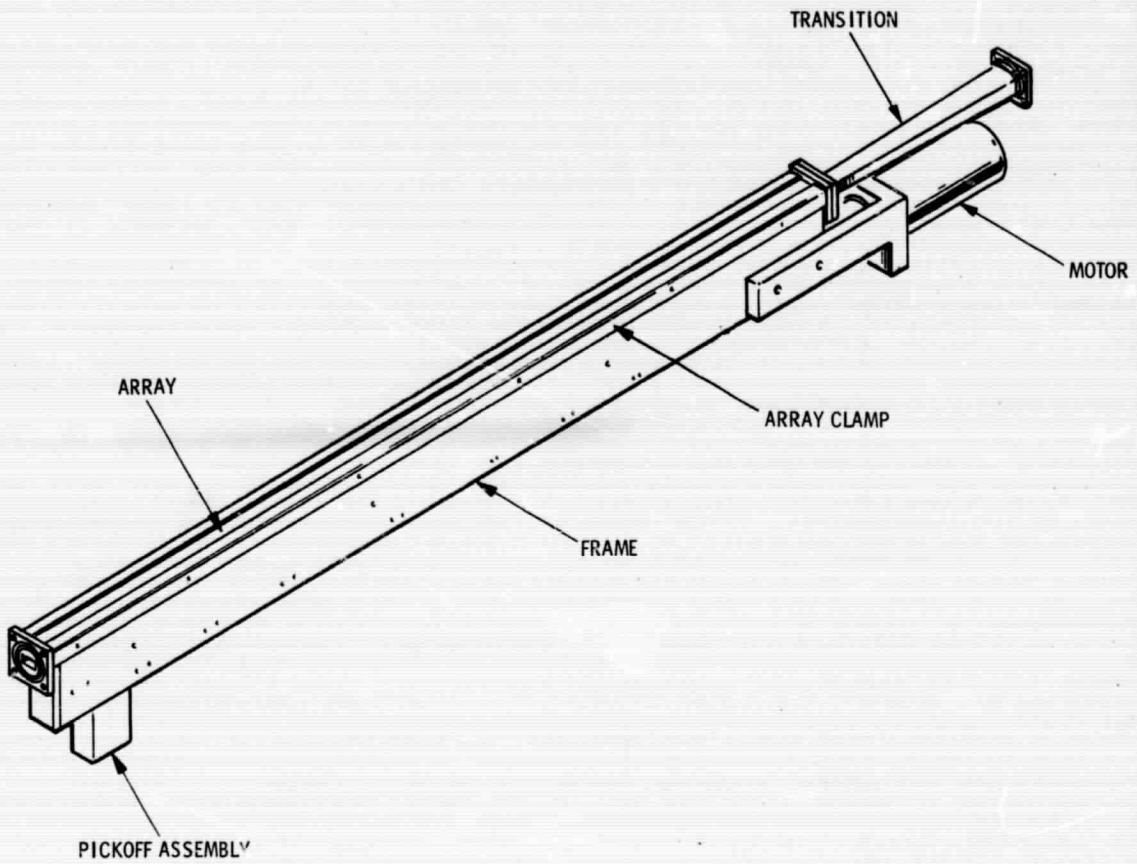

Figure 55. Variable Ridge Scanning Antenna Assembly

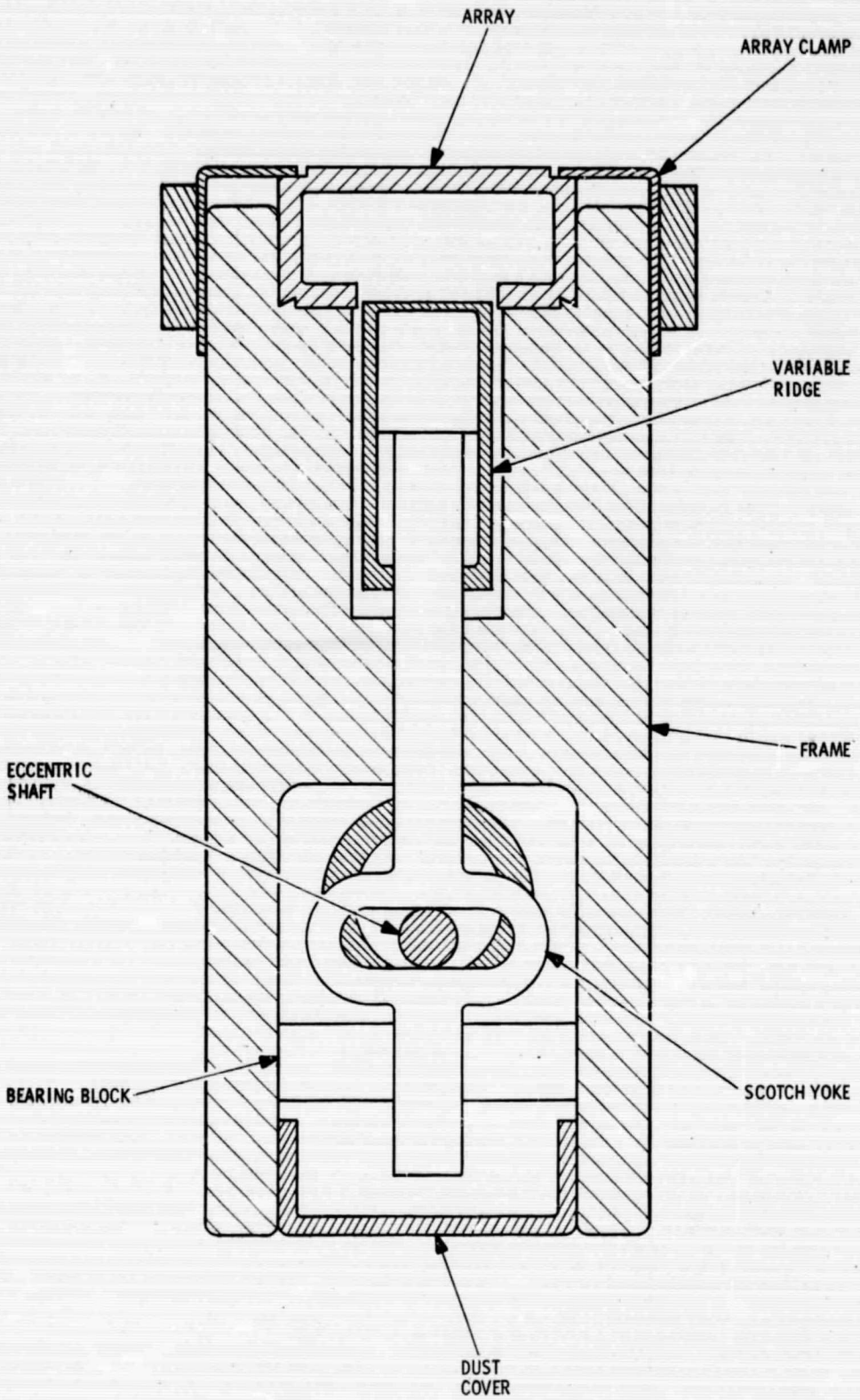

Figure 56. Variable Ridge Scanning Antenna Cross Section

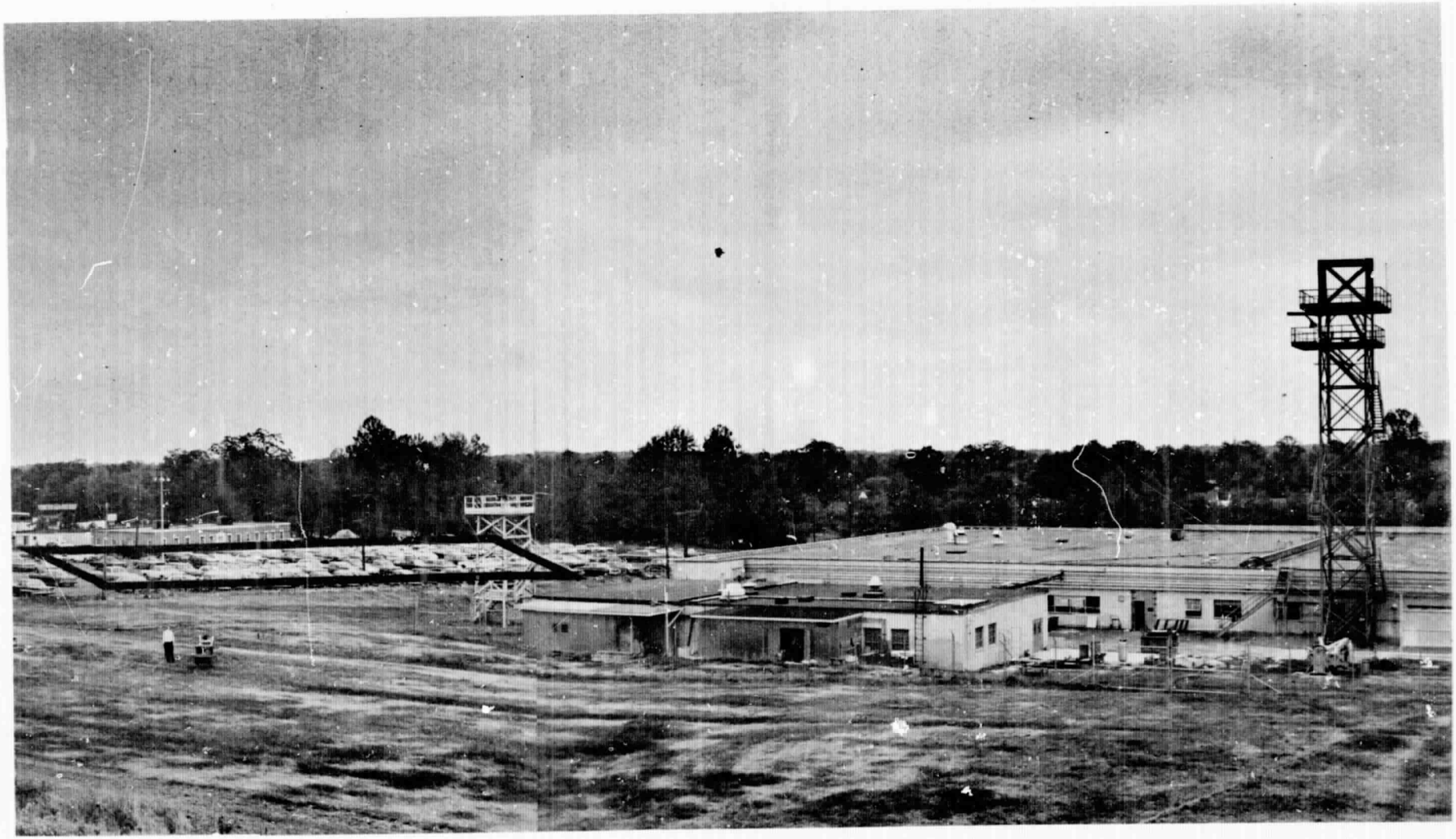

Figure 57. Tower and Ground Area Used in P^3I System Testing

50 foot range resolution. System values used during testing are summarized in Appendix B, except that the scan rate used during testing was 12 frames per second.

Initial adjustment of the system was performed using a 1.2° azimuth beamwidth manually scanned antenna. This resulted in a general familiarity with the radar signature of the surrounding terrain as it appeared on the P^3I display. The ridge scanning antenna was used after the system was adjusted to a satisfactory level of performance.

The most valuable data collected were photographic records of the P^3I display appearance. Still photos were taken using a scope-mounted Polaroid camera, and were compared against photos of the terrain. The Giannini Multidate Model III-B camera used in the LEC helicopter radar program obtained movies of the P^3I display. This electric film advance camera was synchronized to the ridge scanning antenna so that one movie frame was advanced and exposed each time the ridge came to its "out" position (1 revolution or 2 display frames). The ridge scanning antenna was driven at 6 revolutions per second, resulting in a film exposure rate of 6 frames per second and an exposure time of approximately .08 second, during which one complete display frame was presented.

The bulk of the testing evolved about evaluation of the P^3I perspective. Passive radar corner reflectors were arranged in various ground patterns -- triangles, squares, rectangles, etc. -- in the LEC parking lot area shown in Figure 57. The perspective view of these patterns as seen from the tower was photographed and measured in azimuth and depression angle by a transit, enabling the comparison of P^3I perspective and visual perspective. In general, the agreement between visual and P^3I perspective was excellent. This is demonstrated by Figures 58 and 59, showing photographs copied from experimental movie film. Figure 58 shows photographs of a simulated runway obtained by placing 12 corner reflectors in a rectangle that was 32 feet across and 350 feet long, with the horizontal rows perpendicular to the line of sight and 70 feet apart and the vertical rows skewed to the line of sight. In perspective, the base of the rectangle was 5.5° wide and the top 2.5° wide. The first 10 corner reflectors were accompanied by high-intensity lights, resulting in the visual perspective photo on the top. The P^3I perspective

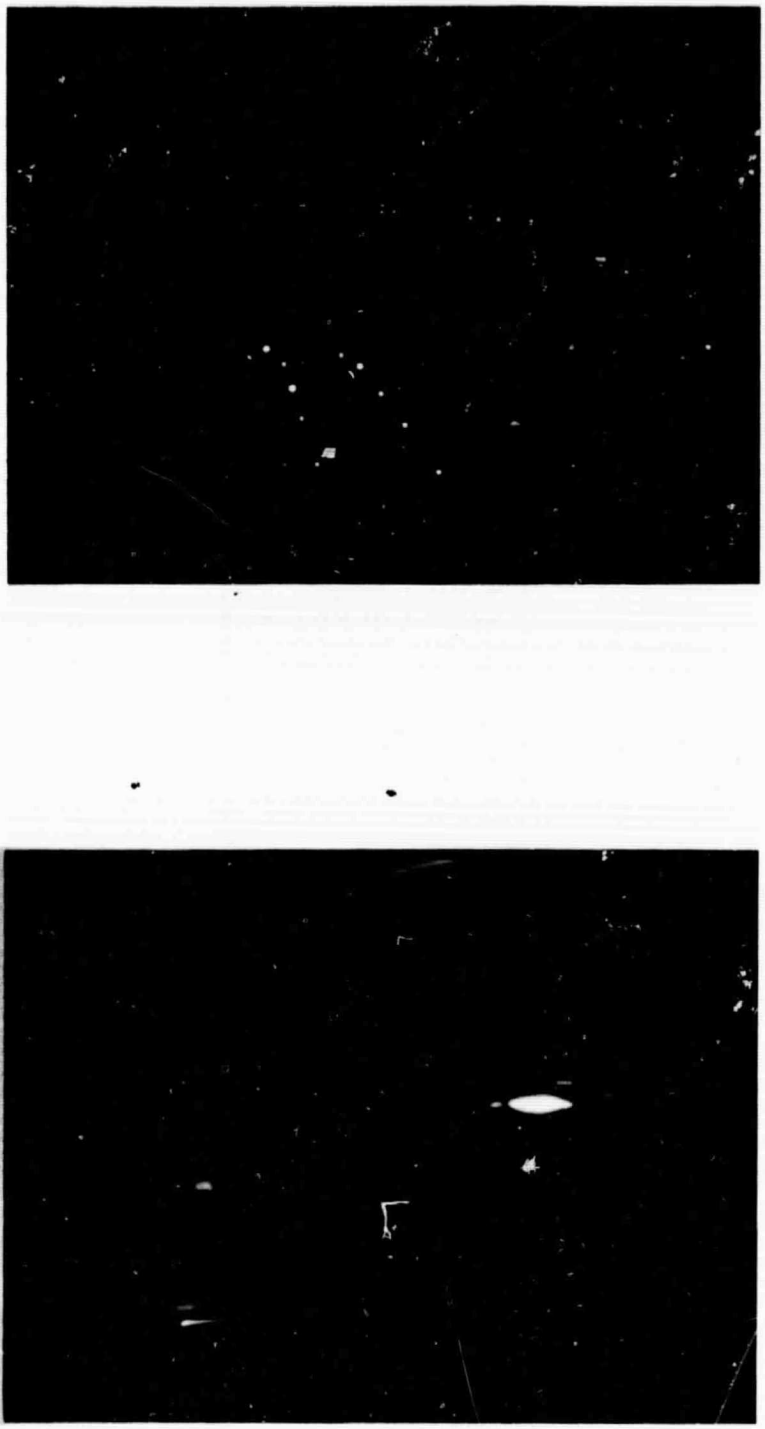

Figure 58. Perspective Appearance of Runway as Seen Visually and on P^3I Display

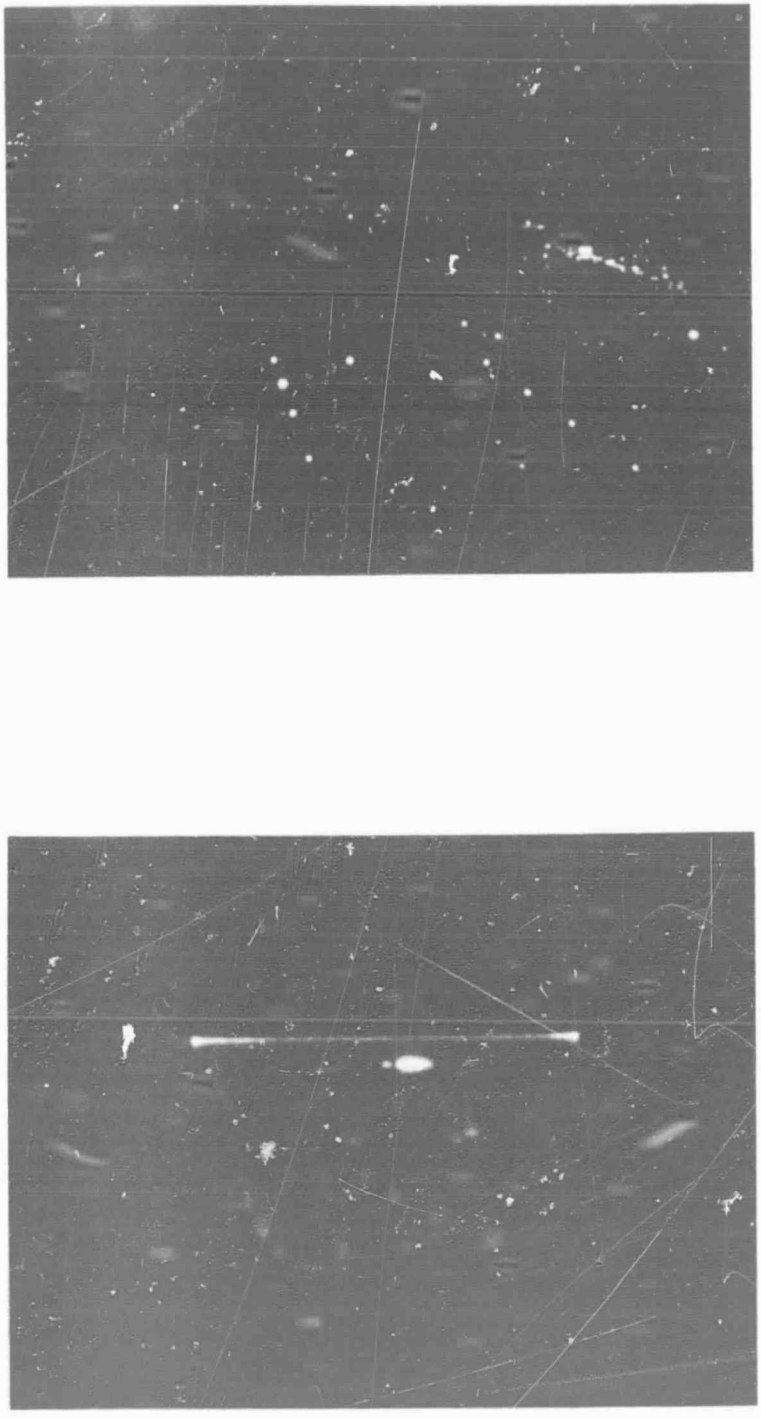

Figure 59. Perspective Appearance of Landing Pad as Seen Visually and on P^3I Display

view of the 12 reflectors, in a slightly smaller scale than the visual, is shown on the bottom, with the close agreement between P^3I and visual perspective being obvious. This simulates the perspective appearance of a 150-foot wide runway as seen from approximately 125 feet altitude of a 3° landing approach or 250 feet altitude of a 6° approach, both toward an aiming point 1000 feet beyond threshold. Figure 59 demonstrates the visual and P^3I perspective appearance of a landing pad 100 feet across and 200 feet long which is outlined by 12 reflectors and 10 lights, spaced 33 feet apart in horizontal rows perpendicular to the line of sight and 67 feet apart in rows skewed to the line of sight. As viewed from the antenna, the pad is 15° across at the base and 5° high, corresponding to the perspective appearance of the pad as seen from approximately 80 feet altitude on a 10° approach toward the center of the pad. Again, considering the scale difference, the P^3I and visual perspective agreement is quite good.

8. RECOMMENDATIONS FOR FURTHER ACTION

The feasibility of the basic P^3I system has been demonstrated, using manual inputs for altitude and attitude and a breadboard system configuration. The main recommendation is that the results obtained during the present contract period be applied to the fabrication of a flying, dynamic, experimental model of the complete P^3I system. This system would include a 60 inch, 1.0° azimuth beamwidth ridge scanning antenna, a 1° elevation beamwidth passive cross-beam antenna for registration, a 2 kW Ku-band transmitter to produce 0.1 μsec pulses at a 25 kHz repetition rate, and a suitable display with at least a 25° by 25° field of view. This system would undergo checkout and adjustment through flight-test in LEC's FH-1100 helicopter prior to installation in the NASA-Ames Convair 340. (This system is described in detail in LEC's proposal to NASA-Ames for a follow-on to the study reported herein.)

It is also recommended that analytical studies be continued to support and advance in-flight research efforts. Included would be feasibility and design studies toward the fabrication of the CBRS system. Study may also be applied to the integration of additional information into the basic P^3I display, such as a ground track line, altitude information, aiming point identification, and flight director information. The feasibility of automatic registration and of making the P^3I system independent of external altitude inputs (through cross-beam use) should also be investigated. Motion cue analysis should also be continued; in particular, it may be possible to electronically outline the instantaneous aiming point by an isovelocity curve or through storage of several key ground returns.

The basic P^3I concept of a radar-derived, aircraft-contained landing display/system has been demonstrated. Work should now be centered on bringing such a system to the level of in-flight performance and sophistication which will enable "better than visual" landings under zero-zero conditions.

9. REFERENCES *

1. Contract NAS2-4091, NASA-Ames Research Center to Lockheed Electronics Company, Plainfield, New Jersey.
2. "Research Study of an Aircraft-Contained Radar Zero-Zero Landing System - First Quarterly Report," Lockheed Electronics Company, Plainfield, New Jersey, April 1, 1967.
3. "Research Study of an Aircraft-Contained Radar Zero-Zero Landing System - Second Quarterly Report," Lockheed Electronics Company, Plainfield, New Jersey, July 1, 1967.
4. "Research Study of an Aircraft-Contained Radar Zero-Zero Landing System - Third Quarterly Report," Lockheed Electronics Company, Plainfield, New Jersey, Oct 1, 1967.
5. Van Sickle, N. D. "Modern Airmanship," Van Nostrand, Princeton, New Jersey, 1961.
6. Wulfeck, J. W. et al, "Vision in Military Aviation," WADC TR 58-399, ASTIA 207 780, Nov., 1958.
7. Stevens, S.S. "Handbook of Experimental Psychology," Wiley, New York, 1951.
8. Lane, J.C. and Cumming, R. W., "The Role of Visual Cues in Final Approach to Landing," Human Engineering Note 1, Aeronautical Research Laboratories, Melbourne, Australia, May, 1956.
9. Baxter, J.R., and Workman, J. D., "Review of Projected Displays of Further Development," Human Engineering Report 2, A. R. L., Melbourne, Australia, August, 1962.
10. Baxter, J.R. "Projected Symbolic Displays for General Aircraft," Human Engineering Note 14, A.R.L., Melbourne, Australia, March, 1963.

---

* Superscript numbers in text correspond to reference numbers.

11. Havron, M. D. "Information Available From Natural Cues During Final Approach and Landing," Human Sciences Research, Inc., ASTIA 285 598, March, 1962.
12. Leary, F. "All-Weather Landing - When?," Space/Aeronautics, February, 1966, pp. 82-94.
13. Litchford, G. B. "The 100-ft Barrier," Astronautics and Aeronautics, July, 1964, pp. 58-90.
14. Woodson, W. E., and Conover, D. W., "Human Engineering Guide for Equipment Designers," 2nd Ed., University of California Press, 1964.
15. Roscoe, S. N., et al, "Flight by Periscope: Making Takeoffs and Landings; The Influence of Image Magnification, Practice, and Various Conditions of Flight," Human Factors, Feb, 1966., pp. 13-40.
16. Kuhlman, R. L. "Approach with Care," Flying, April, 1966, pp. 88-90.
17. Kelley, C. R., et al, "Some Relative Motion Problems in Aviation," U.S. N. Training Device Center, ASTIA 256 346, Jan., 1961.
18. Proposal to NASA-Ames for a Self-Contained Zero-Zero Landing System; D. W. Young and Associates (Subsequently Lockheed Electronics Company, Plainfield, New Jersey), Aug. 29, 1965.
19. Reeder, J. P., "The Impact of V/STOL Aircraft on Instrument Weather Operations," NASA TN D-2703, Feb., 1965.
20. Reeder, J. P., and Kolnick, J. J., "A Brief Study of Closed-Circuit Television for Aircraft Landing," NASA TN D-2185, Feb., 1964.
21. Kibort, B. R., and Drinkwater, F. J., "A Flight Study of Manual Blind Landing Performance Using Closed Circuit Television Displays," NASA TN D-2252, May, 1964.
22. Federal Aviation Regulations, Part 91, "General Operating and Flight Rules."
23. "Vision from Low-Flying Aircraft"; Autonetics: Anaheim, California, EM-1162-103, April 6, 1962.
24. Erickson, R. A., "Visual Detection of Targets: Analysis and Review," U.S. Naval Ordnance Test Station, China Lake, California, February, 1965.
25. Graham, C. H., et al, "Vision and Visual Perception," Wiley: New York, 1965.

26. Young, D. W., Leffel, A. H., and Allen, L. E., "Rotor Blade Antenna Program - PPI Display-Radar-System and Crossed Beam Scan," Rpt 114-005-0011, Lockheed Electronics Company, December 4, 1965.
27. Young, D. W., and Lindenmeyer, L., "Rotor Blade Radar Antenna, Phase I," Bell Helicopter Company, TR No. 299-099-251, January, 1965.
28. Young, D. W. and Palmer, J. E., "Rotor Blade Radar Antenna, Phase II," Bell Helicopter Company, TR No. 299-099-275, ASTIA No. AD-426-744, February, 1965.
29. Young, D. W. "High Speed, Raster Scanning, High Resolution, Radar Sensor for Vertical Display," JANAIR Interim Report, David W. Young and Associates, Inc., ASTIA No. 435-558, July 30, 1963.
30. Young, D. W., "High Speed, Raster Scanning, High Resolution, Radar Sensor for Vertical Display," JANAIR Final Report, Contract Nonr 4032(00), David W. Young and Associates, Inc., July 30, 1964.
31. Soller, T., et al, "Cathode Ray Tube Displays," MIT Radiation Lab Series, Vol. 22, McGraw-Hill, 1948, pp. 384-401.
32. Chance, B., et al, "Waveforms," MIT Radiation Lab Series, Vol. 19, McGraw-Hill, 1949, pp. 301-305.
33. Marcum, J. I., and Swerling, P. "Studies of Target Detection by Pulse Radar," IRE Transactions on Information Theory, Vol. II-6, No. 2, April, 1960.
34. Skolnik, M. I. "Introduction to Radar Systems," McGraw-Hill, 1962.
35. Amendola, J. L. "Effective Radar Cross-Sectional Area of the Terrain as Applied to the Helicopter Radar Program (AAFSS Application)," Lockheed Electronics Company, Rpt. 28-6100-JLA-3, June 27, 1966.
36. "Helicopter Multifunction Radar Study for Naval Air Systems Command," Lockheed Electronics Company, Project 28-7100-9151, August, 1967.
37. Knemeyer, S. and Yingling, G. L. "Results of the USAF Pilot Factors Program as they Apply to Flight Safety," Twelfth Annual Business Aircraft Safety Seminar, May, 1967.
38. Robinson, G. G., and Johnson, N. S. "Subsystem Requirements for an Airborne Laboratory to Study Zero-Zero Landing Systems," 25th Meeting of Flight Mechanics Panel of Advisory Group for Aeronautical Research and Development, October, 1964.

APPENDIX A
DERIVATION OF EQUATIONS FOR MOTION CUE ANALYSIS

Equations defining constant velocity and acceleration curves are derived in order to evaluate the effectiveness of motion cues as a landing aid. An equation is derived in Reference 11 which relates the radial angular velocity to ground coordinates. In this analysis, the radial angular velocity is expressed in terms of azimuth and elevation angle coordinates. This is accomplished in order to get plots of the constant velocity and acceleration contours on a vertical display.

1. Derivation of Equation for Obtaining Isovelocity Curves

The equation derived in Reference 11 is given by:

$$K = \frac{V\sqrt{X^2 + Y^2 \sin^2\alpha}}{X^2 + Y^2 + D^2 + 2DY \cos\alpha} \qquad (1)$$

Where: $K = \frac{d\beta}{dt}$ = radial angular velocity

X and Y = ground coordinates

D = slant range from the aiming point or impact point to the aircraft

V = velocity of aircraft along its glide slope

α = glide slope angle

The geometrical identification of these terms is illustrated in Figure A-1 along with the defining azimuth and elevation angles. We will now proceed to obtain K as a function of (θ, ϕ, D, α and V) from which ϕ = f (K, θ, D, α and V) will be derived to facilitate generating constant K curves directly. X and Y may be solved in terms of θ and ϕ by first substituting Y_o for (Y + D cos α).

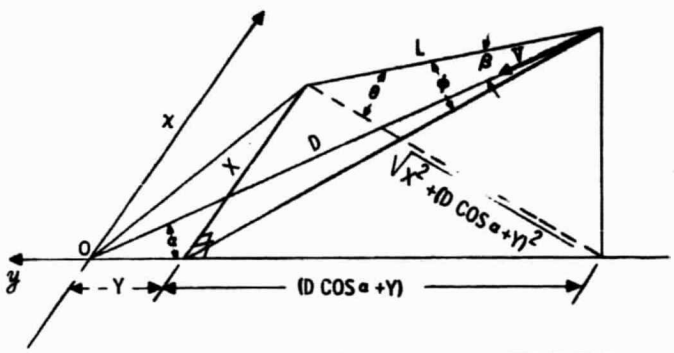

LEGEND: $L = \sqrt{D^2 \sin^2 \alpha + X^2 + (D \cos \alpha + Y)^2}$

ϕ = DEFINED AZIMUTH ANGLE

θ = DEFINED ELEVATION ANGLE

β = RADIAL ANGLE FROM IMPACT POINT O

$(K = \frac{d\beta}{dt})$

Figure A-1. Geometry of Aircraft Descent to Impact Point O.